

## REPORT DOCUMENTATION PAGE

AFRL-SR-BL-TR-98-

is  
on

0305

Public reporting burden for the collection of information is estimated to average 1 hour per response, including gathering and maintaining the data needed, and completing and reviewing the collection of information. Send collection of information, including suggestions for reducing this burden, to Washington Headquarters Service Davis Highway, Suite 1284, Arlington, VA 22202-4302, and to the Office of Management and Budget, Paperwork Reduction Project 0704-0188.

1. AGENCY USE ONLY (Leave blank)		2. REPORT DATE 3/24/98	3. REPORT TYPE AND DATES COVERED Final: 12/16/94 - 12/14/97
4. TITLE AND SUBTITLE  Non-Stoichiometric Layers of III/IV Semiconductors		5. FUNDING NUMBERS F49620-95-1-0091	
6. AUTHOR(S)  Professor Eicke Weber			
7. PERFORMING ORGANIZATION NAME(S) AND ADDRESS(ES)  University of California, Berkeley Electronics Research Laboratory 253 Cory Hall Berkeley, CA 94720		8. PERFORMING ORGANIZATION REPORT NUMBER 442427-22507	
9. SPONSORING / MONITORING AGENCY NAME(S) AND ADDRESS(ES)  AFOSR/PKA 110 Duncan Avenue, Room B115 Bolling AFB DC 20332-8080		10. SPONSORING /MONITORING AGENCY  NE	
11. SUPPLEMENTARY NOTES  19980414 084			
12a. DISTRIBUTION / AVAILABILITY STATEMENT  Unlimited			
13. ABSTRACT (Maximum 200 words)  The objective of this research project was the control of defect formation and thermal stability in non-stoichiometric GaAs thin layers. As-rich GaAs offers unique device applications in layer isolation and optoelectronics because of its insulating capabilities after a thermal annealing and ultrafast time response in the THz range. The introduction of an optical temperature measurement, utilizing the diffuse reflectance spectroscopy enhanced the accuracy of the growth parameter determination, leading to a fairly reproducible growth. This enabled us to determine the limits of the low-temperature growth, a saturation of the lattice dilation at low growth temperatures and/or high BEP ratios, and the onset of polycrystallinity and epitaxial columnar growth as is usually observed in the epitaxial growth of ceramics.			
14. SUBJECT TERMS  non-stoichiometric GaAs thin layers, limits of low-temperature growth			15. NUMBER OF PAGES 75
			16. PRICE CODE
17. SECURITY CLASSIFICATION OF REPORT unclassified	18. SECURITY CLASSIFICATION OF THIS PAGE unclassified	19. SECURITY CLASSIFICATION OF ABSTRACT unclassified	20. LIMITATION OF ABSTRACT n/a

## Table of Contents

<b>Abstract</b>	<b>4</b>
<b>1. Introduction</b>	<b>5</b>
<b>2. Defect control in LT-GaAs</b>	<b>6</b>
2.1 Calibration of the growth temperature (DRS) and As/Ga flux ratio	7
2.2 Lattice expansion due to excess As incorporation	8
2.2.1 Influence of the growth temperature	8
2.2.2 Influence of the As/Ga flux ratio	8
2.3 LT-GaAs, grown in the very low temperature range ( $T_G < 200^\circ\text{C}$ )	10
2.4 Influence of strained diffusion barrier layers	13
2.5 Donors and acceptors in LT-GaAs	14
2.5.1 The double donor $\text{As}_{\text{Ga}}$	14
2.5.2 The triple acceptor $\text{V}_{\text{Ga}}$	15
2.6 Impurities in LT-GaAs (contamination)	16
<b>3. Other non-stoichiometric III-V compounds</b>	<b>17</b>
3.1 As implanted GaAs	17
3.2 LT AlGaAs	18
<b>4. Electrical transport measurements</b>	<b>18</b>
4.1 Vertical & horizontal conductivity	19
4.2 Breakdown voltage	20
<b>5. LT-GaAs:Be for device applications</b>	<b>21</b>
5.1 Lattice mismatch and point defect concentration	21
5.2 Carrier trapping times	23
5.3 Diffusion / Thermal stability	27
5.4 Electrical transport measurements	29

<b>6. Related work in cooperation with other groups</b>	<b>30</b>
<b>7. Summary and Future work</b>	<b>30</b>
<b>8. Personnel</b>	<b>32</b>
<b>9. References</b>	<b>33</b>
<b>10. Publications</b>	<b>36</b>
<b>11. Tables</b>	<b>38</b>
<b>12. Figures</b>	<b>39</b>

## 1. Introduction

Since in 1988 Smith et al. reported the growth of GaAs at low temperatures ( $T_G=200^\circ\text{C}$ ) for buffer layer applications [Smi.88], the amount of research focused on this highly non-stoichiometric GaAs has continuously increased. The interest in LT-GaAs is focused on two electronic properties. First, the material exhibits ultrafast trapping times (< 1ps), when grown below  $T_G=230^\circ\text{C}$  [Gu.92]. Secondly, after an appropriate annealing procedure or if grown at temperatures above  $350^\circ\text{C}$ , LT-GaAs is highly insulating, with resistivities above  $10^7 \Omega\text{cm}$  [Lo.91]. The supersaturation concentration of native point defects such as As antisites ( $\text{As}_{\text{Ga}}$ ), As interstitials ( $\text{As}_{\text{I}}$ ) or Ga vacancies ( $\text{V}_{\text{Ga}}$ ), which cause these special properties, increase the lattice constant of LT-GaAs with decreasing growth temperature. As a result, homoepitaxially MBE-grown LT-GaAs on GaAs is tetragonally distorted (pseudomorphic growth) [Wie.90]. We observed a linear relation between the As antisite concentration [ $\text{As}_{\text{Ga}}$ ] and the lattice mismatch  $\Delta c/c$  [Liu.95]. The incorporation of excess As can reach 1.5% [Yu.92] and increases with decreasing growth temperature and/or increasing As/Ga flux ratio [Luy.98]. In the growth temperature range of  $T_G \in [200^\circ\text{C}, 250^\circ\text{C}]$  and for small excess As fluxes (As/Ga flux ratio  $R > \approx 1.0$ ), the  $\text{As}_{\text{Ga}}$  concentration and therewith the lattice mismatch  $\Delta c/c$  change drastically with small growth parameter variations [Luy.98]. Therefore a precise determination and accurate control of the substrate temperature and the As/Ga flux ratio are essential for LT-GaAs reproducibility. The crystal quality of the highly non-stoichiometric layers is remarkably good. Extended defects (dislocations, stacking faults, precipitates) are rarely found in the as-grown material as long as a certain critical thickness that depends on the growth temperature is not exceeded [Lil.90].

Most of the excess As precipitates to form As clusters and, additionally, outdiffusion of point defects occurs upon thermal annealing at temperatures above  $400^\circ\text{C}$  [Lil.90, Mel.90]. The As antisite concentration decreases from up to  $10^{20}/\text{cm}^3$  down to about  $10^{18}/\text{cm}^3$  [Liu.94] and, as a consequence, the lattice mismatch to the substrate vanishes. This thermal instability requires the growth of diffusion barrier layers [Lin.90], because the outdiffusion can be detrimental to neighboring layers in device structures. Insulation is often required for structures deposited on top of the LT-GaAs layer. Therefore, an annealing step of LT-GaAs is a common procedure in device processing and AlAs diffusion barrier layers are indispensable. These barrier layers, however, influence the incorporation of the native defects because they are strained if grown pseudomorphically on a GaAs substrate.

LT-GaAs, grown below  $T_G=230^\circ\text{C}$ , exhibits ultrafast electron trapping times as measured by optical pump-probe transient absorption or reflection [Gu.92, Lil.94, Spe.97]. These carrier trapping times were reported to correlate in as-grown material with the concentration of ionized As antisites [Lil.94]. In undoped LT-GaAs, however, the  $[\text{As}_{\text{Ga}}^+]$  does not exceed 10% of the total concentration of  $\text{As}_{\text{Ga}}$ . We introduced Be-doping in order to increase and control the amount of ionization of the  $\text{As}_{\text{Ga}}$ . We expected the chemical acceptor to electrically compensate the double donor  $\text{As}_{\text{Ga}}$  and, therefore, increase the fraction of ionized antisite defects. We succeeded by using our standard characterization methods (XRD, Hall, MCDA, NIRA, TEM, SIMS, time-resolved

reflectivity transients) in growing an ultrafast, thermally stabilized and better reproducible non-stoichiometric GaAs. Subpicosecond carrier trapping times were observed at growth temperatures up to 300°C. Thermal treatments were applied for a sandwich structure with LT-GaAs:Be embedded between two GaAs:Si layers. Even after 10 seconds annealing at 850°C or 60 minutes at 700°C no significant change in the Be-doping profile was observed. More detailed investigations to determine the amount of outdiffusion in these layers are ongoing. Additionally, the electrical properties of as-grown and annealed layers are presently investigated and will be object of the following annual report.

Alternatively, non-stoichiometric III-V compounds such as As implanted GaAs, LT-AlGaAs or LT-InP were also subject of our studies. The implanted GaAs turned out to be an inexpensive alternative of producing As-rich GaAs although the results were found to be independent on the chemical nature of the implants. This leads to the conclusion that implanted GaAs is mainly non-stoichiometric due to the high point defect concentration produced because of the lattice damage during implantation. Without the incorporation of additional chemical dopants which can thermally stabilize these native point defects - hypothetically due to complex formation - implanted GaAs will be even less thermally stable than the MBE grown LT-GaAs especially because high  $[V_{Ga}]$  are also present in these layers. LT-Al<sub>0.3</sub>Ga<sub>0.7</sub>As was found to be a superior insulating material with resistivities up to  $10^{11} \Omega\text{cm}$  caused by the deep level defect band which is located about 0.95eV below the conduction band. On the other hand, LT-InP was found to be n-conductive because of a defect level which is resonant with the conduction band [Dre.93]. LT-growth was generally found to produce non-stoichiometry, an issue which found more attention recently in the growth development of III-nitrides. LT-GaAs is a comparably well investigated non-stoichiometric material. Therefore it seems to be a very suitable model substance and might be helpful for overcoming the difficult growth process of the III-nitrides.

## 2. Defect control in LT-GaAs

The substrate temperature and the As/Ga flux ratio (or the BEP ratio) are the most important growth parameters for controlling the As incorporation during the MBE growth of GaAs below 400°C. We demonstrated that an increase in growth temperature reduces the concentration of  $As_{Ga}$  defects, which results in a decrease of the lattice mismatch [Lo.93a,Fuj.95]. This result is confirmed by several growth runs, where the temperature was varied between 155°C and 350°C (Fig. 1). With the currently used DRS temperature calibration (see chapter 2.1) the reproducibility of the temperature dependence is remarkably good. In the temperature range below 200°C the single crystallinity of some of the films broke down as a certain critical thickness was exceeded (blue triangles in Fig. 1). The impact of these low growth temperatures on the structural properties of our films is presented in more detail in chapter 2.3.

The growth on Al<sub>x</sub>Ga<sub>1-x</sub>As diffusion barrier layers was found to reduce the incorporation of As antisites (chapter 2.4). This can be described as a compensation of the hydrostatic stress component introduced by the strained barrier layers if grown pseudomorphically. The acceptor and donor concentrations in the LT-GaAs films were determined (chapter

2.5). The native defect concentrations are by orders of magnitude larger than those of any chemical dopant incorporated in the layers through contamination (chapter 2.6).

## 2.1 Calibration of growth temperature (DRS) and As/Ga flux ratio

Since the As incorporation in the non-stoichiometric GaAs varies dramatically with growth temperature, especially in the temperature range below 250°C (see Fig. 1), it is of great importance to control the growth temperature accurately. Because under standard MBE conditions the accuracy of the low-temperature determination, using a pyrometer extrapolation with a thermocouple, never exceeded  $\pm 10^\circ\text{C}$  [Lo.93b], we introduced a new low-temperature measurement into our MBE system. With the diffuse reflectance spectroscopy (DRS) the substrate temperature can be determined to an accuracy of  $\pm 2^\circ\text{C}$ .

The DRS is an in-situ optical measurement system now commercially distributed by Thermionics NW Inc. Modulated white light from a tungsten halogen lamp is focused onto the substrate wafer through one of the k-cell ports of the MBE machine or the center port, usually used for pyrometer readings. The diffusely reflected light is then measured through a second port (see Fig. 2). The dispersed energy spectrum contains - dependent on the electrical properties and the surface condition of the wafer - the information about the bandgap of the substrate. The signal is therefore sensitive to the temperature of the wafer. More details about the DRS temperature measurement can be found in [Wei.91, Joh.94]. The bandedge absorption changes if an additional LT-GaAs layer has been deposited on the substrate as well as for the deposition of an AlAs buffer layer. Indeed we observed different DRS temperature readings. The DRS temperature changed during in-situ measuring, which could also be partly due to radiation effects from the hot k-cells. After the growth the temperature readings were also different. Therefore, we calibrated the thermocouple readings for wafers with different doping and/or surface quality with the simultaneous DRS temperature reading (see Fig. 3 for  $n^+$  GaAs substrates) and did not measure with the DRS system during the actual growth process. In Fig. 3 the different temperature calibrations for single-sided polished (ssp) and double-sided polished (dsp)  $n^+$ -substrate wafers are shown.

As was previously studied in more detail, the supersaturation of native defects and its related lattice mismatch is as well strongly dependent on the As/Ga flux ratio [Pra.95], here expressed as beam equivalent pressure (BEP) ratios. The BEP of the arsenic and gallium cells are usually determined by an ion gauge, positioned at the backside of the substrate holder station inside the MBE growth chamber. By moving the station, the ion gauge will be rotated into the exact position of the substrate during growth. One disadvantage of this method is that flux variations during the growth process cannot be observed. With our additional mass spectrometer, however, we can monitor the Ga and As peaks of the mass spectrum during growth. Figure 4 shows a comparison between the calibrated signals of the residual gas analyzer (RGA) and a former measured BEP series [Pra.95] with BEP ratio values, obtained with an ion gauge. We expect to avoid inhomogeneous incorporation of excess As due to flux fluctuations during the growth process by further studying "in-situ" the change of the mass spectrum.

## 2.2 Lattice expansion due to excess As incorporation

Since the amount of excess As incorporated during the MBE deposition at low temperatures is decisive for the electronic properties of the LT-GaAs layers, we systematically investigated the influence of the main growth parameters on the incorporation of excess anions. For this purpose, two different types of growth series have been deposited: a temperature series, where the growth temperature was varied from 200°C to 350°C at a beam equivalent pressure (BEP) of 20, and two As/Ga flux series grown at 200°C and 240°C, respectively, where the As/ Ga flux ratio as measured by the BEP was varied from 7 to 40 (see also Fig. 4).

By x-ray diffraction (XRD) the perpendicular lattice constant of the LT-GaAs films was measured from the shift of the (004) reflections with respect to the GaAs substrate peak. The parallel lattice mismatch was evaluated by use of the asymmetrical (224) reflections. Point defect concentrations  $[As_{Ga}^0]$  and  $[As_{Ga}^+]$  were measured by near infrared absorption (NIRA) and magnetic circular dichroism of absorption (MCDA) as described in detail in our previous work, see e.g. [Liu.95].

### 2.2.1 Influence of the growth temperature

The perpendicular lattice constant decreases with increasing growth temperature from  $(0.11\% \pm 0.03\%)$  at 200°C to  $(0.006\% \pm 0.005\%)$  at 345°C (Fig. 1, T1 to T3 series). The parallel lattice constant of the LT-GaAs layers is the same as that of the GaAs substrate. Therefore the LT-GaAs films are tetragonally distorted (pseudomorphic growth). Because of the growth temperature calibration by DRS the dependence of the lattice mismatch on the growth temperature agrees very well for all sample series, which indicates a good reproducibility of the growth conditions. This is also confirmed by the measurement of exactly the same lattice mismatch for samples where the same growth conditions were repeated after two years (T1 compared with T3). The lattice mismatch reaches a saturation level at about 0.16% for low growth temperatures. Below 165°C we did not grow pure single crystalline layers as the top layer became polycrystalline (see also chapter 2.4).

### 2.2.2 Influence of the As/Ga flux ratio (BEP) on the lattice expansion

At the growth temperature of 200°C a steep increase of the lattice mismatch is observed if the BEP ratio is raised from 7 to 20 (Fig. 5). At higher As/Ga flux ratios the lattice mismatch reaches a saturation value at approximately 0.125% (see also Fig. 4). The lattice mismatch of the LT-GaAs layer grown at 200°C with BEP=40 was found to have a reduced lattice mismatch because of flux instabilities during the MBE growth. A similar increase of  $\Delta c/c$  is obtained for the samples grown at 240°C, where the lattice mismatch increases up to 0.050%, which is smaller than the value obtained for 200°C, resulting from the higher growth temperature. However, the onset of the strained growth of the LT-GaAs epilayer occurs at almost the same As/Ga flux ratio corresponding to a BEP of approximately 8 for both temperatures. Below this value the crystal quality of the films

becomes bad as is indicated by a rough surface morphology with a milky appearance. Three additional samples were grown to confirm the plateau-like character and the same nominal temperatures (thermocouple readings) were used. However, since the first set of samples was grown on single sided polished wafers, whereas the second set was deposited onto double sided wafers, the real temperatures determined by DRS are slightly lower for the new samples. This small difference is clearly reflected in the values measured for the saturation lattice constant. The samples deposited at a BEP of 20 and 40 at 195°C exhibit the same lattice mismatch. The lattice constant of the sample grown at 230°C at a BEP of 40 is significantly lower. Our results show that the saturation value is temperature dependent and decreases with higher growth temperature.

A steep onset of the strained growth was previously reported by Missous and O'Hagen [Mis.94], who investigated the influence of a BEP variation in the range of 3 to 6 at 250°C. By Lagadas et al [Lag.94] a linear increase of the lattice mismatch was reported upon a variation of the As/Ga flux ratio for samples grown at 250°C. For BEP values larger than 25 they observed a constant lattice mismatch of 0.056% which is in excellent agreement with our "plateau value" obtained in the growth temperature region of 250°C.

Final remarks:

The concentration of neutral antisites  $[As_{Ga}^0]$  as obtained by near-infrared absorption (NIRA) was found to linearly correlate with the neutral antisite concentration (see Figure 12) [Liu.95]. In this analysis data collected from both the temperature and the BEP series were taken and compared with a former series which was grown at the MIT Lincoln Laboratories [Lil.94,Liu.95]. In all cases except one LT-layer the linear correlation was obvious. This correlation strongly suggests that the dominant defect responsible for the lattice expansion of as-grown LT-GaAs is indeed the  $As_{Ga}$  defect. This conclusion is also supported by the fact that the As-As bond is slightly longer than the As-Ga bond [Cu.78]. Therefore, as long as the linear dependency is observed, most of the excess As can be assumed to be incorporated onto Ga lattice sites, which leads to an expansion of the lattice. This conclusion does not exclude the possibility that each antisite defect has a satellite, i.e. an interstitial As. Because of the linear correlation  $\Delta c/c$  ( $[As_{Ga}^0]$ ) a line was fitted first considering all results and, secondly, without the sample which showed a higher  $As_{Ga}^0$  concentration than was expected from the lattice mismatch (highest  $[As_{Ga}^0]$ ). The fits are shown in Fig. 12 together with the fitting parameters. The layers grown in the very low temperature range were not yet measured by MCDA or NIRA. These data will be provided soon. At present it is unclear if the linear correlation still holds up to the highest lattice mismatch of  $\Delta c/c=0.16\%$  or if a saturation of the lattice mismatch takes place indicating that additional point defects might play a role in the very low growth temperature range.

The saturation value for the tetragonal distortion which is  $\Delta c/c=0.16\%$  corresponds to  $(1.2 - 1.3) \times 10^{20}/cm^3$  neutral As antisites as can be extrapolated from the fit curves of Fig. 6. Assuming a homogeneous distribution of these point defects this results in an average closest distance of 1.44 nm between the  $As_{Ga}$ . As clustering on a nanometer scale seems to be possible at these small distances, which might at first not be detected by TEM (resolution limit is about 2 nm diameter of a nanocluster), but could be measured by wide

angle x-ray scattering methods. In the very low growth temperature range below 200°C such nanoclusters could be the source for dislocations and / or stacking faults if the dislocations split into partials. These clusters can therefore enhance the onset of epitaxial columnar growth.

### 2.3 LT-GaAs, grown in the very low temperature range ( $T_G < 200^\circ\text{C}$ )

Growing LT-GaAs below a growth temperature of 200°C leads to a further increase in the lattice mismatch of the tetragonal distorted lattice up to a saturation value of about  $\Delta c/c = 0.16\%$  (see Fig. 1). This is equivalent to a lattice mismatch in a relaxed lattice of  $\Delta a/a \approx 0.08\%$  ( $\Delta c/c = p * \Delta a/a$  with  $p=c_{11}/(c_{11} + 2c_{12})=0.524$  using the elastic constants from Krieger et al. [Kri.95]). Below 165°C the layers always became partly polycrystalline. With the breakdown of single crystallinity at 155°C we observed a reduction in  $\Delta c/c$ . We determined by x-ray diffraction the parallel and perpendicular lattice mismatch of the layer with the highest reduction in  $\Delta c/c$  using the asymmetric (224) reflection (Fig. 14). Table I shows the results of the lattice mismatches together with  $\Delta c/c$  as determined in (004) reflection for comparison. Within the measured errors no lattice relaxation could be detected. In this temperature range we also observed a large variation in the critical thickness (see also Fig. 16). It seems that at this temperature even slight changes in the growth parameters can change the onset of extended defects. The reduction of the lattice mismatch with decreasing temperature in the low T-range was proposed in recent results on MBE growth simulations of R. Venkat's group at UNLV [Mut.97]. These simulations describe the inverse temperature dependence of LT-GaAs as an effect of negligible As evaporation rate with lowered temperatures, which leaves the thermally activated As adsorption rate as the only determining process for excess As incorporation. Our results can neither support nor disprove this theory because we did not observe a reduction in lattice mismatch with decreasing growth temperature but a large variation of  $\Delta c/c$  after a deposition with nominally the same growth parameters at  $T_G=155^\circ\text{C}$ .

The formation of stacking faults and the related breakdown of single crystallinity was already described in detailed TEM analyses by Liliental-Weber et al. [Lil.91b]. We concentrated our investigation on the temperature and BEP ratio dependence of the defect formation and the critical thickness. In our analysis, the critical thickness is defined as the distance from the substrate (buffer), where a 50% volume fraction remains defect free. An example for the evaluation of the critical thickness is given in Fig. 15. The values, dependent on growth temperature and BEP ratio, as given in Fig.'s 16 and 17, respectively, were found to increase with increasing growth temperature and decreasing BEP ratio. A common procedure to predict the critical thickness of heteroepitaxial growth is to compare the elastic strain energy with the elastic energies of misfit dislocations. This approach, which has been applied in the growth models of People and Bean [Peo.86], Van der Merwe [Mer.63] and Matthews and Blakeslee [Mat.74], fails to describe the transition from pseudomorphic to strain relaxed growth observed in our LT-GaAs layers.

At low temperatures, however, the temperature dependence of the dislocation formation must also be taken into account. Because the dislocation formation (and the dislocation

migration) energy is thermally activated, the critical thickness for equally strained layers should decrease with increasing temperature. This is in contradiction to our results, which show an increase in critical thickness for higher growth temperatures and constant lattice mismatch (Fig. 16 and Table II). For a constant growth temperature these values should decrease with increasing strain. Although the lattice mismatch decreases with increasing BEP ratio (inverse behavior if compared to the  $\Delta c/c$ (BEP) dependence of single crystalline layers, see Table II), the critical thickness decreases for the BEP series grown at 165°C (blue dots in Fig. 17). A drastic decrease in critical thickness with increasing BEP ratio was observed for a Be-doped series, grown at 190°C with  $[Be] = 10^{20} \text{ cm}^{-3}$  (red squares in Fig. 17). Be-doping enhances the excess As incorporation (see chapter 5) similar to a decrease in growth temperature and an increase in BEP ratio. It can be therefore generalized that an increased amount of excess As in the thin layers causes a decrease in critical thickness, although part of these excess As does not contribute to the lattice mismatch (see Table II). We assume that for extreme growth parameters - such as growth temperatures well below 200°C and/or BEP ratios above 30 or high Be-doping in combination with low temperatures and/or high BEP ratios - the excess As cannot be fully substitutionally incorporated into the layer and As nanoclusters will be formed. These clusters are ideal sources for misfit dislocation formation and will therefore reduce the critical thickness although the dislocations present might not be able to glide down to the surface of the LT-layer. Therefore, the single crystalline layers below the defective area of the LT-GaAs are still pseudomorph as was already shown in the x-ray diffraction analysis in figure 7.

The breakdown of the single crystalline growth in LT-GaAs was investigated in more detail in a sample which contained alternating LT-GaAs (thickness: 50 nm) and LT-AlAs (thickness: 1.7 nm) layers grown on top of a 600 nm LT-GaAs layer at 200°C and a BEP ratio of 20. TEM analysis revealed an anisotropic morphology of the growing surface, i.e. hillocks elongated in the [0-11] direction (Fig.s 11). In the (011) orientation the AlAs layers are perfectly straight and perpendicular to the [100] growth direction. The (0-11) projection reveals increasing surface roughness with increasing thickness. Eventually defects nucleate, preferentially at the hillocks. These results clearly demonstrate the influence of surface roughening on the breakdown of single crystallinity in epitaxial growth. Similar results were reported on the transition from epitaxial to amorphous growth of Si and GaAs [Eag.95]. Stress induced surface diffusion which has been evoked to explain surface roughening cannot be a dominant process here because of the low growth temperature. The same argument applies to misfit dislocation formation which is also a thermally activated process. The incorporation of excess As can be assumed to be fairly homogeneous on a macroscopic scale since the size and density of As precipitates formed upon annealing remain constant throughout the whole epilayer [Lil.92,Luy.98]. However, locally the strain field around an As antisite may energetically favor the incorporation of additional  $\text{As}_{\text{Ga}}$  in close vicinity which can gradually increase the buildup of surface undulations. It shall be noted that the critical thickness observed in this sample is not comparable with the ones measured in LT-GaAs without any marker layers (LT-AlAs). The multiple strained layers obviously change the conditions for the onset of polycrystalline growth which starts at a much lower critical thickness than would be

expected in pure LT-GaAs grown with the same growth parameters. On the other hand the LT-AlAs layers themselves cannot be responsible for this effect because the surface undulations are already present at the very first interface.

A discrepancy between critical thickness theories and experimental results was also observed in InGaN/GaN and AlGaN/GaN quantum well structures ([Ki.98], Fig.12). In these systems a transition from 2-dimensional into 3-dimensional growth modes is observed, dependent on the thickness of the layers. However, the critical thickness was found to be 40 times larger in the InGaN/GaN than in the AlGaN/GaN quantum well structures, although for the respective compositions the  $In_xGa_{1-x}N$  had a lattice mismatch  $\Delta a/a \approx 3.6\%$ , while the observed  $Al_xGa_{1-x}N$ -composition exhibited just  $\Delta a/a \approx 1.8\%$ . The growth temperatures, determined by a linear approximation between the respective binary systems, were  $0.45T_m$  (InGaN) and  $0.38T_m$  (AlGaN). The temperatures are given in fractions of the melting temperature ( $T_m$ ) to enable a comparison of the brittleness of the ternary systems. These systems are considerably more difficult than the As-rich GaAs if the heteroepitaxial growth with large lattice mismatches and different thermal expansion coefficients is regarded. It was found recently that non-stoichiometry and cluster formation plays also a role in the GaN growth [Ki.98]. This indicates that these temperature-dependent effects which can be studied separately in LT-GaAs may account for the above described striking results. In this way the well controlled studies of LT-GaAs can improve the low-temperature growth development of the III-nitrides.

Another interesting fact is the coincidence of the temperature range where non-stoichiometric GaAs can be grown and the temperature range for plastic deformation in GaAs. Between  $150^\circ C$  and  $200^\circ C$  the onset of plasticity was observed in GaAs [Yas.88] while the brittle-to-ductile transition (BDT) takes place between  $350^\circ C$  and  $400^\circ C$  [Fu.88]. In the lower temperature range LT-GaAs can be grown single crystalline, but with a limited thickness which in first order is independent of the strain energy because the incorporated stresses are almost constant (saturation level of lattice mismatch). The critical thickness, however, is dependent on the growth temperature and the BEP ratio, which supports the theory of the nanoclusters as sources for crystal defects. The dislocation mobility in this temperature range can still be low and anisotropic. The relaxation of the single crystalline layer will therefore be difficult. On the other hand, inhomogeneities in the incorporation of excess As as caused by minor As flux variations, for example, might have a huge effect in causing the onset of polysrystalline growth above clustered As atoms.

Between  $350^\circ C$  and  $400^\circ C$  the non-stoichiometry of MBE grown GaAs vanishes and the layers are lattice matched to the GaAs substrate. This is the high temperature limit for LT-growth and marks the onset of the BDT. For many polycrystalline materials, single crystalline silicon and some aluminides the temperature range of the BDT is similar to the onset of dislocation climb which is a (bulk) diffusion driven process [Spe.96]. In simulations of LT-growth, however, [Mut.97] the surface diffusion of the Ga atoms was often predicted to be the determining parameter together with the temperature dependent probability of the desorption and absorption of As atoms. However, surface diffusion is expected to have a lower activation energy than the corresponding bulk diffusion so that

these parameters cannot be compared. Nevertheless, the comparison to the III-nitride growth shows that plasticity does play a role in the LT-growth. Further investigations are necessary to clarify in which way the parameters responsible for the mechanical properties of a material are also influencing its epitaxial growth. The extreme conditions of LT-growth are known to take place in the growth process of ceramic materials.

## 2.4 Influence of strained diffusion barrier layers

The results obtained from LT-GaAs layers grown in different laboratories were always difficult to compare. With the temperature and BEP ratio determination obtained by the above described methods (DRS and RGA), however, the dominant growth parameters should lead to reproducible growth. We observed for two different series grown with slightly different growth temperatures due to the usage of different sample holders a systematic variation in lattice mismatch. However, the correction of the growth temperatures even enhanced the difference in lattice mismatch. The remaining difference between these series was determined to be the buffer layer. In one case we used an AlAs lift off layer on which the LT-GaAs layer was grown, the second series was grown on a GaAs buffer layer (Figure 13).

AlAs has a slightly higher lattice constant which produces a lattice mismatch to a GaAs substrate of 0.14%. In a pseudomorphic layer this accounts to  $\Delta c/c = 0.28\%$ . Therefore, the LT-GaAs layers deposited on top of an AlAs layer are grown on a strained layer which is known to influence the incorporation of point defects [Ki.96b]. The biaxial stress introduced by the buffer layer can be partly compensated by a variation in point defect concentration of the top layer.

The biaxial stress introduced by the strained AlAs diffusion barrier layer grown on top of a GaAs substrate leads to a strain according to (isotropic approximation):

$$\varepsilon_a = 1/E_1 * \sigma_a (1-v_1) \quad \text{for the two lattice constants in the growing surface and}$$

$$\varepsilon_c = -1/E_1 * \sigma_a 2v_1 \quad \text{for the growth direction.}$$

( $\varepsilon_a = -0.0014$  and  $\varepsilon_c = 0.0028$  as described above) The hydrostatic component  $\sigma_p$  of the biaxial stress is

$\sigma_p = 2/3 \sigma_a$ . The resulting strain from this component can be compensated by a variation in point defects according to Vegard's law. The reduction in strain accounts to

$$\varepsilon_p = -1/E_2 * \sigma_p (1-2v_2) = -1/E_2 * 2/3 \sigma_a (1-2v_2) = 2/3 \varepsilon_c * E_1/E_2 * (1-2v_2)/(2v_1)$$

with the elastic constants determined from Krieger et al. [Kri.95].

A constant reduction in  $\Delta c/c$  can be calculated for a particular diffusion barrier layer. In Figure 13 this reduction was calculated using the data obtained from LT-GaAs grown directly on GaAs (red squares). The reduction in strain as will be caused by an  $Al_{0.67}Ga_{0.33}As$  barrier layer is shown (blue line). The correspondence of the calculated reduction in  $\Delta c/c$  with the measured values for the series grown at MIT Lincoln Laboratories is amazing. Because these layers were grown in a different MBE system with different temperature and BEP ratio determination methods it was not expected that the calculation fit so well. It is also not necessary that a reduction due to a total compensation

of the stresses will happen. A lowered  $\Delta c/c$ , however, was observed in all cases where LT-GaAs was deposited on top of an AlGaAs layer. This topic will be investigated in more detail with the appropriate growth parameter calibrations and adequate variations in the buffer layer composition.

## 2.5 Donors and acceptors in LT-GaAs

In the following chapter we will discuss the occurrence of the native point defects  $As_{Ga}$  and  $V_{Ga}$ , their dependence on the growth parameters and their charge. These defects are the dominant native donors and acceptors in LT-GaAs. We did not study As interstitials ( $As_I$ ) which does not exclude that this defect might also be present in LT-GaAs. At present, however, we have no experimental evidence that the  $As_I$  has an effect on any of the here discussed properties in LT-GaAs. In chapter 5 the chemical acceptor Be is been discussed in detail. In our MBE grown layers the chemical acceptor C is not present in significant concentrations (see chapter 2.6). The above listed donors and acceptors summarize the currently discussed active dopants in LT-GaAs.

### 2.5.1 The double donor $As_{Ga}$

The As antisite  $As_{Ga}$  was found to be a double donor with a midgap  $As_{Ga}^{0/+}$  level in GaAs [Web.82]. Therefore the Fermi level can be pinned midgap and the material becomes semi-insulating. Our previous work has shown that, with the measurement of the As antisite defect concentration in the neutral and ionized charge state, we gain two very important pieces of information: If the Fermi level is near midgap, the sum of these values represents the total concentration of As antisite defects, whereas the concentration of ionized antisite defects,  $[As_{Ga}^+]$ , corresponds to the effective acceptor concentration. Therefore, the influence of the growth parameters ( $T_G$  and BEP ratio) on the point defect concentrations  $[As_{Ga}^0]$  and  $[As_{Ga}^+]$ , as measured by Near-InfraRed optical Absorption (NIRA) and Magnetic Circular Dichroism of Absorption (MCDA), was studied [Pra.95].

The results obtained upon a variation of the As/Ga flux ratio at 200°C and upon a variation of the growth temperature at a BEP of 20 are shown in Figure 14. In all cases, the positively charged  $[As_{Ga}^+]$  concentration is at least one order of magnitude lower than  $[As_{Ga}^0]$ . The As antisite concentration increases with decreasing growth temperature (see values at BEP=20) and increasing BEP up to a value of 20. In the sample grown at a BEP of 30 the unexpected decrease of the point defect concentrations was found to be due to fluctuations of the As/Ga flux ratio. At higher BEP ratios the point defect concentrations are assumed to reach a saturation value which is in agreement with the lattice mismatch observation (see also Fig. 17).

These results show that a well controlled  $As_{Ga}$  concentration can be achieved by variations in growth temperature and As/Ga flux ratio. However, this holds only in a specific range of growth parameters, since at high As/Ga flux ratios a saturation level is reached. At low As/Ga flux ratios and / or low growth temperatures a deterioration of the crystalline growth is observed, in the first case because of a lack of As (transition to Ga-rich

conditions), in the second case because of reduced thermally activated processes like surface diffusion, adsorption or line defect annihilation.

In undoped As-rich GaAs the concentration of ionized antisites never exceeded 10% of the total  $\text{As}_{\text{Ga}}$  concentration. Low growth temperatures and/or high BEP ratios had to be chosen for achieving a high  $[\text{As}_{\text{Ga}}^+]$ , however, at these conditions usually the lowest fraction of ionized antisites was observed (at most 2% to 5%). Necessarily, a huge amount of excess As was incorporated in the layers under these conditions. The layers showed a high concentration of As precipitates after thermal annealing. If used in device structures, additional AlAs diffusion barrier layers had to be introduced to maintain the properties of the active layers in the devices.

We chose a two step procedure to improve this situation: First we quantified the dominant acceptor, the Gallium vacancy  $\text{V}_{\text{Ga}}$ , compensating the  $\text{As}_{\text{Ga}}$  double donors, and it's temperature dependence. The obtained results indicated that an independent variation of  $\text{As}_{\text{Ga}}$  and  $\text{V}_{\text{Ga}}$  does not seem to be possible in undoped LT-GaAs. Secondly, we increased the ratio of  $[\text{As}_{\text{Ga}}^+]/[\text{As}_{\text{Ga}}]$  ( $[\text{As}_{\text{Ga}}] = [\text{As}_{\text{Ga}}^0] + [\text{As}_{\text{Ga}}^+]$ ) by introducing the chemical acceptor Be (see chapter 5). It was suggested before [Lil.94] that the  $\text{V}_{\text{Ga}}$  might be the dominant acceptor in LT-GaAs. Indications for  $\text{V}_{\text{Ga}}$  were found in LT-GaAs:Be [Bli.92], but never quantified. Therefore, we will describe the slow positron annihilation experiments and the obtained results.

### 2.5.2 The triple acceptor $\text{V}_{\text{Ga}}$

The  $\text{V}_{\text{Ga}}$  concentrations were evaluated from the S-parameter characteristics of the Doppler broadened 511keV positron annihilation peak. The S-parameter is defined as the ratio of the number of counts obtained from the central region of the peak to the total number of counts. The corresponding W-parameter is determined from the shoulder of the peak around 507keV. All positron annihilation spectra, which detect just one dominant defect, show a linear S(W) dependence. If the dominant defect is a single vacancies the (S,W) pair lies on a line with the bulk value (1,1) on the one end and a calculated parameter set (1.024,0.76) on the other end (see Fig. 15). The calculated (S,W) parameter set was experimentally confirmed in Si-doped GaAs [Ge.97a]. If (S,W) for a given layer lies on the described line the  $[\text{V}_{\text{Ga}}]$  can be calculated from the S-parameter value [Ge.97b].

Upon annealing at 600°C, the S-parameter increases to values between 1.03 and 1.05. The corresponding S(W) dependence does no longer follow the linear relation which indicates that different capture centers of the positrons are formed.. Figure 15 shows that in as-grown LT-GaAs the positron capture is dominated by single vacancies. The first as-grown LT-GaAs:Be layers (red dots) are also marked. In annealed LT-GaAs mono-vacancies are no longer present. The additional positron capture centers could be vacancy clusters and / or As precipitates, which were unambiguously identified by TEM.

The concentration of vacancy type defects were determined for samples grown at different temperatures [Ge97a]. The  $[\text{V}_{\text{Ga}}]$  in Fig. 16 is shown in an Arrhenius-type plot. With increasing growth temperature the  $[\text{V}_{\text{Ga}}]$  decrease is similarly to the temperature dependence of the  $[\text{As}_{\text{Ga}}]$ . In addition to our data the vacancy concentrations of two LT-

GaAs samples grown at 170°C and 250°C are given. In these cases the  $V_{Ga}$  concentrations were determined from the vacancy mediated interdiffusion of Al and Ga at LT-GaAs/AlAs interfaces [Ki.96a]. The values are in excellent agreement with our data. The slope of the linear fit to our data corresponds to a negative activation energy of  $0.7 \pm 0.2$  eV. This energy is the result of adsorption, desorption and point defect reactions at the growing surface and may be called an effective binding energy.

The concentration of positively charged  $As_{Ga}^+$  are given in Fig. 16 for comparison. It turned out that the  $[As_{Ga}^+]$  are considerably close to 3 times  $[V_{Ga}]$ . In view of the fact that the  $V_{Ga}$  is indeed expected to act as a triple acceptor, the  $[As_{Ga}^+]$  are shown on a different scale (right y-axis). It is evident that after annealing at 600°C single  $V_{Ga}$  cannot be detected any longer, because its concentration drops below the detection limit of  $5 \times 10^{15} \text{ cm}^{-3}$ . It was herewith demonstrated for the first time that the compensation of the singly ionized  $As_{Ga}$  donors is mainly governed by the triple acceptors  $V_{Ga}$ .

The BEP ratio dependence of the  $V_{Ga}$  concentration was also determined (Figure 17). With increasing BEP ratio the  $[V_{Ga}]$  increases similarly to the  $[As_{Ga}]$  as was expected from the temperature dependence of the  $[V_{Ga}]$ . At high BEP ratios we even observed a saturation of the  $V_{Ga}$  concentration. It shall be noted that the  $[V_{Ga}]$  for a BEP ratio = 20 is about four times lower than the determined  $[V_{Ga}]$  of the corresponding sample of the temperature series (Fig. 16). The reason is still unclear, however, the highest  $V_{Ga}$  concentration was never reproduced.

## 2.6 Impurities in LT-GaAs

The discussion about donor and acceptor concentrations in LT-GaAs always included the search for additional point defects. For the time being we do not exclude the possibility of As interstitials, present in the layers. It is simply noted that we never saw any indication for them, except the fact that different methods for measuring excess As showed different results. We do exclude the possibility of having further chemical acceptors or donors in our MBE grown layers at a concentration level, which can influence the obtained electrical or mechanical (strain) results. Table 2 shows the results of several SIMS analyses. The highest observed concentrations of the most prominent contamination elements carbon (acceptor), oxygen and hydrogen (both interstitials) are given together with the values from our last growth runs ("current level"). Nitrogen was never obtained above the detection limit for the chosen SIMS conditions ( $3 \times 10^{15} \text{ cm}^{-3}$ ). The highest observed carbon concentration is  $6 \times 10^{16} \text{ cm}^{-3}$ , far below the values of the ionized  $As_{Ga}$  donors. We did find segregation at all interfaces, mostly from oxygen, when high contamination levels were observed. Currently all determined concentrations of contamination elements are below the respective detection limits (see Table III). Other elements (except the ones which are or were present in the sources) are even more unlikely to be found in MBE grown samples under UHV conditions. The observed concentrations of impurities cannot account for electrical or mechanical compensation effects.

### 3. Other non-stoichiometric III-V compounds

During the first year of the AFOSR contract we mainly concentrated on studying the native point defects, especially the anion antisites, in LT-GaAs and other non-stoichiometric III-V compounds and observed their effect on the material's properties. A cheap alternative to MBE grown LT-GaAs is the production of As-rich GaAs by As, Ga or Ar implantation into GaAs. These materials were investigated and their point defect concentration and electrical properties were compared to the performance of LT-GaAs. LT-AlGaAs and LT-InP were additionally investigated materials. The n-type conductivity in LT-InP was found to originate from the anion antisite levels whose first level ( $P_{In}^{0/+}$ :  $E_c + 0.12\text{eV}$ ) is resonant with the conduction band. The results obtained in As implanted GaAs and LT-AlGaAs will be presented here in more detail.

#### 3.1 As implanted GaAs

The basic properties of implanted GaAs are comparable with LT GaAs. The chemical nature of the implanted element is of minor interest; since implanting with Ga, As or Ar leads to similar results. This indicates that the defect population in implanted GaAs is produced by damaging the crystal rather than by incorporating special atoms. However, one distinct difference was observed in Ar implanted GaAs: after annealing voids rather than As precipitates were formed [Wal.96]. The saturation limit for the lattice mismatch obtained in LT-GaAs does not hold for As implanted GaAs: a lattice mismatch in growth direction of  $\Delta c/c = 0.36\%$  was measured due to the incorporation of excess As while in LT-GaAs the maximal lattice mismatch is much lower. Additionally the annealing behavior is slightly different from that of the non-stoichiometric GaAs grown by MBE, especially for low annealing temperatures.

In Figure 18 the ionized  $[As_{Ga}^+]$  as measured as-implanted and after different 20 minutes annealing steps is given for As implanted GaAs. SI,  $n^+$  and  $p^+$  GaAs substrates were used. In the as-implanted material the concentration of ionized  $As_{Ga}^+$  is not maximal, indicating that at first high concentrations of interstitials will diffuse into substitutional positions during the annealing procedure. Therefore, the substitutional point defects increase with low temperature annealing. The high concentration of ionized antisites up to  $10^{20}/\text{cm}^3$  also reflects the high concentration of compensating acceptors ( $V_{Ga}$ ) which are still present after annealing at temperatures below  $400^\circ\text{C}$ . Due to the process of point defect formation by crystal damage the concentration of ionized  $As_{Ga}^+$  is greater by more than one order of magnitude than the concentrations in conventional MBE grown LT-GaAs (neutral antisite concentrations are about three times higher than in LT-GaAs). At higher annealing temperatures the ionized antisite concentration decreases in As implanted GaAs, probably due to both reduction of  $V_{Ga}$  and  $As_{Ga}$  (precipitate formation). In Ar implanted GaAs the maximal  $[As_{Ga}^+]$  was reached after annealing at  $500^\circ\text{C}$  and then decreases due to the clustering of  $V_{Ga}$  into voids [Wal.96]. After annealing at  $600^\circ\text{C}$  As and Ar implanted GaAs also showed high electrical resistivity [Fuj.95, Liu.95, Wal.96]. Ultrafast time response was observed in both Ar and As implanted GaAs [Wal.96, Wan.96]. One technical problem of producing non-stoichiometric GaAs is the uniformity of the excess As in the layers. The

implantation requires a thermal treatment to enhance the uniformity of the material. Because of the high defect concentration, especially the high vacancy concentration, implanted GaAs is even less thermally stable than the usual LT-GaAs. An alternative which might improve the thermal stability is to implant elements who can stabilize the native point defects (like Be in LT-GaAs).

### 3.2 LT-AlGaAs

LT-Al<sub>x</sub>Ga<sub>1-x</sub>As has a high antisite concentration similar to that of LT-GaAs. The MCDA spectra of LT-Al<sub>x</sub>Ga<sub>1-x</sub>As and LT-GaAs are similar as can be seen in Figure 19. At low Al percentage the MCDA spectrum has the same features of two negative peaks. As the amount of Al increases the two peaks start to shift to higher energies with the paramagnetic peak shifting faster than the diamagnetic peak. Eventually the paramagnetic peak merges into the diamagnetic peak (around x=0.2), but a definite shoulder at lower energies is still visible up to x=0.3. For x=0.3 the only MCDA band observed is located at 1.35eV [Pra.98]. Photoquenching studies made with white light illumination indicate that these two peaks and eventually the one peak are associated with the EL2 defect. Unlike in LT-GaAs, the peaks in LT- Al<sub>x</sub>Ga<sub>1-x</sub>As are quenchable to a greater extent about 80% to 90%. Temperature dependent MCDA showed that the MCDA signal after white light illumination is fully recovered from the quenching process around 140K, which is identical to the recovery process of quenched EL2 in bulk GaAs.

With increasing x the bandgap increases in the Al<sub>x</sub>Ga<sub>1-x</sub>As alloy system. The highly localized antisite level at 0.95eV below the conduction band results in the formation of insulating material with specific resistivities above 10<sup>11</sup> Ωcm as can be seen in figure 20 [Ver.96]. Current transient spectroscopy of these samples yields a deep level activation energy of 1.01eV, in close agreement with the value obtained from conductivity measurements. The high resistivity in LT-Al<sub>x</sub>Ga<sub>1-x</sub>As offers device isolation properties that are even superior to LT-GaAs.

### 4. Electrical transport measurements

The high resistivity of annealed LT-GaAs layers led to it's first application as insulation layer with reduced sidегating and backgating effects [Smi.88]. We studied the electric transport properties of as-grown and in-situ annealed LT-GaAs dependent on the growth temperature and BEP ratio. Therefore, two sets of samples were grown for the determination of the horizontal conductivity by Hall effect measurements and of the vertical conductivity by use of n-i-n structures. The "Hall samples" contained an AlAs layer for lift-off and were grown at different growth temperatures. The annealed series for Hall measurements were produced inside the MBE chamber at 580°C under As overpressure. The n-i-n structures contained a LT-GaAs layer which was embedded between two n<sup>+</sup> layers. Since the growth of the n<sup>+</sup> top layer is performed at 580°C, the underlying LT-GaAs layer is in-situ annealed for approximately 30 min. The Hall effect measurements were carried out at the Slovac Academy of Science in Bratislava. The n-i-n

structures were additionally tested in an I-V system until breakdown occurred (chapter 4.2).

#### 4.1 Vertical & horizontal conductivity

The resistivity and mobility for as-grown LT-GaAs is shown in Figure 21 dependent on the lattice mismatch. This correlation was chosen because the LT-layers were grown on top of the strained AlAs lift-off layer and are not quite comparable to LT-GaAs which was directly grown on GaAs. The lattice mismatch, however, is a great measure for the defect density in the midgap defect band and the corresponding growth temperatures can be calibrated from the  $\Delta c/c(T_G)$  graphic (see Fig. 1). These growth temperatures are given in the top x-axis. The results are compared with the resistivity data as determined by Kaminska and Weber for low growth temperatures [Kam.92]. Regarding the fact that the growth parameters in the 1992 experiments still varied significantly and, therefore, the lattice mismatch also changed up to 25%, the agreement is satisfactory.

The planar resistivity increases rapidly with increasing growth temperature (decreasing lattice mismatch). This is due to the decreasing defect density of midgap As antisites. For growth temperatures around 400°C (with buffer layer growth around 350°C) the as-grown value reaches already  $10^7 \Omega\text{cm}$  and the material is semi-insulating (without containing any As precipitates). The remaining total As antisite concentration drops into the  $10^{18}/\text{cm}^3$  range, still enough to pin the Fermi level at midgap. On the other end of the temperature range the resistivity drops below  $100 \Omega\text{cm}$  at about 220°C. The As antisite concentration reaches the  $10^{20}/\text{cm}^3$  range and hopping conductivity with a simultaneously apparent negligible carrier mobility dominates the electric behavior. The new Hall series did not quite reach this behavior because the effect of the lift-off layer on the  $[\text{As}_{\text{Ga}}]$  was not clear when the MBE growth runs were performed and therefore, the nominal temperatures were chosen too high. However, hopping conduction is already dominant at higher growth temperatures.

The influence of different growth temperatures and different As/Ga flux ratios, specifically on the vertical conductivity, was further investigated. The results are summarized in Figs. 22 and 23. Whereas at low growth temperatures a residual hopping contribution can be observed, the samples grown at higher temperatures show only one activation energy, as is obvious from the linear behavior of the Arrhenius plot in Figure 22. At room temperature, the resistivity is high for all samples, namely above  $10^6 \Omega\text{cm}$ . Note that no As precipitates were detected by TEM in the annealed samples grown at high temperatures. This gives further support for the notion that the high resistivity in undoped, annealed LT-GaAs layers is caused by the residual  $\text{As}_{\text{Ga}}$ , which form deep donor states pinning the Fermi level near midgap.

Different As/Ga flux ratios affect the conductivity only slightly, as can be deduced from the temperature dependence of the vertical conductivity of samples grown at 240°C (Fig. 23). With increasing As/Ga flux ratio an increase of the contribution due to hopping conduction can be observed.

Since the temperature dependence of the mobility is not known for all samples, the activation energies of the band conductivity cannot be evaluated unambiguously. However, for each sample the range of possible values can be determined by assuming two different variations of the mobility with temperature: (a) a  $T^{-3/2}$  dependency due to phonon scattering and (b) a constant mobility, which was found in Hall effect measurements of our samples at high measurement temperatures [Nov.96]. With these assumptions the activation energy e.g. for the sample grown at 240°C is estimated to lie within the range of 0.73 to 0.77 eV, which is indicated by the vertical bar in the inset of Figure 22. These values agree with our previous results of a n-i-n sample containing a semi-insulating LT-GaAs layer grown at 240°C, where an activation energy of 0.77 eV was determined assuming a temperature independent mobility [Fuj.95]. Furthermore, it can be deduced (see inset Fig. 22), that the activation energy is significantly lower for high growth temperatures ( $>300^\circ\text{C}$ ) compared to lower growth temperatures. Similar low activation energies were previously reported by Look et al. [Lo.93a], who found an activation energy of 0.65 eV for as-grown samples deposited in a temperature range of 200°C to 400°C. Upon annealing, no change of the temperature dependence of the conductivity was found. Only at higher growth temperatures one single conduction mechanism, the band conduction, was observed by Look et al. [Lo.93a], which is in agreement with our value.

A variation of the As/Ga flux ratio also influences the band conduction behavior. Whereas at lower As/Ga flux ratios, i.e. at a BEP of 10 and 20, the activation energy is the same, a high As/Ga flux ratio induces a decrease of the activation energy (see inset in Fig.23)

The high activation energies at low growth temperatures of about 0.73 to 0.77 eV and low As/Ga flux ratios are close to that of undoped semi-insulating GaAs, in which EL2 is the dominant deep donor. A decrease of the activation energy for higher growth temperatures can be explained in two ways: a decrease of the acceptor concentration which would change the position of the Fermi level, or a modification of the deep donor level. The existence of a deep donor level 0.65 eV below the conduction band edge, which is associated with As antisites, has been suggested previously [Lo.93b], but this question requires further study.

## 4.2 Breakdown voltage

An important parameter for device application is the maximum electric field that can be applied to a material before irreversible damage occurs. The breakdown voltage of LT-GaAs samples was measured using a vertical n-i-n etched mesa structure, where the insulating layer was the in-situ during the growth of the top n-layer annealed LT-GaAs. To date, only samples with undoped LT-GaAs have been measured, the first measurements of LT-GaAs:Be will be processed and measured similarly.

The values obtained for undoped LT-GaAs are shown in Figure 24. The breakdown voltage shows a marked dependence on the growth conditions. Namely, it decreases as the growth temperature increases. The breakdown field changed from  $3.0 \times 10^5 \text{ V/cm}$  at  $203^\circ\text{C}$  to  $1.7 \times 10^5 \text{ V/cm}$  at  $275^\circ\text{C}$  and dropped below  $1.2 \times 10^5 \text{ V/cm}$  for higher growth temperatures. Repeating the measurement on the same mesa after breakdown resulted in

greatly decreased breakdown voltage. If the first measurement stopped short of the breakdown voltage, almost identical measurements up to the highest voltage of the first test were obtained upon repeating the test.

## 5. LT-GaAs:Be for device applications

MBE-grown LT-GaAs exhibits ultrashort carrier response time (< 1psec), when grown below 230°C, as measured by transient absorption or reflection [Lil.90,Gu.92,Sos.97, Spe.97]. The response times seemed to correlate with the concentration of ionized  $\text{As}_{\text{Ga}}^+$ . In undoped LT-GaAs [ $\text{As}_{\text{Ga}}^+$ ] is mainly determined by the concentration of the native acceptors [ $\text{V}_{\text{Ga}}$ ] (see also chapter 2.5). However, the undoped LT-GaAs is metastable: thermal annealing above 400°C causes lattice relaxation due to As outdiffusion and As precipitate formation. At first, the carrier trapping times are not affected by a thermal treatment because the ionized As antisites are thermally more stable than the neutral  $\text{As}_{\text{Ga}}^0$  [Liu.94]. This fact is astonishing because it requires the thermal stability of the compensating acceptors, the  $\text{V}_{\text{Ga}}$ , in order to keep the concentration of ionized  $\text{As}_{\text{Ga}}$  constant. Additionally, the As precipitates can act as carrier traps in the annealed LT-GaAs layers.

This thermal instability requires the growth of diffusion barrier layers [Lin.90], because the outdiffusion can be detrimental to neighboring layers in device structures. For a device it is therefore desirable to avoid As outdiffusion and develop thermally stable non-stoichiometric material, which contains just enough point defects to exhibit ultrafast carrier response times. Therefore, we studied high p-doping with Be acceptors to achieve a higher ionization fraction of the  $\text{As}_{\text{Ga}}$  and avoid unnecessary amounts of thermally unstable neutral antisites. The Be concentration [Be] in the layers was determined by SIMS, while the [Be] calibration was obtained from Hall measurements of GaAs grown at  $T_G=580^\circ\text{C}$ . Different annealing treatments were carried out: The annealing treatments we refer to in chapter 5.1 and 5.2 were performed in proximity at 600°C or 700°C for 30 minutes each. Additional high annealing treatments were chosen to prove the thermal stability of the Be acceptors in LT-GaAs:Be (SIMS analyses in chapter 5.3). Here a rapid thermal annealing (RTA) at 850°C for 10 seconds was compared with a proximity anneal at 700°C for 60 minutes. The annealing procedures for the first layers to be measured by Hall were performed at the Forschungszentrum Juelich, Germany in As containing quartz ampoules for different time periods (chapter 5.4).

### 5.1 Lattice mismatch and point defect concentration

It was noticed already (chapter 2), that the lattice mismatch in LT-GaAs scales linearly with the amount of neutral As antisites. On the other hand, the incorporation of a high concentration of Be, which is a comparably small atom compared with the Ga host atom, should contract the lattice. Consequently an incorporation of Be into the expanded LT-GaAs lattice will compensate the strain caused by the non-stoichiometry. This effect can be seen in Figure 25 for LT-GaAs:Be, grown at different growth temperatures with varied Be concentrations (BEP ratio 20). Upon Be-doping the (positive) lattice mismatch to the substrate indeed decreases. The lattice mismatch of GaAs:Be grown at a high temperature

(600°C), is shown for comparison. In the Be-doping range around  $7 \times 10^{19}/\text{cm}^3$ ,  $\Delta c/c$  is similar for the samples grown at 250°C and 275°C, while the lattice mismatch of the 240°C series is significantly smaller. The carrier trapping times show a similar behavior (see Table IV).  $\Delta c/c$  becomes negative if the Be concentration is high enough, which is dependent on the growth temperature.

To estimate the effect of strain compensation we calculated the strain on the GaAs lattice as caused in undoped LT-GaAs and high temperature GaAs:Be, assuming that the strains will be additive in LT-GaAs:Be. The  $[\text{As}_{\text{Ga}}^0]$  amounts to  $10^{20}/\text{cm}^3$  in a sample, grown at 200°C. This causes a lattice mismatch of  $\Delta c/c = +0.12\%$ . In contrast, the lattice constant of a Be-doped sample,  $[\text{Be}] = 7 \times 10^{19}/\text{cm}^3$ , grown at  $T_G = 600^\circ\text{C}$  amounts to  $\Delta c/c = -0.032\%$ . Therefore, we would need more than 2.5 times more Be than As antisites to compensate the strain in the LT-GaAs. Following, we describe the microscopical strain of these point defects:

Strain induced by substitutional point defects can be expressed by Vegard's law as follows:

$$\varepsilon = b C \quad (\text{Eq. 1})$$

Here  $\varepsilon = \Delta a/a = \Delta c/c$  for an isotropically expanded or compressed lattice,  $C$  stands for the point defect concentration and the coefficient  $b$  can be derived to ([Ki.96b])

$$b = 1/3 [(r_s/r_H)^3 - 1] N^{-1} \quad (\text{Eq. 2})$$

with  $N$ : number of lattice sites in the observed lattice,  $r_H$ : covalent radius of host atom,  $r_s$ : covalent radius of solute atom.

For the pseudomorphically grown thin layers the tetragonal distorted lattice mismatch has to be corrected by a factor  $p$ , which accounts for the elastic constants of the lattice. The isotropic lattice mismatch  $\Delta a'/a'$  corresponds to the measured  $\Delta c/c$  according to:

$$\Delta c/c = 1/p * \Delta a'/a' = \varepsilon/p \quad (\text{Eq. 3})$$

with  $p(\text{GaAs}_{001}) = c_{11}/[c_{11} + 2 c_{12}] = 0.524$ , using the elastic constant measurements in [Kri.95]. It is worth noting that this calculation for the radius of the solute atom does not consider the concept of volume conservation, but involves the elastic response of the lattice. With  $N = 2.2 \times 10^{22}/\text{cm}^3$  for the number of sites in the Ga-sublattice and  $r_H = 2.45\text{\AA}$ , we calculated the bond lengths of  $\text{As}_{\text{Ga}}\text{-As}$  and  $\text{Be}_{\text{Ga}}\text{-As}$  to

$$r_{\text{As}(\text{Ga})} = 2.75\text{\AA} \quad \text{and} \quad r_{\text{Be}(\text{Ga})} = 2.31\text{\AA}$$

These values are calculated with the assumption that the elastic constants and the thermal expansion coefficients of LT-GaAs are similar to those for GaAs. The difference of the  $\text{As}_{\text{Ga}}\text{-As}$  to the Ga-As bond length amounts to 12%. Landman et al. obtained in recent first principle calculations, the increase in bond length to 9% for the As antisite and to 12% for an As split interstitial [Lan.97], which is in reasonable agreement with our data. Taking the expansive and compressive contributions to the lattice constant into account, we can predict the lattice mismatch for our samples. However, the calculated and measured values differ significantly as can be seen in Figure 25.

The amount of strain compensation upon Be-doping is much higher than calculated, assuming an additive strain of the single point defects. This effect can either be due to the smaller covalent radius of the ionized  $\text{As}_{\text{Ga}}^+$ , when compared to the host atom Ga or due to a considerable amount of complex formation between the  $\text{As}_{\text{Ga}}$  and the  $\text{Be}_{\text{Ga}}$ , which was suggested earlier [Bli.92]. Present results do not yet allow us to distinguish between these alternatives. A complex in the Ga-sublattice is not a new concept. The existence of  $\text{Si}_{\text{Ga}}\text{-V}_{\text{Ga}}$  complexes in Si-doped GaAs was recently directly confirmed by STM observations with accompanying slow positron annihilation [Ge.97b]. The concentration of the  $\text{V}_{\text{Ga}}$  is far too low to play a role in strain compensation of LT-GaAs:Be and eventually present As interstitials are expected to increase the lattice distortion [Lan.97] which is in contradiction to the above described results. Furthermore, it is not likely that other impurities in concentrations able to produce a lattice distortion are incorporated during the MBE growth (see also chapter 2.6), which leaves us with the explanations described above.

Additionally, very high Be concentrations were achieved in As-rich GaAs: while MBE grown GaAs usually showed surface roughening and a decrease in absolute lattice mismatch for  $[\text{Be}] > 10^{20}/\text{cm}^3$ , in LT-GaAs:Be even the highest Be concentration of  $5*10^{20}/\text{cm}^3$  did not have any effect on the surface roughness and a lattice mismatch of -0.25% was measured (see Figure 26). In Figure 27 the change in lattice mismatch upon thermal annealing is shown for LT-GaAs:Be, grown at 250°C. The as-grown  $\Delta c/c$  is positive for LT-GaAs:Be with the lowest [Be]. LT-GaAs:Be is lattice matched for  $[\text{Be}] = 2*10^{19}/\text{cm}^3$ , while for higher Be concentrations  $\Delta c/c$  becomes negative. Upon thermal annealing at 600°C the lattice mismatch in the low-doped layers vanishes as it does in undoped LT-GaAs. The layers with high Be-doping show no change in the lattice mismatch upon thermal annealing. The increase of the annealing temperature to 700°C does not change these results.

The annealing behaviour of low-doped LT-GaAs:Be is similar to that of undoped LT-GaAs (Fig. 27). The neutral antisites  $\text{As}_{\text{Ga}}^0$ , which are responsible for the tetragonal distortion of the LT-layers and therewith for the increase in strain energy of the system, were found before to be more thermally unstable than the ionized antisites  $\text{As}_{\text{Ga}}^+$  [Liu.94] which will increase with increasing Be-doping. The samples with a negative lattice mismatch seem to be even more thermally stable despite the increased strain energy in the layers. This effect will be discussed in more detail in chapter 5.3.

## 5.2 Carrier trapping times

The time resolved reflectivity transients were recorded in a pump-probe laser pulse experiment. The used laser operated at a wavelength of 800 nm, 100 fs short pulses were repeated at a frequency of 100 MHz. The recorded data could be modeled by at most two exponential decays, providing two time constants. The shorter time constant is influenced by the experimental resolution, but may contain as well thermalization effects. Carrier trapping times, given in this section, refer to the longer time constant whenever two

exponential functions were fitted. Carrier trapping times above 0.1 ps can be reliably resolved.

Figure 28 gives the change of the carrier trapping time (CTT) upon Be-doping in as-grown material. According to our initial expectations the carrier trapping time was significantly reduced upon Be-doping. Similar results were obtained for all growth temperatures, although the reduction in carrier trapping time seems to increase with increasing growth temperature. A reduction in CTT of more than one order of magnitude can be achieved with  $7 \times 10^{19}/\text{cm}^3$  Be for  $T_G=275^\circ\text{C}$ , whereas for LT-GaAs, grown at  $T_G=240^\circ\text{C}$ , at least  $3 \times 10^{20}/\text{cm}^3$  Be are required to achieve a similar reduction.

The reduction in carrier trapping time upon increasing growth temperature for a constant Be concentration is shown in figure 29. The decays of the given spectra are similar for  $250^\circ\text{C}$  and  $270^\circ\text{C}$ , but change to shorter response times for the layers grown at  $295^\circ\text{C}$  or  $320^\circ\text{C}$ . Because the Be concentration was kept constant the amount of ionized  $\text{As}_{\text{Ga}}^+$  should be also similar. The results, however, indicate that for  $T_G > 270^\circ\text{C}$  the total  $[\text{As}_{\text{Ga}}]$  dropped below the Be concentration so that some  $\text{As}_{\text{Ga}}$  are already doubly charged.

In Figures 30.a and 30.b the changes in the time-resolved transients upon thermal annealing are shown for two layers grown at  $250^\circ\text{C}$  with different  $[\text{Be}]$ . Overall, only small changes were observed between the transients recorded for as-grown and at  $600^\circ\text{C}$  annealed layers in contrast to the annealing behavior of the lattice mismatch. Upon thermal annealing at  $700^\circ\text{C}$ , however, the carrier trapping times for the low doped LT-GaAs layers - as shown in Fig. 30.a - decreased significantly, including even the lattice matched sample (see also Figure 27). The highly doped LT-layers show ultrafast time response for all annealing conditions (Fig. 30.b).

These results show that a higher annealing temperature is needed to change the carrier trapping time than to eliminate the lattice mismatch. The samples with a negative lattice mismatch seem to be even more thermally stable. Neither  $\Delta c/c$  nor the carrier trapping time change upon annealing despite the increased strain energy in the layers. Interestingly, the high annealing temperature of  $700^\circ\text{C}$  leads to ultrafast trapping times in the low Be-doped layers (Fig.s 30.a+b), although the concentration of  $\text{As}_{\text{Ga}}^+$  seems to decrease [Liu.94,Spe.97]. This can be due either to the formation of a more effective trapping center like  $\text{As}_{\text{Ga}}^{++}$  or due to less interaction with other defects which might increase the effective carrier cross section.

Because we are not aware of any published effective carrier capture cross sections  $\sigma_{\text{eff}}$  for LT-GaAs, we collected data about neutral and ionized antisite concentrations or concentrations of the compensating acceptor,  $\text{V}_{\text{Ga}}$  (Figure 31).  $\text{V}_{\text{Ga}}$  acts as a triple acceptor and, therefore, counts as  $3 \times [\text{V}_{\text{Ga}}]$ , when compared to the ionized antisite concentration [Luy.98]. The corresponding carrier trapping times, already partly published in [Lil.94,Kru96,Spe97], are inversely plotted versus these concentrations to obtain  $\sigma_{\text{eff}}$  according to

$$1/\tau = \langle v_{\text{th}} \rangle * N_T * \sigma_{\text{eff}}$$

with:  $\tau$ : carrier trapping time,  $\langle v_{th} \rangle$ : mean thermal velocity,  $N_T$ : concentration of the deep trapping center (after Shockley-Read-Hall). The mean thermal velocities for electron, light and heavy holes in GaAs at  $T=300K$  are  $1.77 \cdot 10^7 \text{ cm/s}$ ,  $1.76 \cdot 10^7 \text{ cm/s}$  and  $0.68 \cdot 10^7 \text{ cm/s}$ , respectively [Sze.81]. The data are plotted in Figure 31 together with the result from the low-doped LT-GaAs:Be, grown at  $250^\circ\text{C}$ . The presently available trapping frequencies versus the  $[\text{As}_{\text{Ga}}^0]$  are also given because the probability of hole trapping (at neutral antisite defects) is high due to the high  $[\text{As}_{\text{Ga}}^0]$  in LT-GaAs and the similar thermal velocities of electrons and light holes. Results from samples with high Be concentrations are not included, because these layers most likely contain doubly charged  $\text{As}_{\text{Ga}}^{++}$  which will act as an additional carrier trap. In the chosen Be-doped series the concentration of compensating Be is known, because we determined with Hall measurements the amount of electrically active Be, which could be subtracted from the total [Be]. The results obtained from the Hall measurements will be completed and discussed in the next annual report.

The following different possible deep level trapping centers are discussed:

$\text{As}_{\text{Ga}}^+$ : electron trap,  $\text{As}_{\text{Ga}}^{++}$ : electron trap,  $\text{As}_{\text{Ga}}^0$ : hole trap.

Deep level contamination elements (e.g. Cr, O) or extended defects such as As precipitates and dislocations are not present in as-grown LT-GaAs layers in a significant amount and their influence on the carrier trapping time is therefore negligible (see also [Luy.98,Spe97]) as are the hole traps  $V_{\text{Ga}}$  in LT-GaAs because of their comparably low concentration.

An apparent  $\sigma_{\text{eff}}$  was determined for the electron trap  $\text{As}_{\text{Ga}}^+$  in all undoped LT-GaAs layers as:  $\sigma_{\text{eff}}(\text{As}_{\text{Ga}}^+) \approx 4 \cdot 10^{-14} \text{ cm}^2$ . The known neutral antisite concentrations also give a constant  $\sigma_{\text{eff}}$ , which would then be a hole trap with  $\sigma_{\text{eff}}(\text{As}_{\text{Ga}}^0) \approx 4 \cdot 10^{-15} \text{ cm}^2$ , one order of magnitude lower than the value of the electron trap  $\text{As}_{\text{Ga}}^+$ . The Be-doped LT-GaAs and the neutron-irradiated bulk GaAs [Kru96] have a slightly smaller effective carrier capture cross section:  $\sigma_{\text{eff}}(\text{As}_{\text{Ga}}^+) \approx 10^{-14} \text{ cm}^2$  for an electron trap, which is probably due to a different ratio between the neutral and ionized antisite concentrations.  $[\text{As}_{\text{Ga}}^+]/[\text{As}_{\text{Ga}}^0]$  can become as high as 1.7 in LT-GaAs:Be and was determined to be 0.6 - 0.7 in neutron irradiated GaAs. In undoped LT-GaAs, however, this ratio never exceeded 0.1 and usually reaches about 0.05. Regarding these facts, we conclude that in undoped LT-GaAs, both neutral and ionized  $\text{As}_{\text{Ga}}$  can act as carrier capture centers, resulting in a comparable trapping time for both holes and electrons. Therefore, the measured CTT is influenced by both traps according to:

$$1/\tau_{\text{total}} = 1/\tau_1 + 1/\tau_2$$

and the carrier capture cross section for each trap is smaller than the above given value. The  $\sigma_{\text{eff}}$  as obtained in neutron irradiated bulk GaAs and the LT-GaAs:Be layer is probably dominated by electron capture and therefore gives a more accurate estimation of  $\sigma_{\text{electron}}(\text{As}_{\text{Ga}}^+)$ . An extended analysis, including many low Be-doped LT-GaAs layers, might further clarify the carrier trapping behaviour, because in this material the formation of neutral antisites can be suppressed, while extended defects or other deep level point defects are negligible. However, the formation of doubly charged antisites might occur if the Be-doping is too high for the given growth temperature (and therewith the initial  $[\text{As}_{\text{Ga}}]$ ).

Because of the high ionization rate of the  $\text{As}_{\text{Ga}}$  we conclude that the  $\sigma_{\text{eff}}$ , as calculated from the neutron-irradiated bulk GaAs and the Be-doped LT-GaAs data, is close to the value of the  $\sigma_{\text{electron}}$  ( $\text{As}_{\text{Ga}}^+$ ). Then the  $\sigma_{\text{eff}}$  for the neutral  $\text{As}_{\text{Ga}}^0$  must be corrected for the undoped LT-GaAs. The resulting carrier capture cross sections, calculated according to the above equations, are:

$$\text{electron capture: } \sigma_{\text{electron}}(\text{As}_{\text{Ga}}^+) = (1.5 \pm 0.7) * 10^{-14}/\text{cm}^2$$

$$\text{hole capture: } \sigma_{\text{hole}}(\text{As}_{\text{Ga}}^0) = (4 \pm 2) * 10^{-15}/\text{cm}^2$$

The given error for  $\sigma_{\text{hole}}$  includes the different thermal velocities for light and heavy holes. The estimated hole capture cross section corresponds very well with the results obtained by DLTS [Zai.92]. Zaidi et al. determined  $\sigma_{\text{eff}}$  to  $5 * 10^{-15}/\text{cm}^2$  and attributed this to a hole capture. Plastically deformed GaAs and annealed LT-GaAs contain dislocations and As precipitates, respectively, which may also act as carrier traps. Therefore, the determination of  $\sigma_{\text{eff}}$  in plastically deformed GaAs [Oes.94] and the hypothesis of different carrier traps present in annealed LT-GaAs [Sos.97] account for different traps and cannot be compared with this analysis. It is therefore not surprising that Sosnowski et al. [Sos.97] could not correlate their results, determined in annealed LT-GaAs, to the as-grown material. The electron capture cross section determined by Mitonneau et al. [Mit.79] is orders of magnitude lower than  $\sigma_{\text{eff}}$ , obtained from the neutron irradiated bulk GaAs and the LT-GaAs:Be. Because in [Mit.79] the influence of the prominent deep level impurity Cr is still a matter for debate (see, e.g., [Zai.92, Kru.96]), this additional trap might account for a part of the large difference. On the other hand a field enhancement of the capture cross section cannot be excluded from our measurement, which might also lead to an increased  $\sigma_{\text{eff}}$ . Summarized, our estimation shows that the double donor  $\text{As}_{\text{Ga}}$  can act in both neutral and single positively charged state as a recombination center for holes and electrons, respectively.

The pump-probe pulse technique will then, dependent on the amount of excited carriers for each pump and probe pulse, lead to an indirect exchange of charge between the  $\text{As}_{\text{Ga}}^0$  and  $\text{As}_{\text{Ga}}^+$ . This continuous change in carrier capture center concentrations for electrons and holes can result in long time responses, during which these defects remain in an excited state. The trapped carriers can be re-excited and trapped again, before the onset of recombination processes occurs. Long "total relaxation" times up to some hundred picoseconds after a pump-probe pulse experiment were reported recently [Sie.96, Gre.97]. Although trapped electron and hole recombination times were found to be around 10ps [Gre.97], the LT-GaAs layer remained in an excited state for a period of time at least one order of magnitude longer, which might be described as a multiple conversion of a  $\text{As}_{\text{Ga}}^0$  into a  $\text{As}_{\text{Ga}}^+$  and vice versa upon each applied pulse.

The annealing behaviour of the carrier trapping time in low-doped LT-GaAs:Be can be now described as an initial decrease of neutral antisites  $\text{As}_{\text{Ga}}^0$ , which do not influence the CTT because of the dominant electron trapping at  $\text{As}_{\text{Ga}}^+$ . The ionized antisites cannot decrease initially upon thermal annealing because the Be acceptors are stable, as confirmed in SIMS analysis (see chapt. 5.3). The decrease in CTT occurs if the  $[\text{As}_{\text{Ga}}]$  becomes smaller than the  $[\text{Be}]$  and some of the  $\text{As}_{\text{Ga}}^+$  become doubly charged. This also explains why the high-doped LT-GaAs:Be does not show any difference in CTT upon thermal

annealing, because in these layers  $\text{As}_{\text{Ga}}^{++}$  are probably already present in the as-grown layers. This hypothesis includes the assumption that  $\text{As}_{\text{Ga}}^{++}$  is a more effective electron trap than the singly charged  $\text{As}_{\text{Ga}}^+$  (cf. [Spe.97]). Furthermore, the  $\text{As}_{\text{Ga}}^{++}$ , which are the assumed dominant carrier capture centers in high-doped LT-GaAs:Be, are stable even after an annealing step of 30 minutes at 700°C.

### 5.3 Diffusion / Thermal stability

The thermal stability of LT-GaAs:Be depends strongly on the chosen growth parameters which are the growth temperature, the BEP ratio and the Be concentration. The first two parameters determine the “initial”  $\text{As}_{\text{Ga}}$  concentration while the [Be] further increases this concentration and changes the fraction of ionization. Both effects are demonstrated in Figure 32 for LT-GaAs:Be layers grown at 240°C and 275°C. The graphic shows the neutral and singly charged antisite concentrations for undoped (red) and Be-doped (green) LT-GaAs with a  $[\text{Be}] = 7 \times 10^{19}/\text{cm}^3$  (as-grown: full columns, annealed: textured columns). We chose the annealing procedure according to the known conditions which will fully eliminate the lattice mismatch in undoped LT-GaAs (600°C, 30 minutes, in-situ MBE in  $\text{As}_4$  flux).

The  $\text{As}_{\text{Ga}}$  concentrations in both charged states drop below the detection limit, when the Be concentration exceeds  $10^{20}/\text{cm}^3$  (for  $T_G=240^\circ\text{C}$ ). We assume that the  $\text{As}_{\text{Ga}}$  in these cases are still present and therefore doubly charged, and a large part of the Be concentration will be electrically active. At present we cannot access the  $[\text{As}_{\text{Ga}}^{++}]$ . Therefore, we cannot determine or even estimate the  $[\text{As}_{\text{Ga}}^{++}]$  from the [Be] and in Fig. 32 the total amount of  $\text{As}_{\text{Ga}}$  consists of  $[\text{As}_{\text{Ga}}^0]$  and  $[\text{As}_{\text{Ga}}^+]$  only. We observed a steep increase in the antisite concentration upon Be-doping in both the ionized  $[\text{As}_{\text{Ga}}^+]$  and the total  $[\text{As}_{\text{Ga}}]$ . The total antisite concentration in the LT-GaAs:Be, grown at 240°C, equals the concentration in LT-GaAs, grown at 200°C and is more than twice as large as in undoped material, grown at the same temperature.

The fraction of  $[\text{As}_{\text{Ga}}^+]/[\text{As}_{\text{Ga}}]$  increases from about 5% in undoped layers to more than 50% in the Be-doped layers. Under different conditions it can naturally reach 100%. However, an unexpected reduction in ionization occurs in the sample grown at 275°C, compared to the LT-GaAs:Be grown at 240°C. Because the Be concentration remains constant, this reduction can be only described if further donors and/or electrically active Be are present (p-type conductivity). Because of the lack of chemical donors (see chapter 2.6) we propose that part of the As antisites are already doubly charged which does not exclude that some Be acceptors might be also electrically active. However, this has to be due to a localized bending of the conduction and/or valence band because we simultaneously observe neutral antisites  $\text{As}_{\text{Ga}}^0$ . In the sample, grown at 275°C, both (measurable) antisite concentrations remained constant upon thermal annealing, while in the sample, grown at 240°C, the antisite concentrations were reduced, but still well above the detection limit [Spe.97].

The thermal stabilization of the  $\text{As}_{\text{Ga}}$ , as was demonstrated in Fig. 32, might be caused by complex formation with the Be acceptor [13] and/or an ineffective ratio between the

$[As_{Ga}]$  and the comparably low concentration of the  $V_{Ga}$ , which are assumed to promote the As diffusion: whereas in undoped LT-GaAs  $[V_{Ga}] / [As_{Ga}] \approx 2\%$ , this ratio is reduced to 0.1% and 0.2% in LT-GaAs:Be, grown at  $T_G=240^\circ C$  and  $T_G=275^\circ C$ , respectively. The strain compensation between the  $Be_{Ga}$  and the  $As_{Ga}$  atoms might have also enhanced the incorporation of  $As_{Ga}$  as was found in the increase of total  $[As_{Ga}]$ . Of course, the change of the Fermi level is known to increase the incorporation rate of several elements. At present we cannot determine which mechanism is dominant. Further studies including the introduction of different dopants are necessary to evaluate the different models for the increased excess As in LT-GaAs:Be. One topic which will be addressed is the question how well the concepts made for thermal equilibrium (e.g. the change of the Fermi level) still fit for the low temperature growth.

The thermal stability of the Be was investigated by SIMS depth profiles. Therefore, a sandwich structure with LT-GaAs:Be embedded into two GaAs:Si layers was grown. During the growth of the top n-GaAs layer the LT-layer was in-situ annealed at  $600^\circ C$  for about 30 minutes. This structure was post-annealed at  $700^\circ C$  for 60 minutes or at  $850^\circ C$  for 10 seconds (RTA). The SIMS profiles of the Be and the Si concentrations were measured by Charles Evans & Associates. The results are shown in Figures 33.a, b & c.

The as-grown profile (Fig. 33a) shows the high Be concentration ( $\approx 5 \cdot 10^{18}/cm^3$ ) in the LT-layer which was grown at  $295^\circ C$  (BEP=20). On both sides of the LT-layer the low Si-doped barrier layers are visible ( $[Si] \approx 2 \cdot 10^{16}/cm^3$ ). A steep increase of the Si concentration appears at the interface to the substrate ( $n^+ \text{-GaAs}$ ). The in-situ annealing of the LT-GaAs:Be might have led to a segregation of Be at the substrate interface where a small Be peak appeared. However, these peaks can also occur as an artifact at interfaces if the uniformity of the sputtering during the SIMS analysis changes. The increase of both Si and Be concentrations at the surface of the sample is most likely artificial.

Upon RTA at  $850^\circ C$  (Fig. 33b) the Si and Be profiles remain almost constant, just a slight increase of the Be segregation peak at the substrate interface occurs. This is an indication for a real segregation of Be at the substrate, which can be confirmed with electrochemical capacitance voltage measurements (ECV). Also Si from the n-GaAs barriers seem to diffuse to the interfaces of the LT-GaAs:Be layer. Upon annealing at  $700^\circ C$  for 60 minutes (Fig. 33c) the Si diffuses out of the substrate and an unusually broad Si peak appears at the sample surface. Be, however, mainly remains in the LT-GaAs:Be layer, the LT-interface close to the surface is slightly broadened and also a small peak occurs at the surface. The main diffusion effects are supposed to be due to the high Si concentration of the substrate and the thermal instabilities of the Si rather than those of Be.

These first results on the thermal stability are very promising. A similar LT-GaAs:Be layer was determined to still exhibit a carrier trapping time below 1ps which allows to further decrease the Be concentration (and probably increase the growth temperature) by still matching the requirements for a first application of LT-GaAs:Be in a radiation hardened HIGFET structure [Abr.93]. Further investigations of the diffusion profiles will follow including ECV measurements to determine eventual compensation effects at the interfaces.

Also detailed investigations of the  $V_{Ga}$  concentrations in LT-GaAs:Be are ongoing. The first results of  $[V_{Ga}]$  are shown in Figure 15. The data show that single vacancies are present in the as-grown layers and not in annealed LT-GaAs:Be although the changes are less drastic than in undoped LT-GaAs. At present we have not enough data to correlate the  $V_{Ga}$  concentration with the growth parameters. Furthermore, the change in the Fermi level due to the Be-doping leads to difficulties in the determination of  $[V_{Ga}]$  because with the dropping Fermi level the acceptors change their charge which also influences the positron lifetime.

#### 5.4 Electrical transport measurements

During the last years, several groups investigated the electrical activity of dopants, incorporated into LT-GaAs. Be-doping was reported in Refs. [Bli.92,Ati.95,Mis.96]. All authors report hopping conductivity of the as-grown samples due to the  $As_{Ga}$  point defect band in the band gap. With increasing annealing temperature the resistivity of the LT-GaAs:Be increases [Bli.92], but then rapidly drops above 700°C [Ati.95]. Slight differences were observed, dependent on the Be concentration and / or the growth temperature, but the general trends are similar. Our first studies, carried out in collaboration with M. Luysberg's group in Jülich, Germany, were focused on the BEP dependence and annealing behavior of heavily Be doped LT-GaAs.

For this purpose four LT-GaAs:Be layers were grown on an AlAs buffer layer at 190°C and BEP ratios of 10, 20, 23 and 40 with  $[Be] = 10^{20} \text{ cm}^{-3}$ . The layers, grown with the two highest BEP ratios exceeded the transition to partly relaxed growth by introducing stacking faults (see chapter 2.2), which will influence the results of the Hall measurements. Therefore, we studied the electrical properties for the two low BEP ratios only. For these measurements a standard Hall system in Van der Pauw geometry was used. The annealing was performed for 20 minutes in quartz ampoules containing As, except at 600°C, where different time periods were chosen. Figure 34 shows the resistivity of these samples for the different annealing temperatures and time periods. The highest resistivity was always observed after annealing at 600°C for 20 minutes. The resistivity then decreased with increasing annealing time (for 600°C) and with higher annealing temperatures. The corresponding carrier concentration approached the initially incorporated Be concentration for annealing temperatures above 700°C.

The highest Be-doped LT-GaAs from [Ati.95] is shown for comparison ( $T_G=250^\circ\text{C}$ ,  $BEP=20$ ,  $[Be]=5*10^{19} \text{ cm}^{-3}$ ). The annealing temperature dependence is similar, if the position of the maximal resistivity is not considered. The carrier concentration reached the Be-doping concentration for the highest annealing temperature (900°C). The evaluation of the maximum shows the trend towards higher resistivity by incorporating a lower  $As_{Ga}$  concentration (lower BEP ratio). It is likely that a lower  $As_{Ga}$  /  $Be_{Ga}$  ratio further increases and thermally stabilizes the resistivity. A detailed investigation on the resistivity of various LT-GaAs:Be layers will be performed in the following AFOSR contract. The annealing procedures (RTA in [Ati.95] versus ampoule annealing in this study) are not quite comparable because of the large difference in annealing time of the two methods (30 seconds versus 20 minutes). It is worth noting that the studied material is still far off the

thermally stabilized conditions for LT-GaAs:Be. The  $[As_{Ga}]$  is much higher than the  $[Be]$ , even in the case of the material grown at 250°C with  $[Be]=5*10^{19} cm^{-3}$  (red triangles in Fig. 15, [ati.95]).

In conclusion, we are at present investigating the electrical properties of thermally stabilized material in detail. Especially in the case of  $[As_{Ga}] / [Be_{Ga}]$  ratio approaching 1.0 (see chapter 3.1), this special material seems to exhibit unique resistivity and annealing behavior. In our future work we will continue Hall measurements of the thermally stabilized LT-GaAs:Be. To gain insulating behavior, we will further reduce the  $[As_{Ga}]$  by increasing the growth temperature and decreasing the  $[Be]$ . It is our goal to maximally ionize the As antisites while retaining - or even improving - the thermal stability in a less As-rich material and finally achieve insulating material with ultrafast carrier trapping time.

## 6. Related work in cooperation with other groups

We collaborate with several groups in the LT-GaAs research project. Because of the varied requirements of investigations in the LT-GaAs:Be topic we recently started new collaborations or renewed longstanding connections to other groups. Issues like diffusion mechanisms, the general aspects of LT-growth (e.g. for the use in GaN growth research), the probability of complex formation or the applicability of LT-GaAs:Be changed the priorities in our research projects. This is reflected in the increased number of collaborations. We did not list groups that we just provide with MBE grown LT-GaAs layers for their research projects which is also increasing.

### I. Existing cooperations:

Dr. Liliental-Weber, LBNL Berkeley	TEM
Dr. Kisielowski, NCEM, LBNL Berkeley	<i>LT growth mechanisms, HREM</i>
Prof. Bokor, EECS Berkeley	<i>time-resolved reflectivity transients</i>
Dr. Luysberg, FZ Jülich, Germany	TEM & SIMS
Prof. Krause-Rehberg, Universität Halle, Germany	<i>slow positron annihilation</i>
Prof. Weatherford, NPS Monterey	<i>Be-doped LT-GaAs in HIGFET's</i>
Prof. Keller, ETH Zürich, Switzerland	<i>applications in laser technology</i>
Prof. Venkat, UNLV, Las Vegas	<i>MBE growth simulation</i>

### II. Recently established new collaborations:

Prof. Morgan, WS University, Detroit	<i>Defect complex simulations in LT-GaAs:Be</i>
Prof. Whitaker, University of Michigan	<i>Be-doped LT-GaAs in THz - photomixers</i>
Dr. Hollis, MIT Lincoln Lab., Boston	<i>Be-doped LT-GaAs in MISFET's</i>
Dr. Liu, QED, Bethlehem, PA	<i>C-doped LT-GaAs, p-doped LT-InP (in preparation)</i>

## 7. Summary and Future work

The work performed within the last year has resulted in several new and exciting research directions. The lattice expansion of samples deposited with precise substrate temperature and in-situ As/Ga flux ratio control can be used as standards in systems that lack the direct determination of substrate temperature, a problem that has plagued research and

application of nonstoichiometric GaAs from its very beginning. The results of our study of the lowest growth temperatures show similarities to the GaN MBE-growth. The well controlled As-rich GaAs serves as a model substance for low temperature growth mechanisms, which is a fundamental issue in the research of the III-nitrides [Ki.98].

In addition we have established the reduction in temporal response in LT-GaAs due to Be-doping. For the LT-GaAs:Be, grown at 275°C, almost two orders of magnitude were gained in carrier trapping time for appropriate Be concentrations. It is evident that the ionized  $\text{As}_{\text{Ga}}^+$  are not the only trapping centers in these materials and we expect  $\text{As}_{\text{Ga}}^{++}$  to be present and even more efficient in carrier trapping than the  $\text{As}_{\text{Ga}}^+$ . LT-GaAs:Be is far more thermally stable than undoped LT-GaAs with comparable growth parameters, in terms of retaining subpicosecond time response. Lattice matched As-rich GaAs can be grown and - by choosing appropriate growth parameters - can exhibit ultrafast time response due to a balanced  $[\text{As}_{\text{Ga}}]$  and  $[\text{Be}_{\text{Ga}}]$ . Ultrafast LT-GaAs:Be can be grown at higher growth temperatures than ever obtained before (around 300°C), where the growth parameters are easier to control. We deduce from the strain compensation behaviour and the increase in thermal stability that a localization or even a complex formation between the  $\text{As}_{\text{Ga}}$  and the  $\text{Be}_{\text{Ga}}$  is likely to occur. First electrical measurements reveal similarities to literature studies, however, systematic studies of the resistivity of LT-GaAs:Be, dependent on BEP ratio and growth temperature, are ongoing.

The carrier capture cross section analysis for undoped and low Be-doped LT-GaAs reveals a dominant electron trapping for As-rich GaAs with high  $\text{As}_{\text{Ga}}$  ionization fraction as also found in neutron irradiated bulk GaAs. In as-grown and undoped LT-GaAs a simultaneous electron and hole trapping at  $\text{As}_{\text{Ga}}^+$  and  $\text{As}_{\text{Ga}}^0$ , respectively, are expected. The calculated carrier capture cross sections give a slightly higher value for the electron capture than for the hole capture, which can be easily compensated in LT-GaAs by the extreme high concentrations of neutral As antisites. The actual carrier trapping and recombination processes after a pump-probe pulsing, however, can become very complex because of the interdependence between the electron and hole traps.

With this new development towards thermal stability, the As-rich GaAs offers further application prospects in devices, which require thermal stability in addition to ultrafast carrier trapping time. This new material might make the incorporation of diffusion barriers (to avoid detrimental effects from As outdiffusion) obsolete. Tailoring the response of this material upon annealing at higher temperatures than 600°C is one of our next steps in this research field. In chapter 5.3 the first results are already shown. Electrochemical Capacitance Voltage measurements to determine eventual outdiffusion of vacancies will soon follow. We are currently working on the first application for thermally stabilized LT-GaAs:Be which is its radiation hardening effect on a HIGFET structure as used in satellite technology [Abr.93]. This radiation hardening effect due to ultrafast carrier capture was predicted by Weatherford et al. [Wea.95].

Our future work will contain two major points: First the applicability of LT-GaAs in THz-technology and as insulation layer which we will try to extend with different dopants. Our hope is to gain significant knowledge about the physical background of the previously described thermal stability mechanisms in LT-GaAs:Be. Simultaneous to the investigation

of different dopants in LT-GaAs we will concentrate on the electrical properties such as semi-insulating behavior or breakdown voltage. Our goal is to control the properties of the non-stoichiometric GaAs even better and design LT-layers which meet the requirements of different industrial needs. Secondly, the fundamental research of LT-growth mechanisms which is of major interest for the III-nitrides but also for the epitaxial growth of ceramics will be studied. The above described investigations will give us the opportunity to monitor the interdependence of dopants and non-stoichiometry. Also we can simulate the growth on strained buffer layers by using AlGaAs barrier layers which we anyway need for lift-off or as optical mirrors in time-resolved absorption measurements. LT-GaAs with a ten years research knowledge background developed into a useful model substance for new material systems which are by far more complicated and difficult to produce.

## 8. Personnel

### Eicke R. Weber, P.I.

Joachim Krueger, postdoctoral scholar	(1995)
Hiroshi Fujioka, visiting scholar	(1995)
Xiao Liu, postdoctoral scholar	(1995)
Hyunchul Sohn, postdoctoral scholar	(1995 / 1996)
Arti Prasad, Ph.D. in 1996	(1995 / 1996)
Ralf Klockenbrink, DAAD fellow	(1996)
Martina Luysberg, Humboldt fellow	(1996 / 1997)
Petra Specht, postdoctoral scholar	(1996 / 1997)
Ri'an Zhao, graduate student	(1997)
Robert C. Lutz, graduate student	(1997)
Klaus Thul, visiting student	(1997)
Michael G. Cich, graduate student	(1997)

## 9. References

[Abr.93] J.K. Abrokwa, J.H. Huang, W. Ooms, C. Shurboff, J.A. Hallmark, R. Lucero, J. Gilbert, B. Bernhardt, G. Hansell, IEEE GaAs IC Symposium Technical Digest, 1993, p. 127

[Ati.95] N. Atique, E.S. Harmon, J.C.P. Chang, J.M. Woodall, M.R. Melloch, N. Otsuka, *J. Appl. Phys.* **77**, 1471 (1995)

[Bli.92] D.E. Bliss, W. Walukiewicz, K.T. Chan, J.W. Ager III, S. Tanigawa, E.E. Haller, *Mat. Res. Soc. Symp. Proc.* **241**, 93 (1992)

[Cu.78] J. A. Del Cueto and N.J. Shevlik, *J. Phys C*, **11**, 829 (1978)

[Dre.93] P. Dreszer, W.M. Chen, K. Seendripu, J.A. Wolk, W. Walukiewicz, B.W. Liang, C.W. Tu, E.R. Weber, *Phys. Rev. B* **47**, 4111 (1993)

[Eag.95] D.J. Eaglesham, *J. Appl. Phys.* **77**, 3597 (1995)

[Fu.88] S. Fujita, K. Maeda, S. Hyodo, *Phys. Stat. Sol.* **109** (1988) 383

[Fuj.95] H. Fujioka, E.R. Weber, A. K. Verma, *Appl. Phys. Lett.*, **66**, 2834 (1995)

[Ge.97a] J. Gebauer, R. Krause-Rehberg, S. Eichler, M. Luysberg, H. Sohn, E.R. Weber, *Appl. Phys. Lett.* **71**, 638 (1997)

[Ge.97b] J. Gebauer, R. Krause-Rehberg, C. Domke, Ph. Ebert, K. Urban, *Phys. Rev. Lett.* **78**, 3334 (1997)

[Gre.97] P. Grenier, J.F. Whitaker, *Appl. Phys. Lett.* **70**, 1998(1997)

[Gu.92] S. Gupta, J.F. Whitaker, G.A. Mourou, *IEEE Journal of Quantum Electronics* **28**, 2464 (1992)

[Joh.94] S.R. Johnson, C. Lavoie, E. Nodwell, M.K. Nissen, T. Tiedje, J.A. MacKenzie, *J. Vac. Sci. Technol.* **B12**, 1225 (1994)

[Kam.92] M. Kaminska, E.R. Weber, *Mat. Sci. Forum* **83-87**, 1033 (1992)

[Ki.96a] C. Kisielowski, A.R. Calawa, Z. Liliental-Weber, *J. Appl. Phys.* **80**, 156 (1996)

[Ki.96b] C. Kisielowski, J. Krueger, S. Ruvimov, T. Suski, J.W. Ager III, E. Jones, Z. Liliental-Weber, M. Rubin, E.R. Weber, M.D. Bremser, R.F. Davis, *Phys. Rev. B* **54**, 17745 (1996)

[Ki.98] C. Kisielowski, in: "Gallium Nitride", J.I. Pankove & T.D. Moustakas eds., Academic Press, (1998) in press

[Kri.95] M. Krieger, H. Sigg, N. Herres, K. Bachem, K. Kähler, *Appl. Phys. Lett.* **66**, 682 (1995)

[Kru.96] J. Krueger, Y.C. Shih, L. Xiao, C.L. Wang, J.D. Morse, M. Rogalla, K. Runge, E.R. Weber, Proc. of the IEEE SIMC-9, Toulouse 1996, p. 345

[Lag.94] M Lagadas, Z. Hatzopoulos, M. Calamiotou, M. Kayiambaki, and A. Christou, *Mat. Res. Soc. Symp. Proc.*, **325**, 383 (1994)

[Lan.97] J.I. Landman, C.G. Morgan, J.T. Schick, P. Papoulias, A. Kumar, *Phys. Rev. B* **55**, 15581 (1997)

[Lil.90] Z. Liliental-Weber, *Mat. Res. Soc. Symp. Proc.* **198**, 371 (1990)

[Lil.91] Z. Liliental-Weber, W. Swider, K.M. Yu, J. Kortright, F.W. Smith, A.R. Calawa, *Appl. Phys. Lett.* **58**, 2153 (1991)

[Lil.92] Z. Liliental-Weber, *MRS Symp. Proc.* **241**, 101 (1992)

[Lil.94] Z. Liliental-Weber, J. Ager III, D. Look, X.W. Lin, X. Liu, J. Nishio, K. Nichols, W. Schaff, W. Swider, K. Wang, J. Washburn, E.R. Weber, J.

Whitaker, in: "Proc. of the 8<sup>th</sup> Conf. on Semiinsulating III-V Materials", ed. M. Godlewski (World Scientific, 1994) p.305

[Lin.90] B.J.-F. Lin, C.P. Kocot, D.E. Mars, R. Jaeger, IEEE ED37, 46 (1990)

[Liu.94] X. Liu, A. Prasad, W.M. Chen, A. Kurpiewski, A. Stoschek, Z. Liliental-Weber, E.R. Weber, Appl. Phys. Lett. **65**, 3002 (1994)

[Liu.95] X. Liu, A. Prasad, J. Nishio, E.R. Weber, Z. Liliental-Weber, W. Walukiewicz, Appl. Phys. Lett. **67**, 279 (1995)

[Lo.91] D.C. Look, J. Appl. Phys. **70**, 3148 (1991)

[Lo.93a] D. C. Look, G. D. Robinson, J. R. Sizelove, and C. E. Stutz, J. Electron. Mat., **22**, 1425 (1993)

[Lo.93b] D. C. Look, Z.-Q. Fang, J. R. Sizelove, and C. E. Stutz, Phys. Rev. Lett., **70**, 465, (1993)

[Luy.98] M. Luysberg, H. Sohn, A. Prasad, P. Specht, Z. Liliental-Weber, E.R. Weber, J. Appl. Phys. **83**, 561 (1998)

[Mat.74] J.W. Matthews, A.E. Blakeslee, J. Cryst. Growth **27**, 118 (1974)

[Mel.90] M.R. Melloch, N. Otsuka, J.M. Woodall, A.C. Warren, J.L. Freeouf, Appl. Phys. Lett. **57**, 1531 (1990)

[Mer.63] J. H. van der Merwe, J. Appl. Phys. **34**, 117, 123 (1963)

[Mis.94] M. Missous and S. O'Hagen, J. Appl. Phys., **75**, 3396 (1994)

[Mis.96] M. Missous, Microelectronics J. **27**, 393 (1996)

[Mit.79] A. Mitonneau, A. Mircea, G.M. Martin, D. Pons, Rev. Phys. Appl. **14**, 853 (1979)

[Mut.97] S. Muthuvenkatraman, S. Gorantla, R. Venkat, D.L. Dorsey, submitted to J. Appl. Phys., 1997

[Nov.96] J. Novak, J. Betko, L. Lubomir, P. Kordos, private communications

[Oes.94] M. Oestreich, W.W. Ruehle, J. Krueger, H. Alexander, J. of Luminescence **58**, 123 (1994)

[Peo.86] R. People, J. C. Bean, Appl. Phys. Lett. **49**, 28 (1986)

[Pra.95] A. Prasad, X. Liu, H. Fujioka, N.D. Jaeger, J. Nishio, and E.R. Weber, in: Defects in Semiconductors 18, edited by S. Sumino (Trans Tech Zürich 1995), Materials Science Forum, vol. 196-201, p.189

[Pra.98] A. Prasad, P. Stallinga, X. Liu, E.R. Weber, to be published in Phys. Rev. B (1998)

[Sie.96] U. Siegner, R. Fluck, G. Zhang, U. Keller, Appl. Phys. Lett. **69**, 2566 (1996)

[Smi.88] F. Smith, A. Calawa, Appl. Phys. Lett. **42**, 818 (1988)

[Sos.97] T.S. Sosnowski, T.B. Norris, H.H. Wang, P. Grenier, J.F. Whitaker, C. Y. Sung, Appl. Phys. Lett. **70**, 3245 (1997)

[Spe.96] "Deformation and fracture in stoichiometric FeAl- and NiAl single crystals", P. Specht, Ph.D. thesis, Aachen 1996 (in german)

[Spe.97] P. Specht, S. Jeong, H. Sohn, M. Luysberg, A. Prasad, J. Gebauer, R. Krause-Rehberg, E.R. Weber, in: Proc. of the Int. Conf. on Defects in Semiconductors ICDS 19, Aveiro, Portugal, Mater. Sci. Forum **258-263**, 951 (1997)

[Sze.81] Electron & hole masses were taken from S.M. Sze: *Physics of Semiconductor Devices*, 2<sup>nd</sup> edition, John Wiley & Sons, Inc., New York, 1981, Appendix H

- [Ver.96] A.K. Verma, J. Tu, J.S. Smith, H. Fujioka, E.R. Weber, *Appl. Phys. Lett.* **68**, 699 (1996)
- [Wal.96] W. Walukiewicz, Z. Liliental-Weber, J. Jasinski, M. Almonte, E. E. Haller, A. Prasad, E. R. Weber, K. Wang, and J. Whitaker, *Appl. Phys. Lett.* **69**, 2569 (1996)
- [Wan.96] H.-H. Wang, P. Grenier, J.F. Whitaker, H. Fujioka, J. Jasinski, Z. Liliental-Weber, *IEEE J. Select. Top. Quantum Electronics* **2**, 630 (1996)
- [Wea.95] T.R. Weatherford, D. McMorrow, A.B. Campbell, W.R. Curtice, *Appl. Phys. Lett.* **67**, 703 (1995)
- [Web.82] E.R. Weber, H. Ennen, U. Kaufmann, J. Windscheif, J. Schneider, T. Wosinski, *J. Appl. Phys.* **53**, 6140 (1982)
- [Wei.91] M.K. Weilmeier, K.M. Colbow, T. Tiedje, T. van Burren, L. Xu, *Can. J. Phys.* **69**, 422 (1991)
- [Wie.90] C.R. Wie, K. Xie, D.C. Look, K.R. Evans, C.E. Stutz, in "Proc. of Semi-Insulating III-V Materials", eds. A. Milnes & C.J. Miner (Hilger, Bristol, 1990) p.71
- [Yas.88] K. Yasutake, Y. Konishi, K. Adachi, K. Yoshi, M. Umeno, H. Kawabe, *Jap. J. of Appl. Phys.* **27** (1988) 2238
- [Yu.92] K.M. Yu, M. Kaminska, Z. Liliental-Weber, *J. Appl. Phys.* **72**, 1850 (1992)
- [Zai.92] M.A. Zaidi, H. Maaref, J.C. Bourgoin, *Appl. Phys. Lett.* **61**, 2452 (1992)

## 10. Publications

*Annealing dynamics of arsenic-rich GaAs formed by ion-implantation,*  
 H. Fujioka, J. Krueger, A. Prasad, X. Liu, E.R. Weber, A.K. Verma, *J. Appl. Phys.* **78**, 1470 (1995)

*Native point defects in low-temperature-grown GaAs,*  
 X. Liu, A. Prasad, J. Nishio, E.R. Weber, Z. Liliental-Weber, W. Walukiewicz, *Appl. Phys. Lett.* **67**, 279 (1995)

*Magnetic circular dichroism of low-temperature-grown  $Al_xGa_{1-x}As$ ,*  
 A. Prasad, X. Liu, P. Stallinga, E.R. Weber, *MRS Symp. Proc.* **378**, 207 (1995)

*Conduction Mechanism in Arsenic Implanted GaAs,*  
 H. Fujioka, E.R. Weber, A.K. Verma, *Appl. Phys. Lett.* **66**, 2116 (1995)

*Transient Current Study of Low-Temperature Grown GaAs Using an n-i-n Structure,*  
 H. Fujioka, E.R. Weber, A.K. Verma, *Appl. Phys. Lett.* **66**, 2834 (1995)

*Characterization of Low-Temperature AlGaAs Lattice Properties Using High Resolution X-Ray Diffraction,*  
 A.K. Verma, J.S. Smith, H. Fujioka, E.R. Weber, *J. Appl. Phys.* **77**, 4452 (1995)

*Synthesis of Semi-insulating GaAs by As Implantation and Thermal Annealing: Structural and Electrical Properties,*  
 A. Claverie, H. Fujioka, L. Laanab, Z. Liliental-Weber, E.R. Weber, *Nuclear Physics Methods in Materials Research* **B96**, 327 (1995)

*The Role of Point Defects in Non-Stoichiometric III-V Compounds,*  
 A. Prasad, X. Liu, H. Fujioka, N.D. Jaeger, J. Nishio, E.R. Weber, in: *Defects in Semiconductors* **18**, Ed.: S. Sumino, *Trans. Tech. Zuerich, Mater. Sci. Forum* **196-201** (1995) p.189

*Electrical Characterization of Low-Temperature  $Al_{0.3}Ga_{0.7}As$  Using n-i-n Structures,*  
 A.K. Verma, J. Tu, J.S. Smith, H. Fujioka, E.R. Weber, *Appl. Phys. Lett.* **68**, 699 (1996)

*Quantitative HRTEM: a Step Towards Application Oriented Basic Research,*  
 C. Kisielowski, Z. Liliental-Weber, and E. R. Weber, *Brazilian Journal of Physics* **26**, 83 (1996)

*Control of stoichiometry dependent defects in low temperature GaAs,*  
 M. Luysberg, H. Sohn, A. Prasad, H. Fujioka, R. Klockenbrink, E.R. Weber, in: *Semiconducting and Insulating Materials 1996*, Ed.: C. Fontaine, *IEEE* (1996), p.21

*High resistivity and ultrafast carrier lifetime in argon implanted GaAs,*  
 W. Walukiewicz, Z. Liliental-Weber, J. Jasinski, M. Almonte, E. E. Haller, A. Prasad, E. R. Weber, K. Wang, and J. Whitaker, *Appl. Phys. Lett.* **69**, 2569 (1996)

*Electrical and structural properties of LT-GaAs: Influence of As/Ga flux ratio and growth temperature,*

M. Luysberg, H. Sohn, A. Prasad, P. Specht, H. Fujioka, R. Klockenbrink, E.R. Weber,  
MRS Symp. Proc. **442**, 485 (1997)

*Ga vacancies in low-temperature-grown GaAs identified by slow positrons,*

J. Gebauer, R. Krause-Rehberg, S. Eichler, M. Luysberg, H. Sohn, E.R. Weber, Appl.  
Phys. Lett. **71**, 638 (1997)

*Vacancy defects in low-temperature-grown GaAs observed by continuous and pulsed slow positrons,*

J. Gebauer, R. Krause-Rehberg, S. Eichler, W. Bauer-Kugelmann, G. Kögel, W.  
Triftshäuser, M. Luysberg, H. Sohn, E.R. Weber, Mater. Sci. Forum **255-257**, 204 (1997)

*Defect control in As-rich GaAs,*

P. Specht, S. Jeong, M. Luysberg, A. Prasad, H. Sohn, J. Gebauer, R. Krause-Rehberg,  
E.R. Weber, in: Proc. of the Int. Conf. on Defects in Semiconductors ICDS 19, Aveiro,  
Portugal, Mater. Sci. Forum **258-263**, 951 (1997)

*Effects of the growth temperature and As/Ga flux ratio on the incorporation of excess As into low-temperature-grown GaAs,*

M. Luysberg, H. Sohn, A. Prasad, P. Specht, Z. Liliental-Weber, E.R. Weber, J. Gebauer,  
R. Krause-Rehberg, J. Appl. Phys. **83**, 561 (1998)

*The origin of the Magnetic Circular Dichroism of Absorption of the Arsenic Antisite in GaAs and AlGaAs,*

A. Prasad, P. Stallinga, X. Liu, E.R. Weber, to be published in Phys. Rev. B (1998)

*Ultrafast carrier trapping & thermal stability in As-rich GaAs through Be-doping,*

P. Specht, R. Zhao, S. Jeong, J. Bokor, E.R. Weber, submitted to Phys. Rev. B (1998)

*Ultrafast response times and enhanced optical nonlinearity in Beryllium doped low-temperature grown GaAs,*

A. Prasad, M. Haiml, I.D. Jung, J. Kunde, F. Morier-Genoud, E.R. Weber, U. Siegner, U.  
Keller, accepted as oral presentation at CLEO, May 1998

*Transition from epitaxial to columnar growth of non-stoichiometric GaAs deposited at low temperatures,* M. Luysberg, P. Specht, H. Sohn, E.R. Weber, submitted to ICEM-14,  
Cancun, 1998

## 11. Tables

**Table I:  $\Delta c/c$  and  $\Delta a/a$  of partly polycrystalline LT-GaAs layer (sample M101)**

$\Omega'$	0.009°	0.010°	0.009°
$\Omega$	0.077°	0.078°	0.079°
$\Delta\tau$ {224}	0.034°	0.034°	0.035°
$\Delta\Theta$ {224}	-0.043°	-0.044°	-0.044°
$\Delta a/a$ {224}	0%	0.0017%	-0.0007%
$\Delta c/c$ {224}	0.126%	0.128%	0.129%
$\Delta\Theta$ (004)	0.047°	0.047°	0.048°
$\Delta c/c$ (004)	0.126%	0.126%	0.129%

**Table II: Critical thickness ( $d_{LT}$ ) and related data in LT-GaAs ( $T_G < 200^\circ\text{C}$ )**  
 $(d_0$  : total thickness of the LT-layer)

Sample no.	$T_G$ [°C]	BEP ratio	$\Delta c/c$ [%]	$d_0$ [nm]	$d_{LT}$ [nm]	$d_{LT}/d_0$ [%]
M126	155	20	0.156	1000	630	63
M152	155	20	0.137	500	286	57
M101	155	25	0.129	1000	391	39
M138	165	11	0.161	1700	993	58
M125	165	20	0.160	1500	763	51
M141	165	40	0.140	1000	463	46
M124	175	20	0.158	1500	890	59
M127	185	20	0.141	2250	1580	70

**Table III: SIMS data (contamination)**

	C [cm <sup>-3</sup> ]	O [cm <sup>-3</sup> ]	H [cm <sup>-3</sup> ]
highest level	$6*10^{16}$	$6*10^{17}$	$2*10^{17}$
current level	$<2*10^{16}$	$<3*10^{16}$	$<1*10^{17}$

## 12. Figures

## Lattice Mismatch of the Temperature Series

(BEP=20, growth rate: 1 $\mu$ m/h)

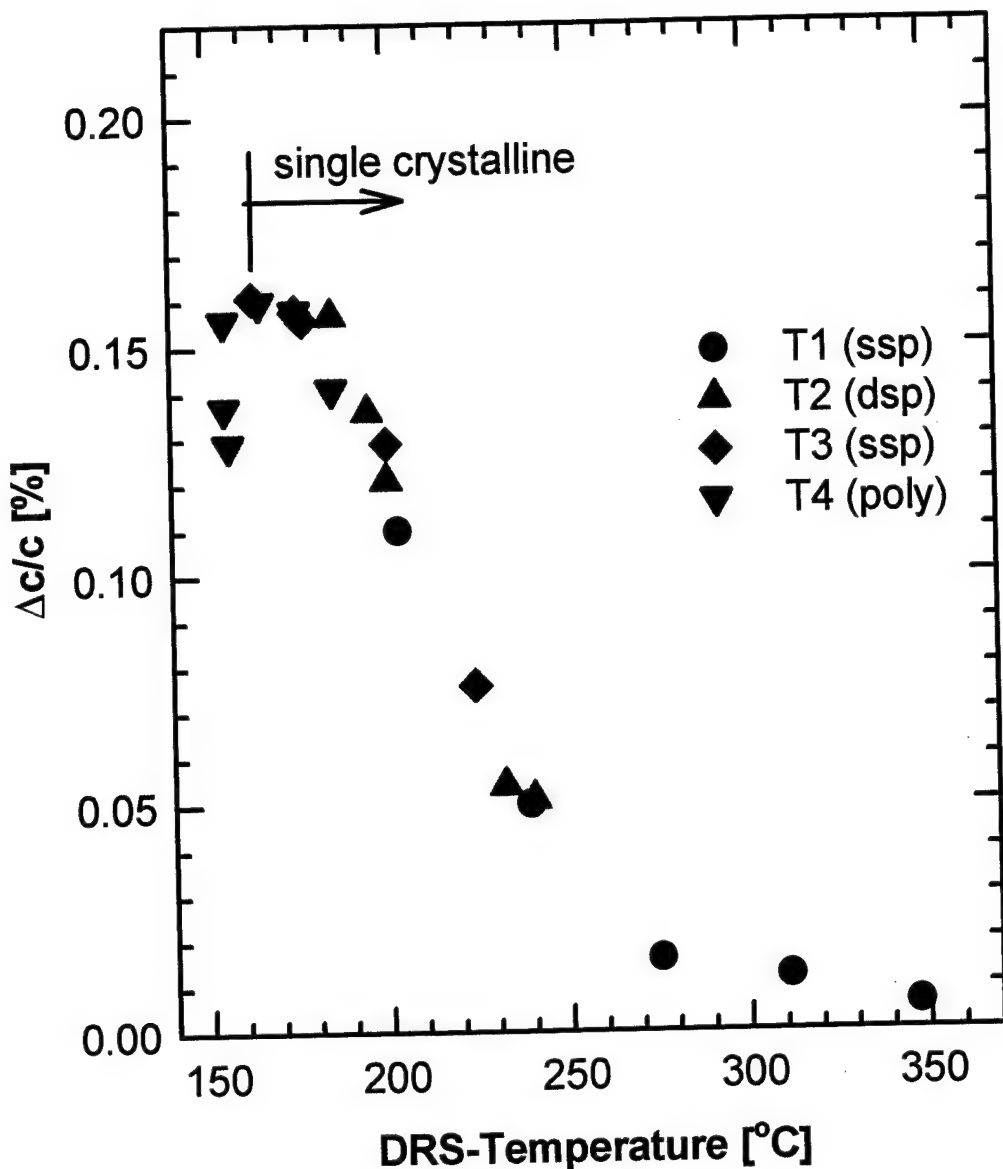


Figure 1

# Measurement geometry of the diffuse reflectance spectroscopy (DRS)

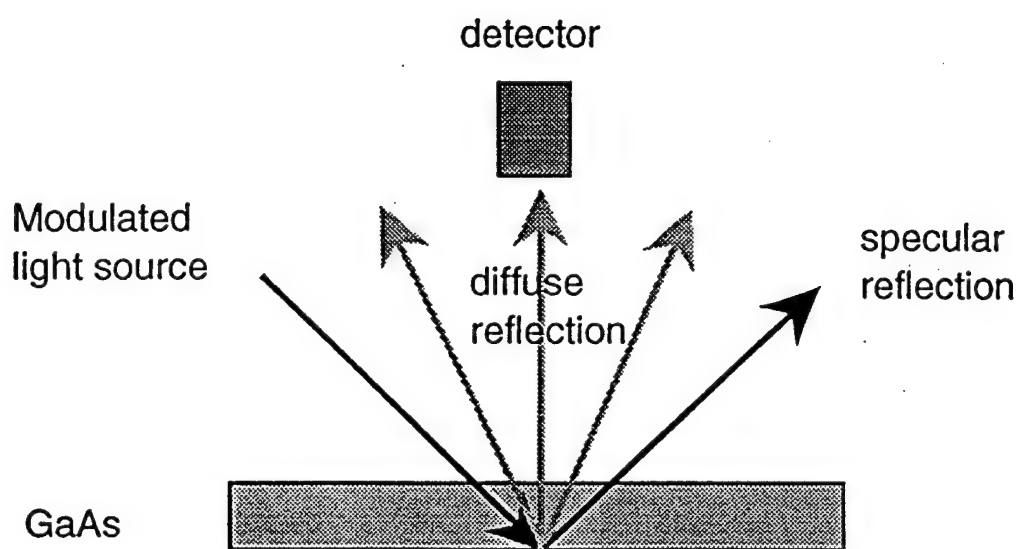


Figure 2

# Calibration of the growth temperature for n<sup>+</sup> GaAs substrate

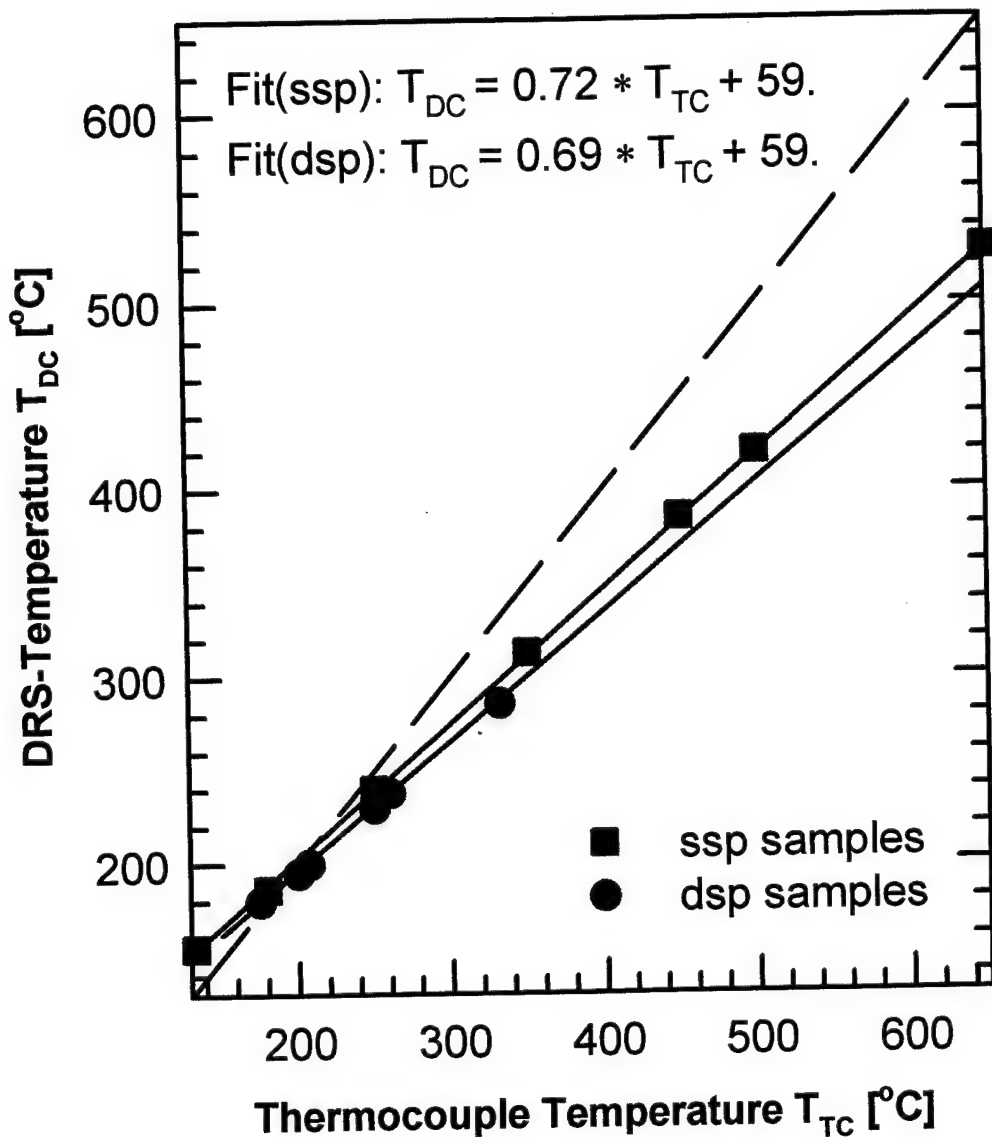


Figure 3

## BEP ratio determination methods

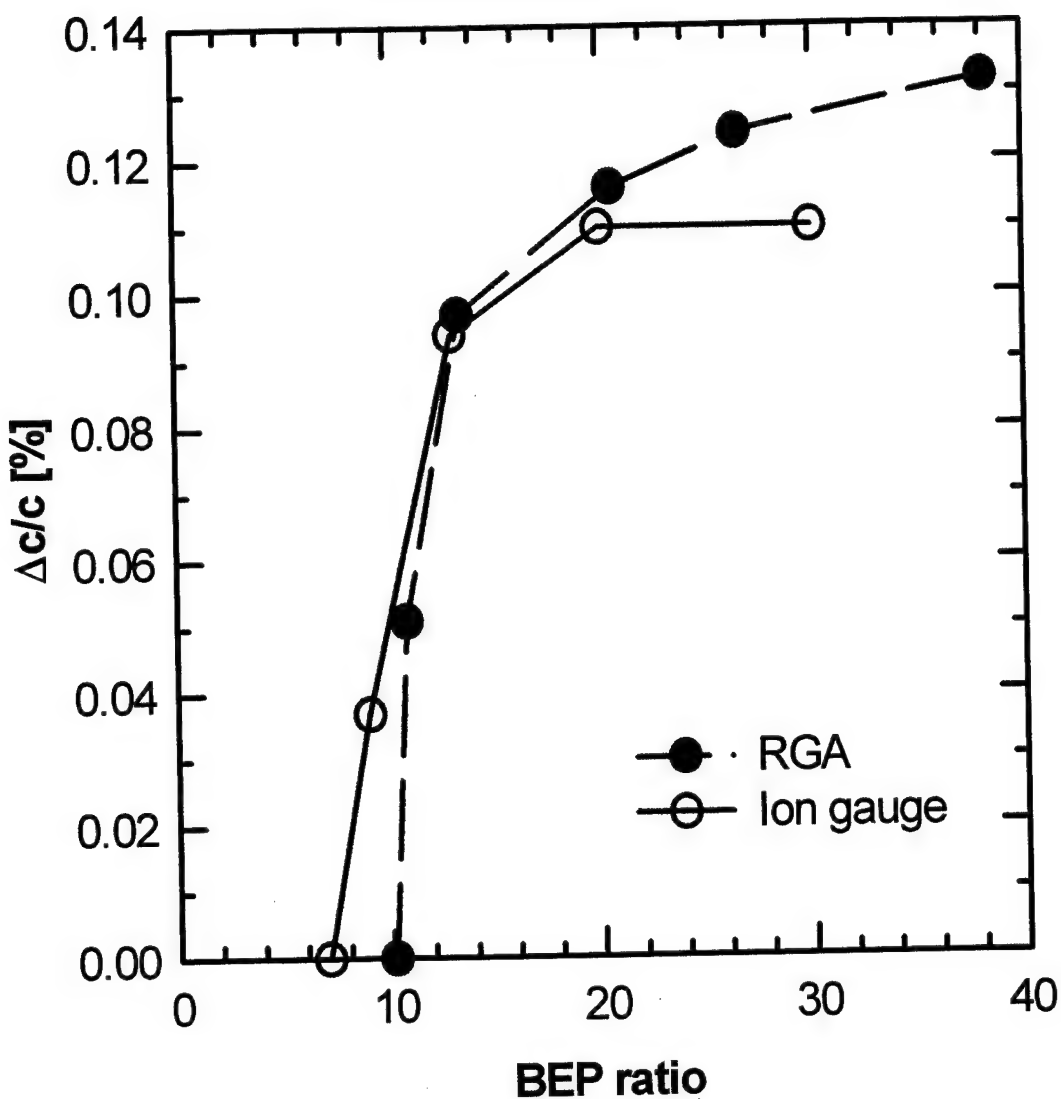


Figure 4

## Lattice expansion of LT-GaAs grown at different As/Ga flux ratios (BEP ratio)

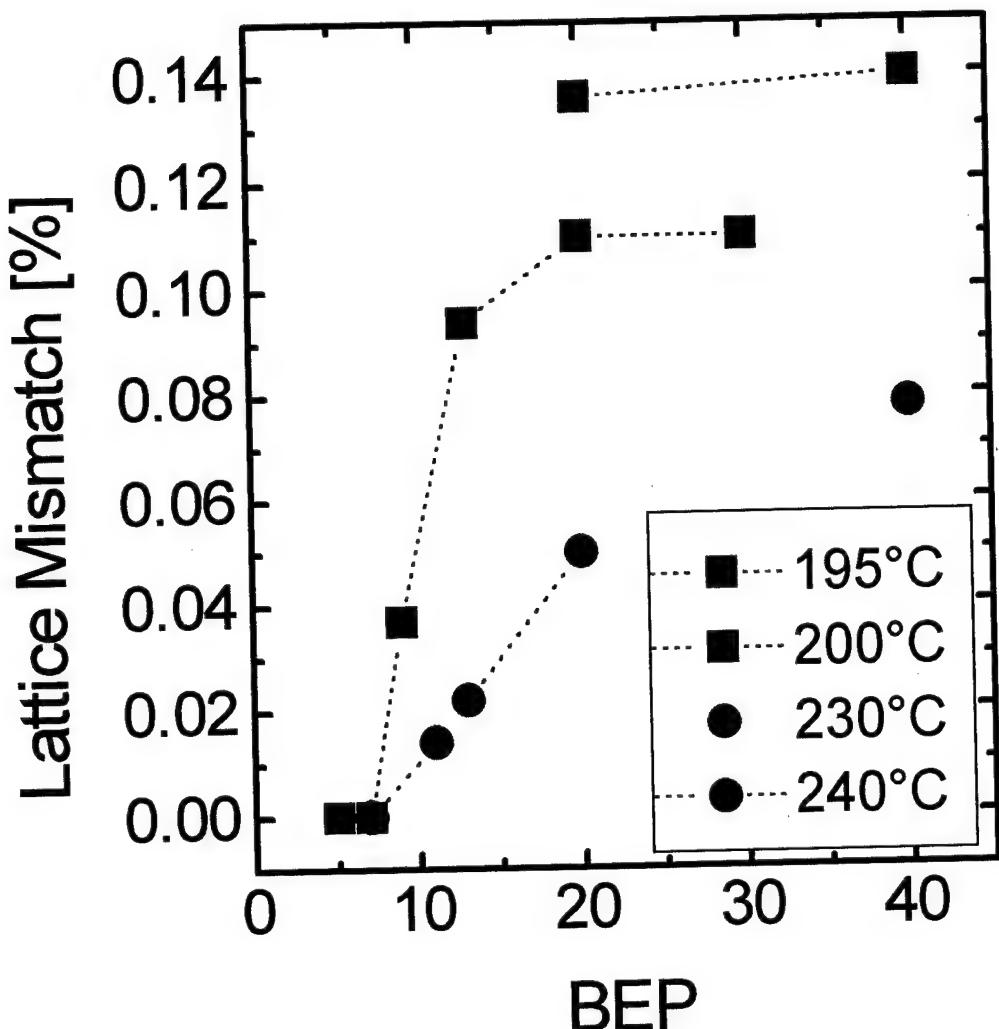


Figure 5

# Correlation of lattice mismatch and $\text{As}_{\text{Ga}}$ concentration

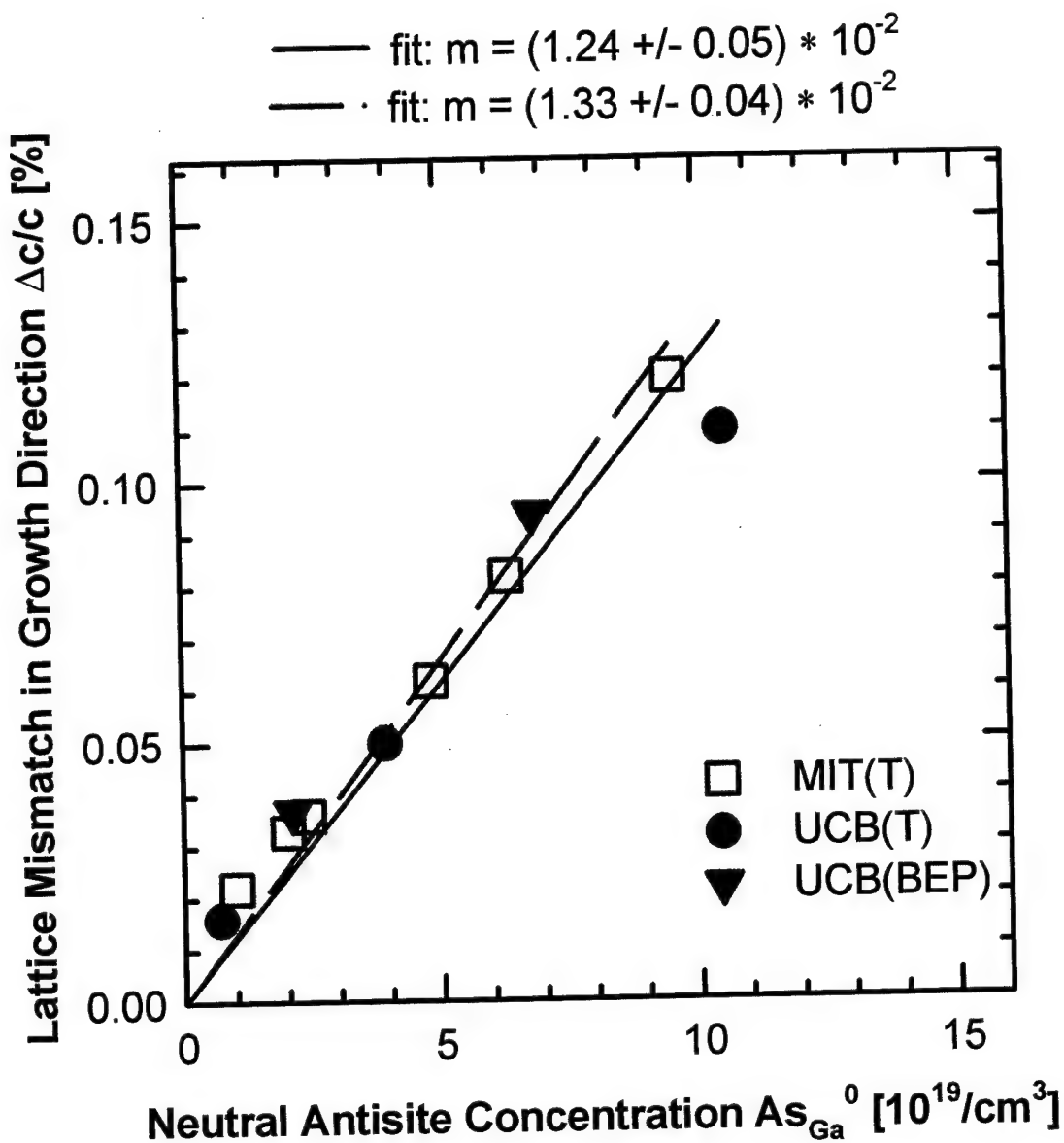


Figure 6

# Determination of $\Delta a/a$ and $\Delta c/c$ by (224) x-ray reflection ( $T_G=155^\circ\text{C}$ )

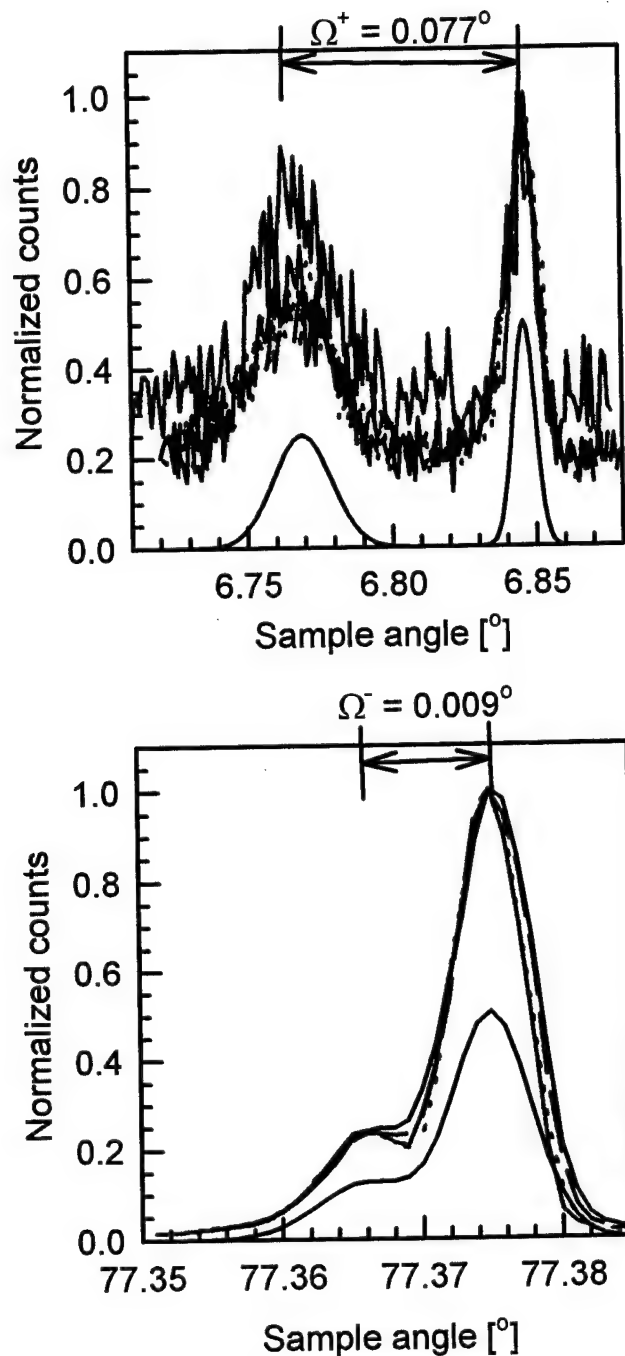


Figure 7

## Critical thickness of LT-GaAs ( $T_G=165^\circ\text{C}$ , BEP=40, $\Delta c/c=0.14\%$ )

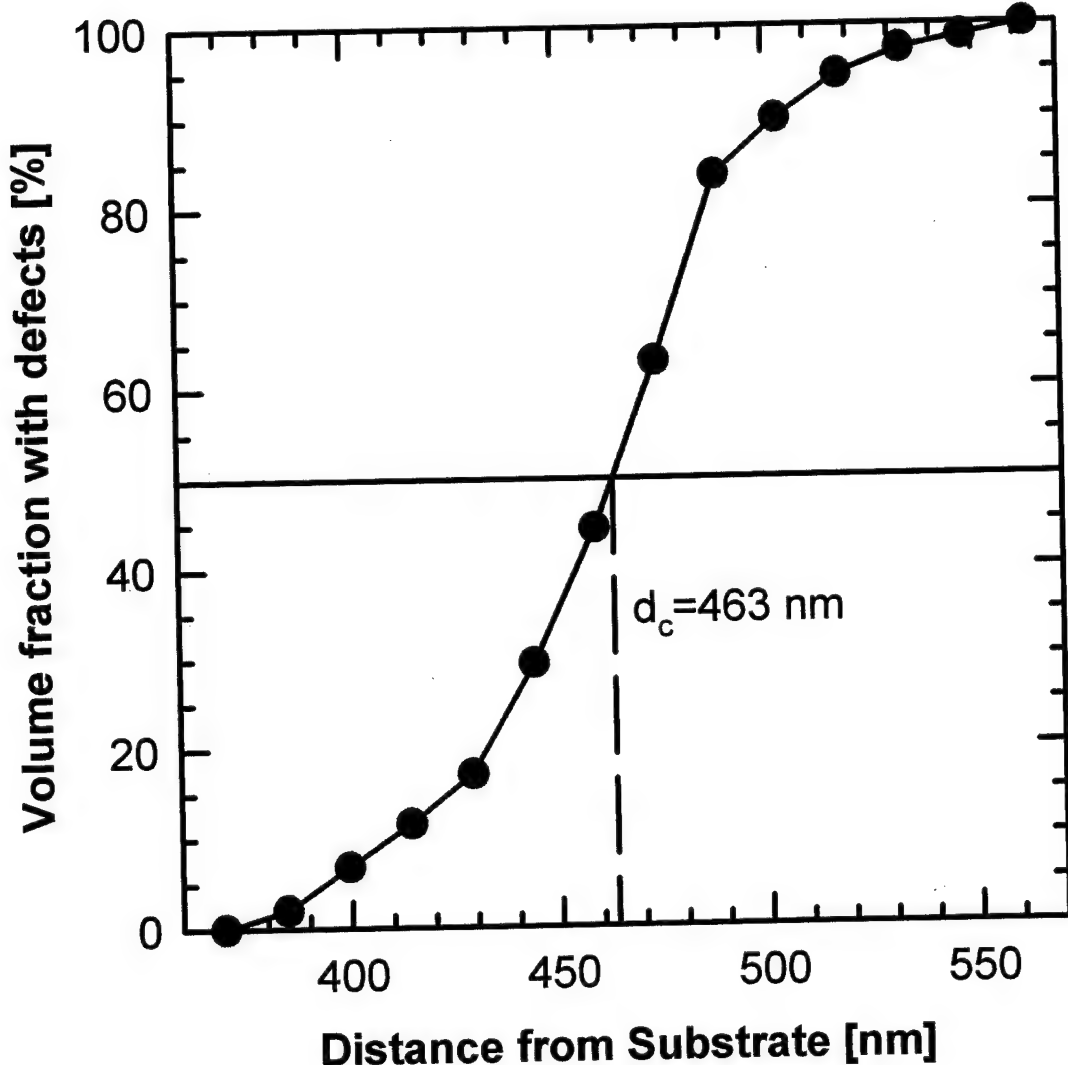


Figure 8

# Breakdown of single crystallinity in LT-GaAs

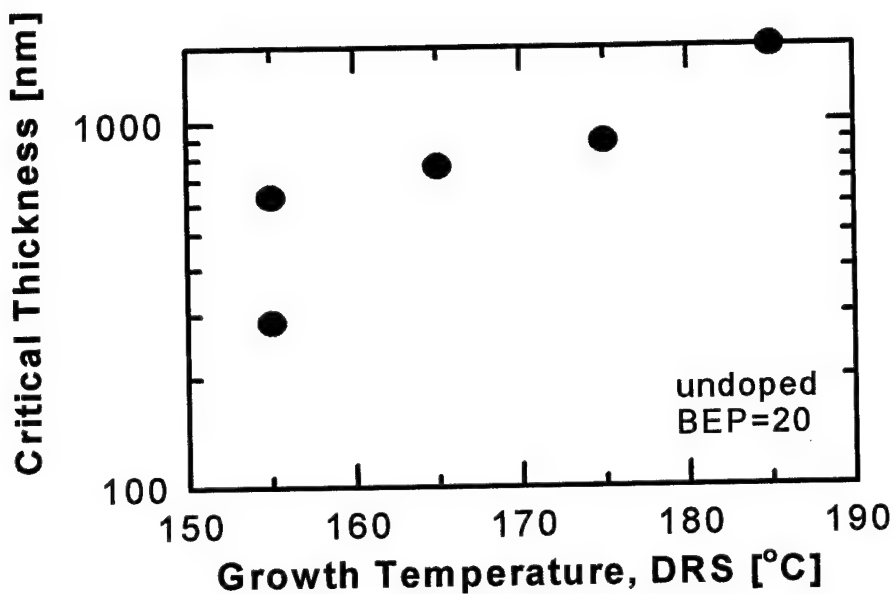


Figure 9

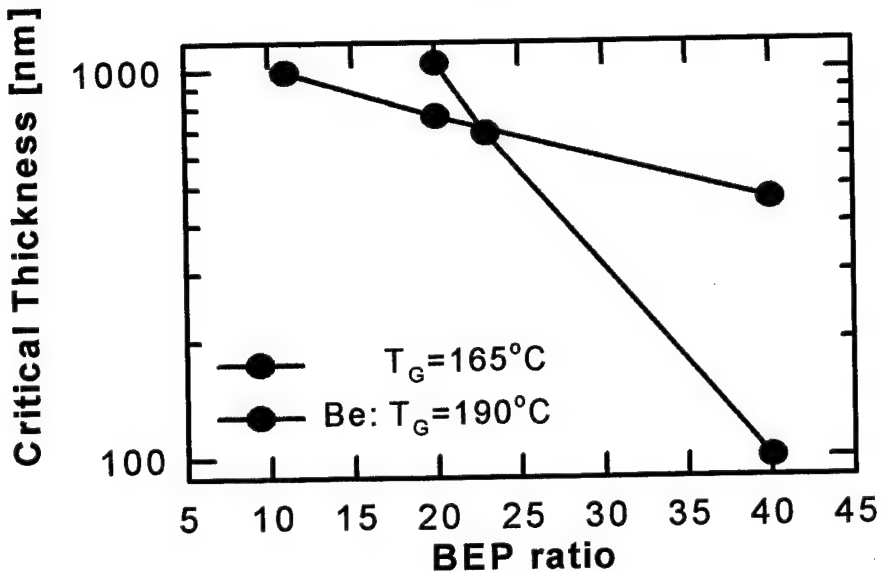


Figure 10

## Transition from single crystalline to polycrystalline growth (011)



Figure 11.a

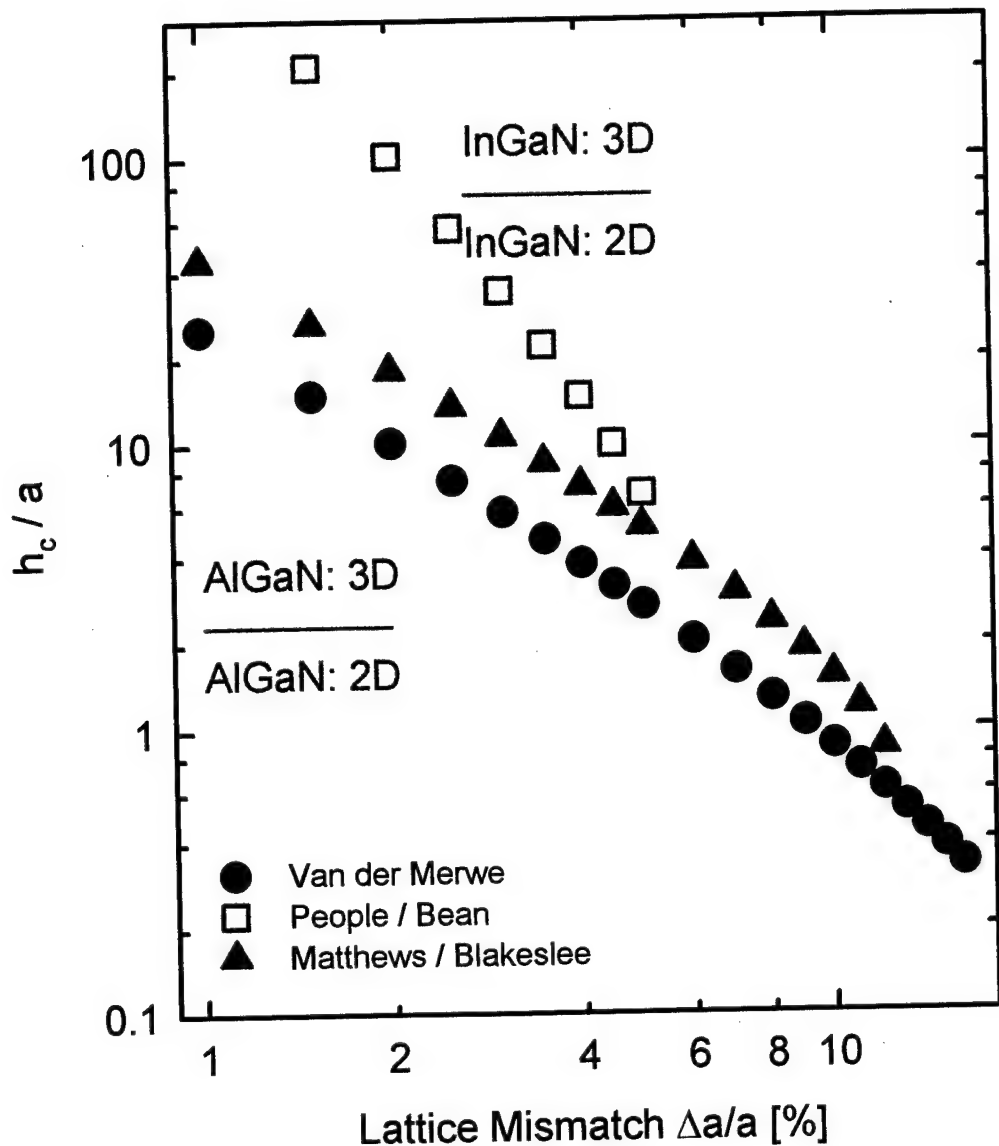
## Transition from single crystalline to polycrystalline growth (0-11)



Figure 11.b

# Critical thickness for GaN

( $v=0.23$ ,  $a=b$ )



C. Kisielowski, in: "Gallium Nitride", J.I. Pankove & T.D. Moustakas eds.,  
Academic Press, (1997) in press

Figure 12

# Growth on strained diffusion barrier layers (LT-GaAs on $\text{Al}_{0.67}\text{Ga}_{0.33}\text{As}$ )

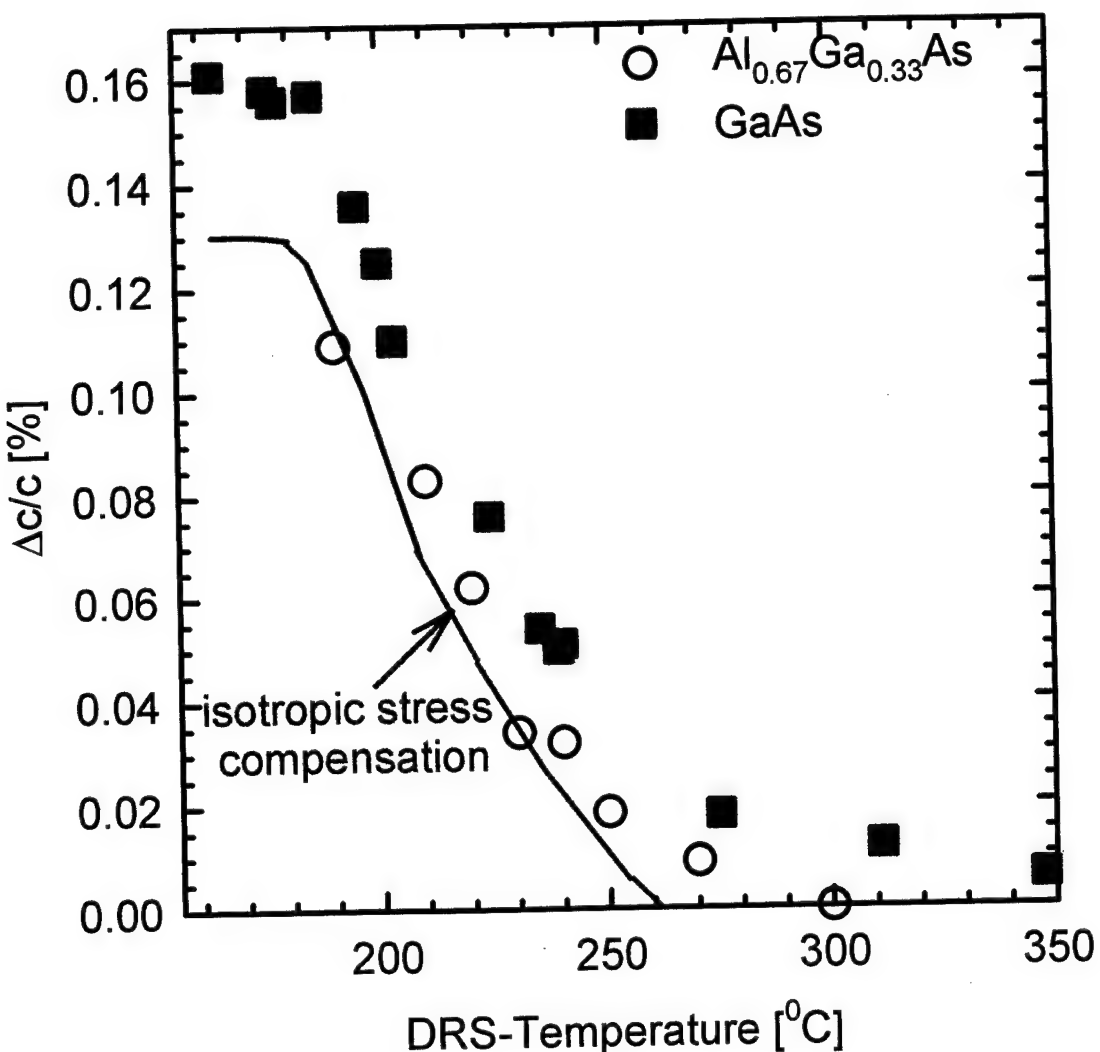


Figure 13

# As<sub>Ga</sub> concentrations as a function of growth parameters

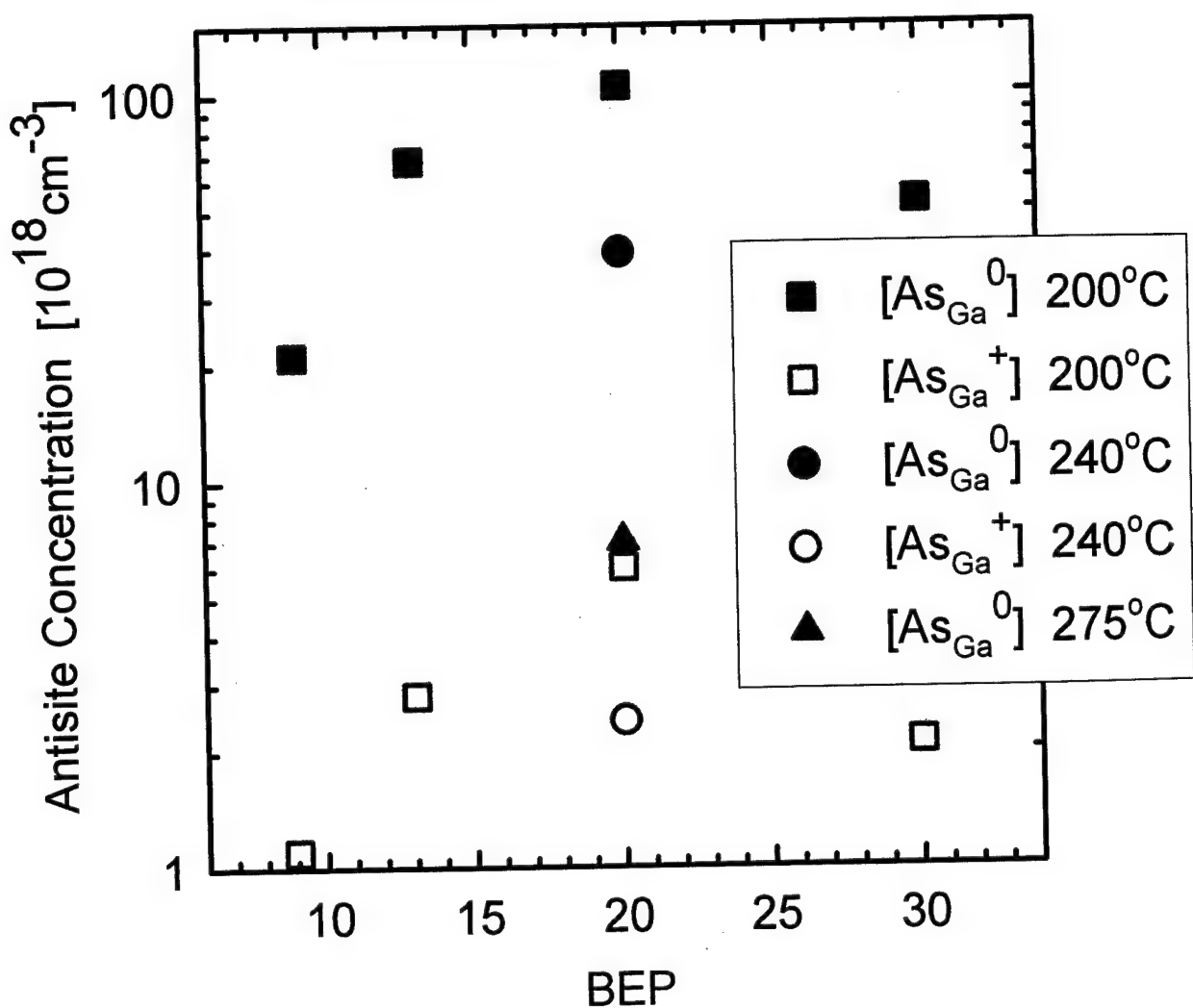


Figure 14

# S(W) dependence for $V_{Ga}$

## as-grown LT-GaAs

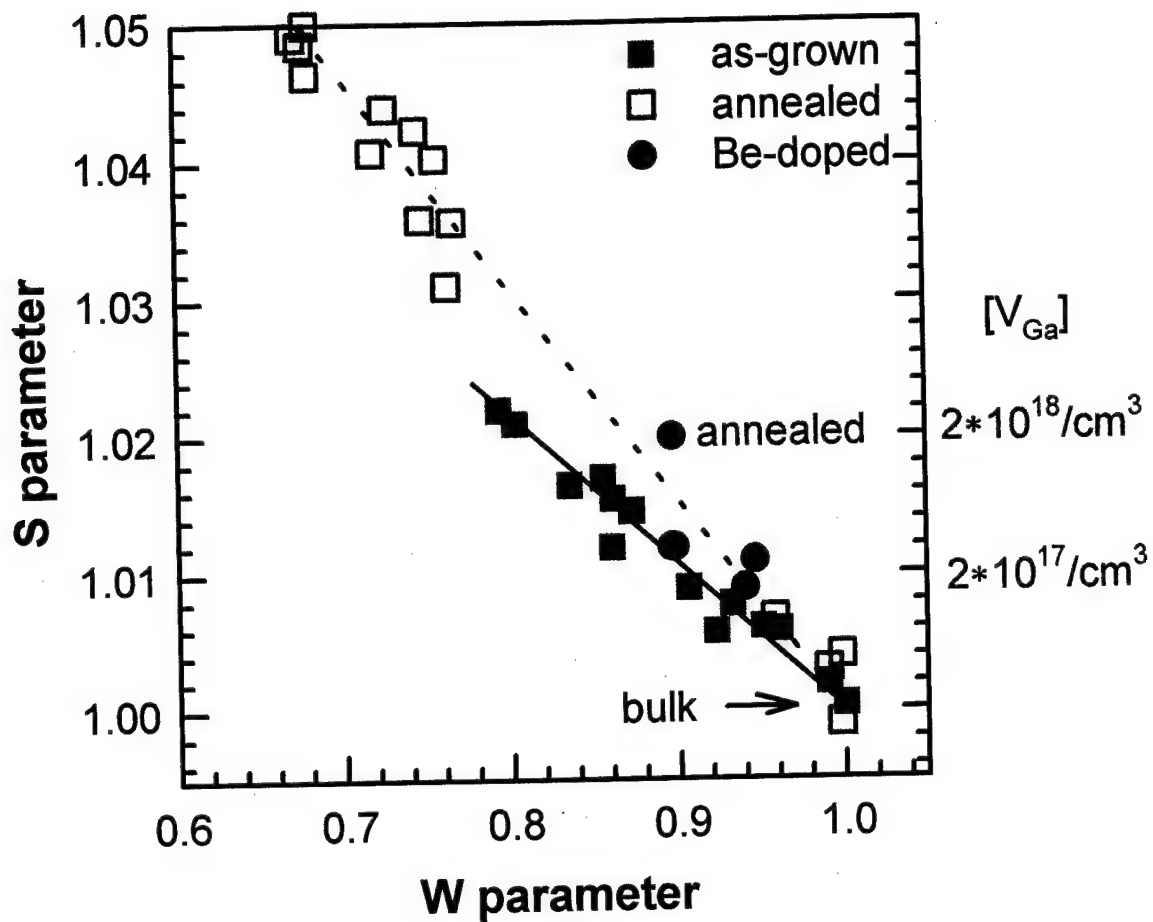


Figure 15

# V<sub>Ga</sub> concentration in As-rich GaAs

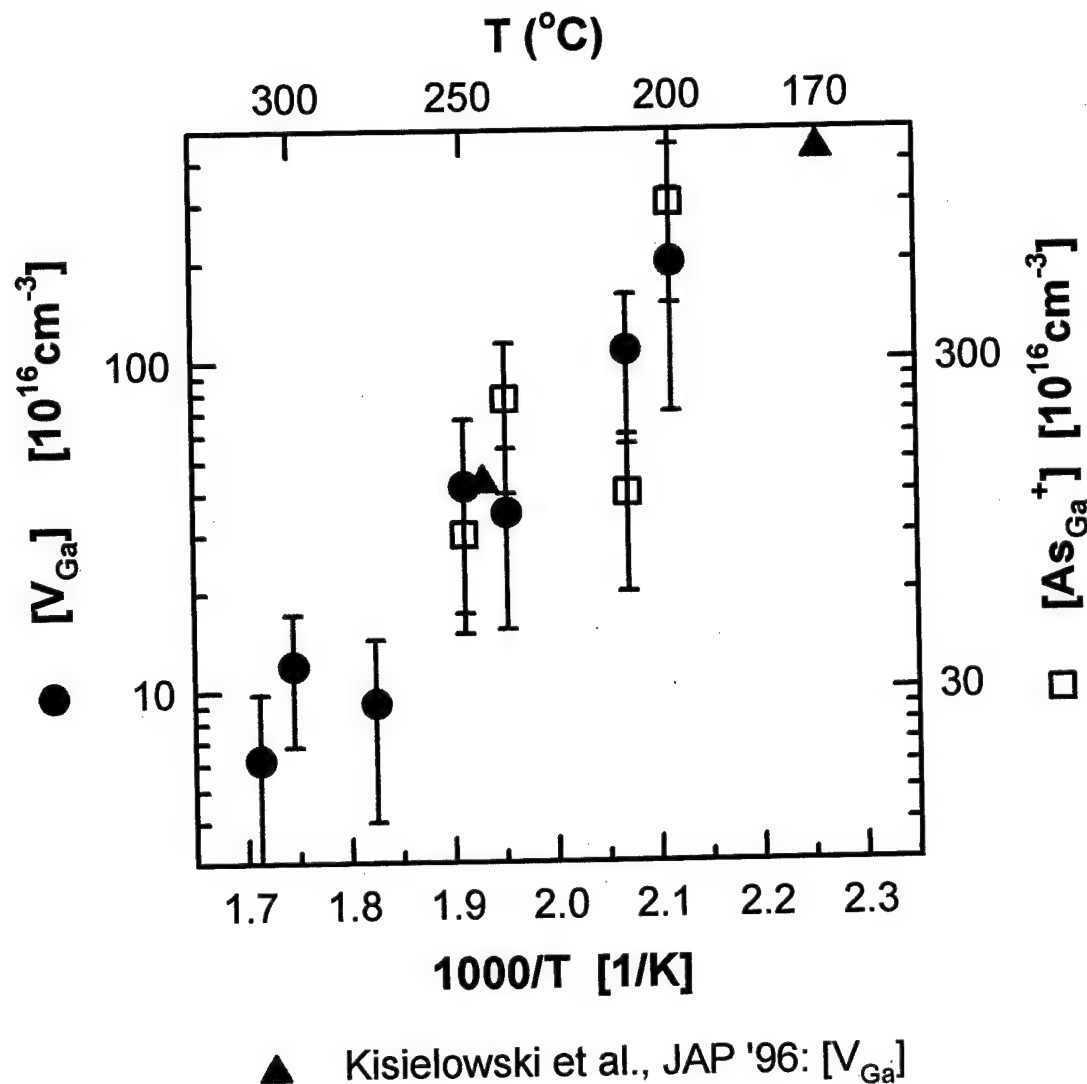


Figure 16

## [V<sub>Ga</sub>] dependence on the As/Ga flux ratio

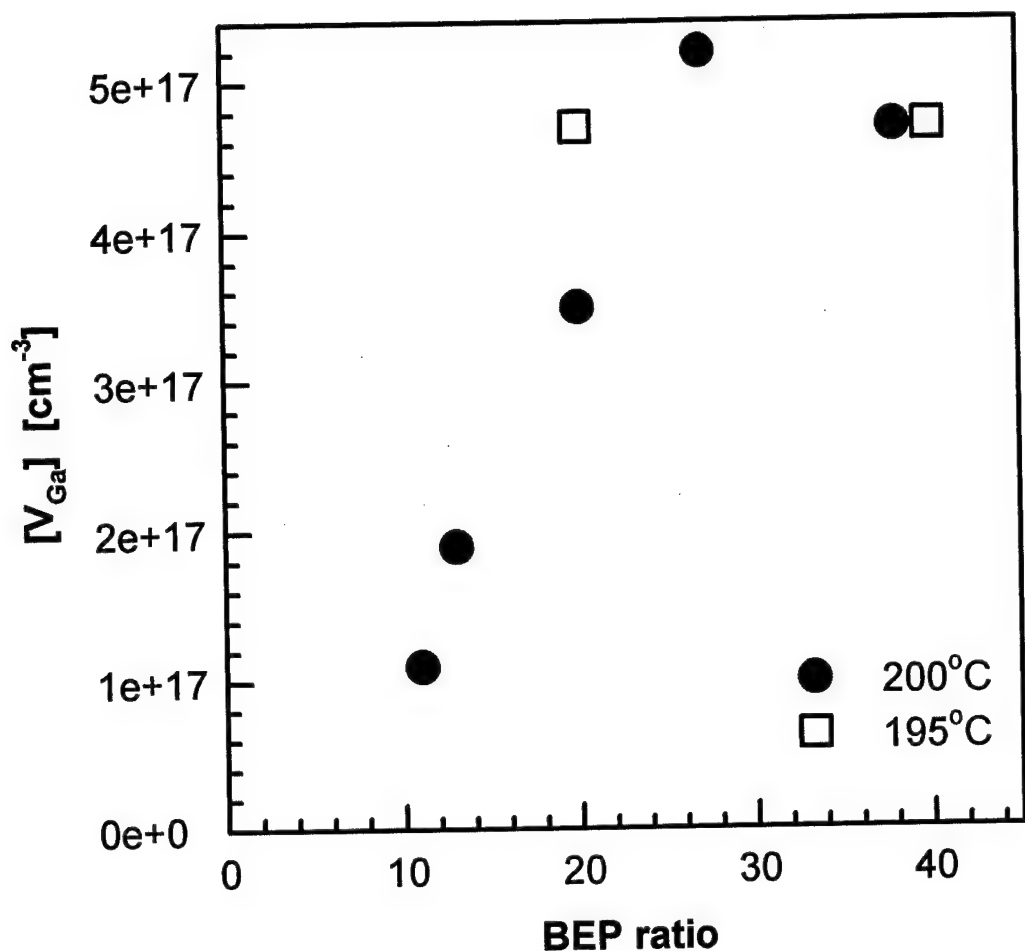


Figure 17

# [As<sub>Ga</sub><sup>+</sup>] in As implanted GaAs: Annealing behavior

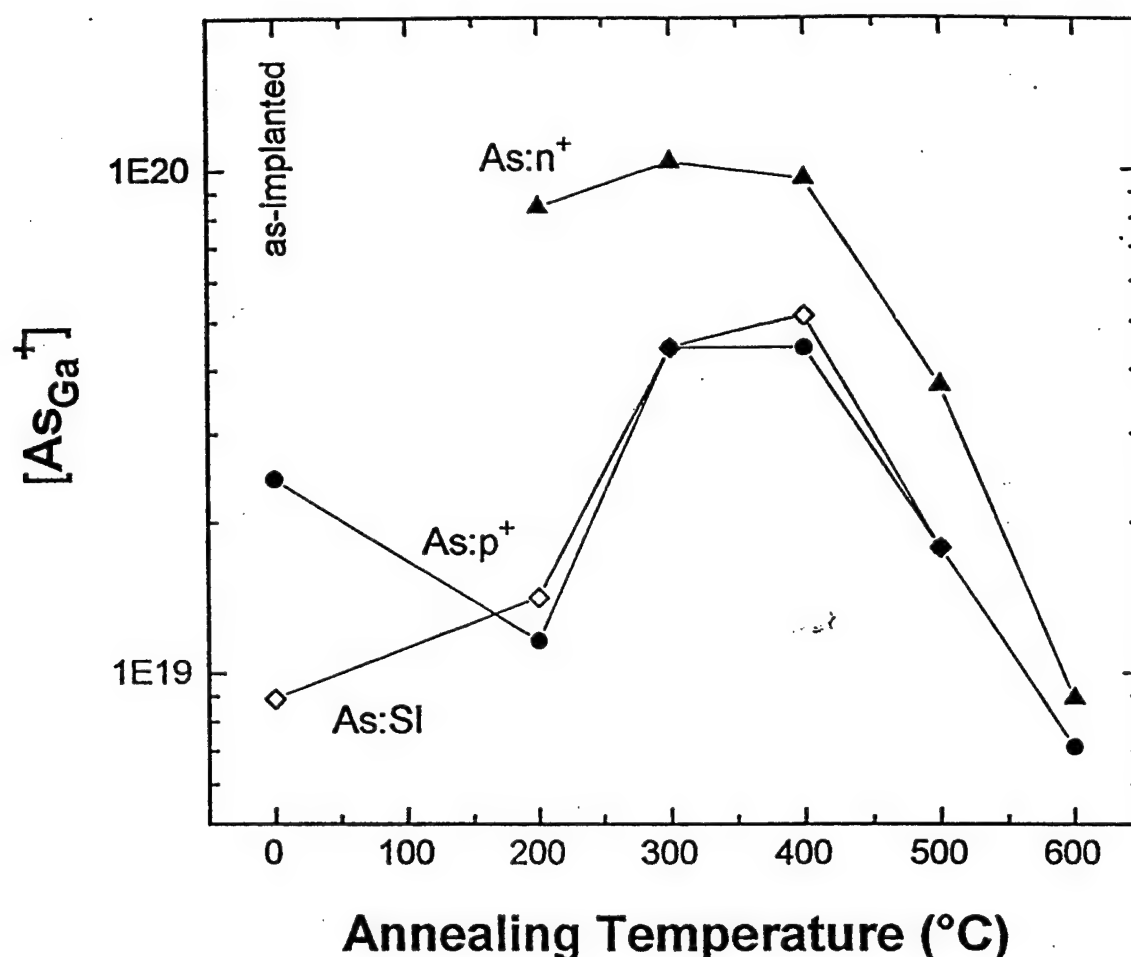


Figure 18

## MCDA spectra of LT-Al<sub>x</sub>Ga<sub>1-x</sub>As

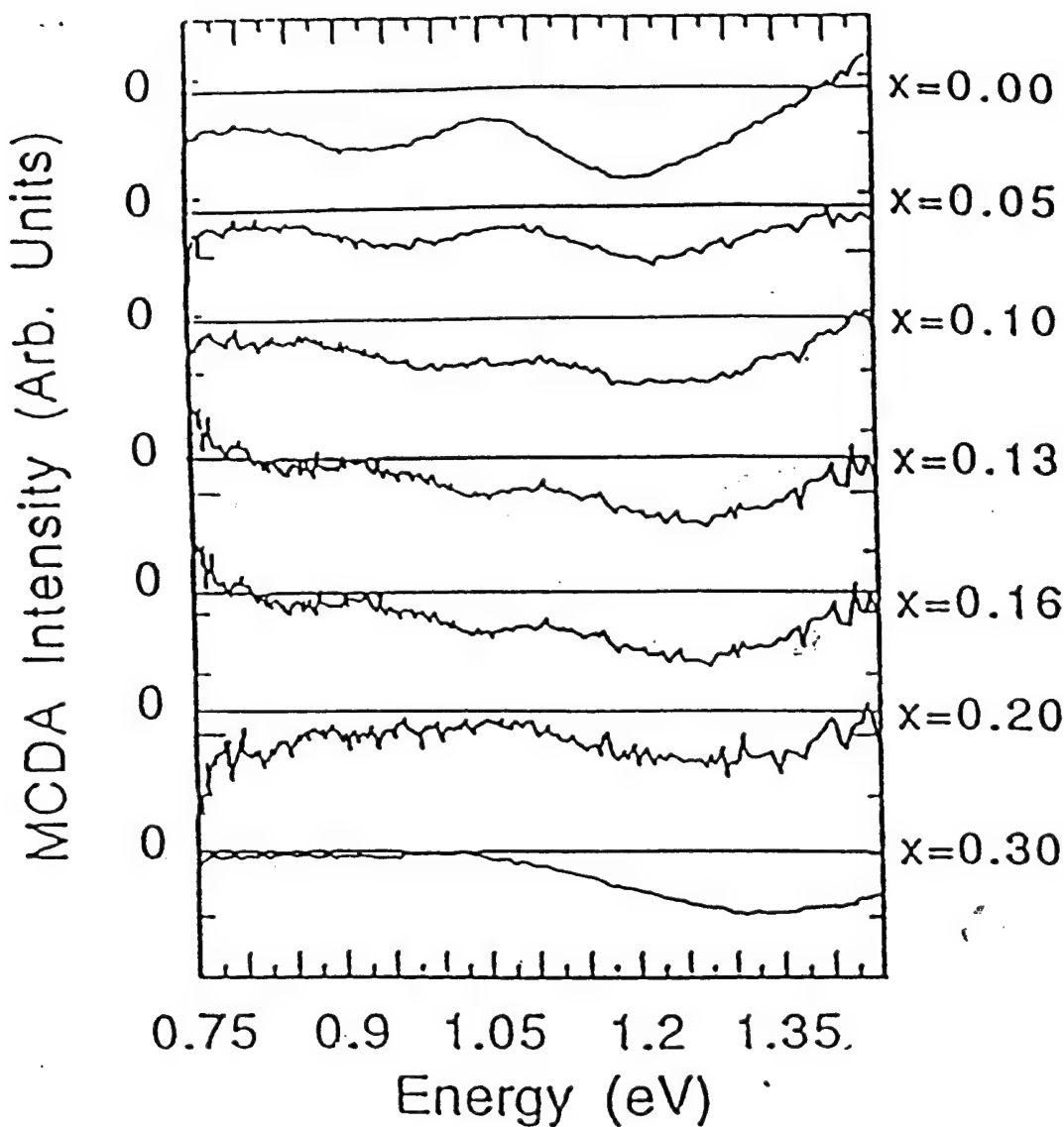


Figure 19

# Conductivity vs 1/T for LT-Al<sub>0.3</sub>Ga<sub>0.7</sub>As

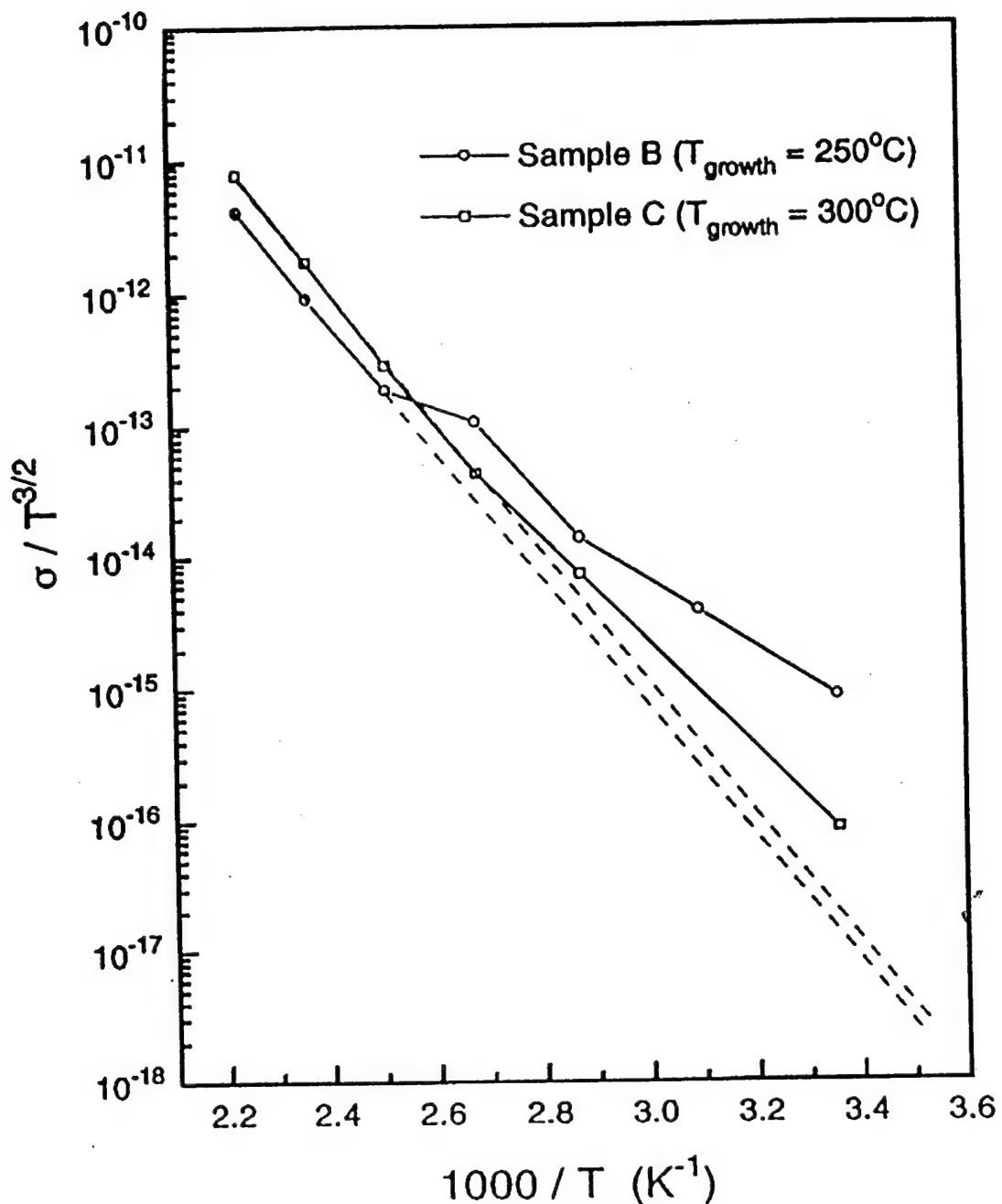


Figure 20

# Planar Resistivity of as-grown LT-GaAs

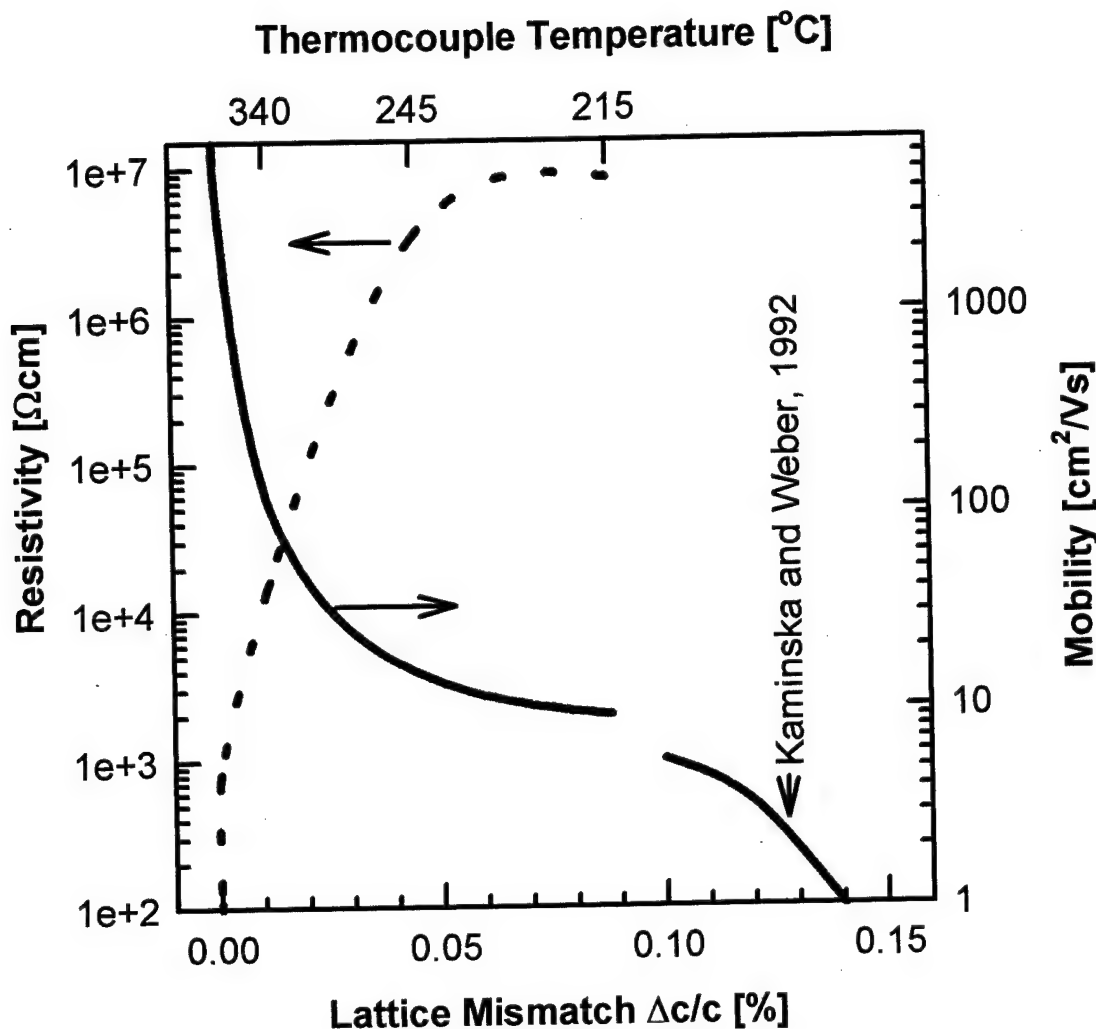


Figure 21

# Vertical conductivity of LT-GaAs: influence of growth temperature $T_g$

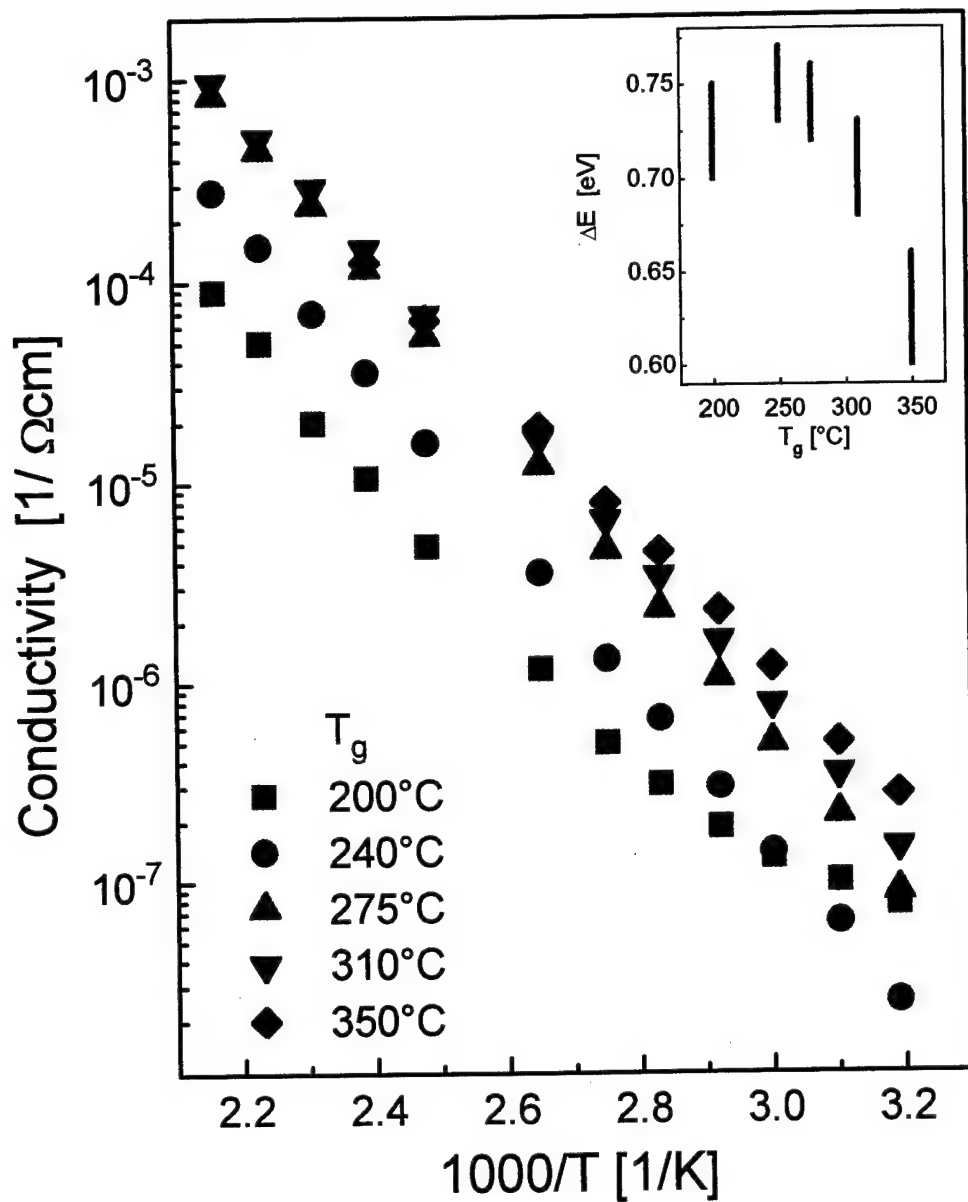


Figure 22

# Vertical conductivity of LT-GaAs: influence of As/Ga flux ratio (BEP)

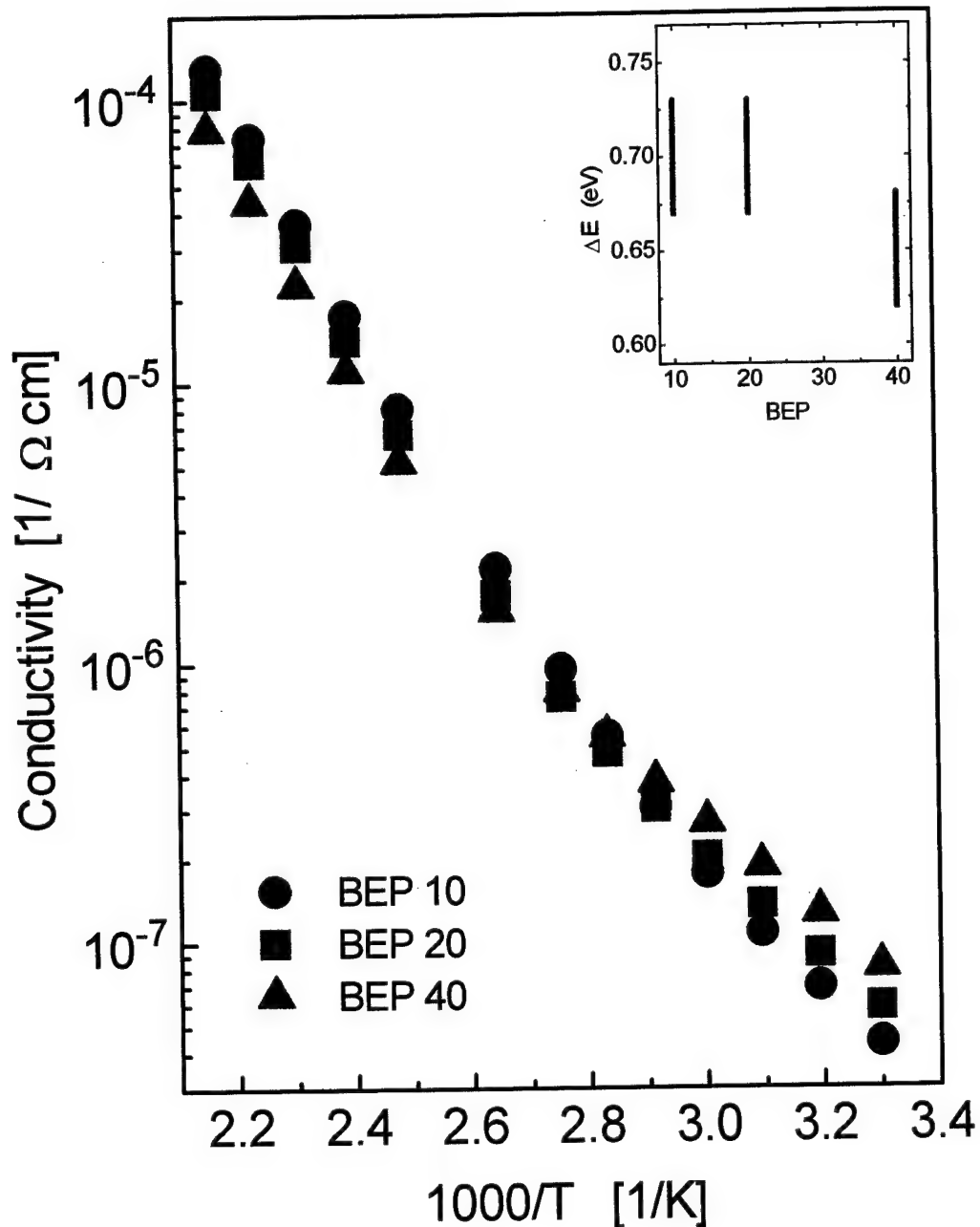


Figure 23

# Breakdown voltage in LT-GaAs

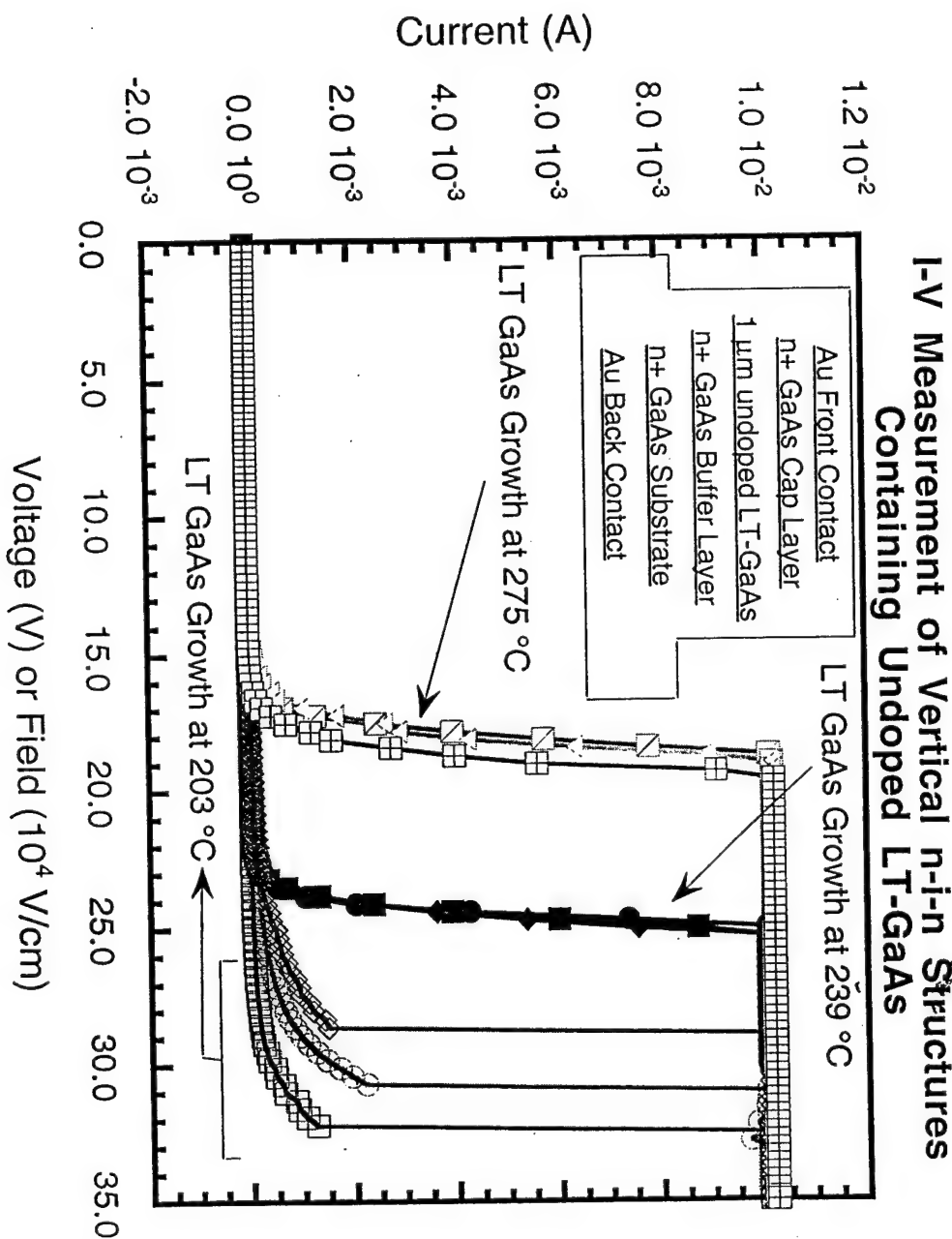


Figure 24

# Lattice mismatch of LT-GaAs:Be

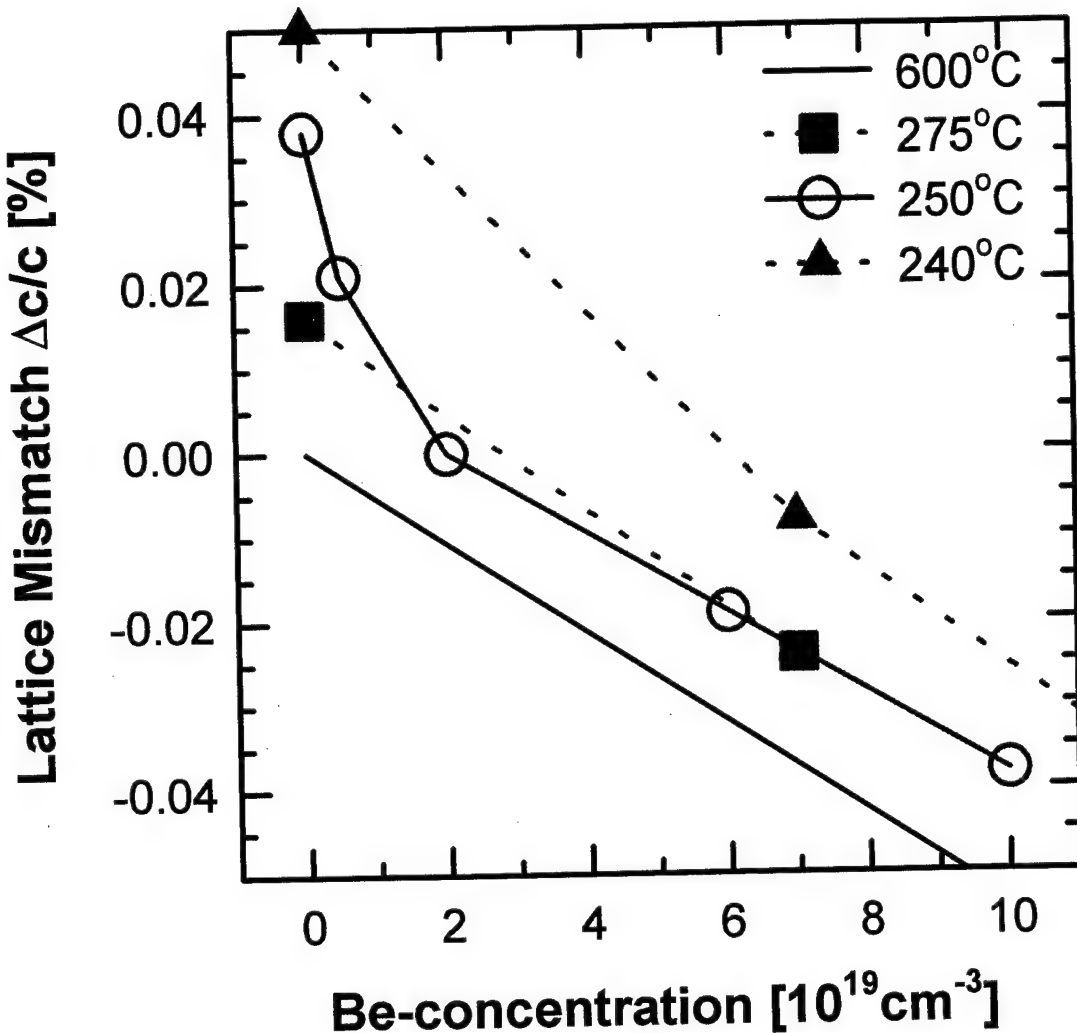


Figure 25

# Ultra-high Be concentrations in LT-GaAs

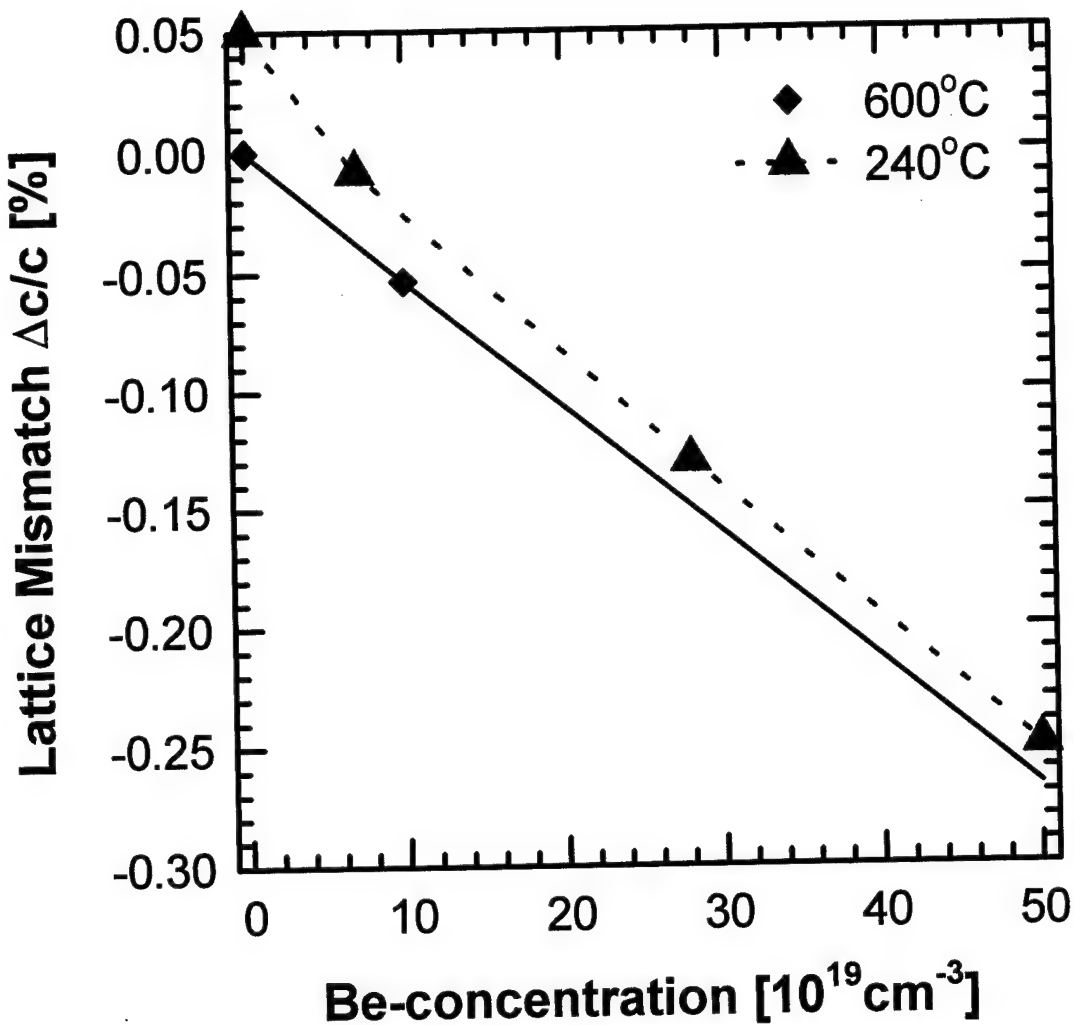


Figure 26

# Annealing behaviour of LT-GaAs:Be

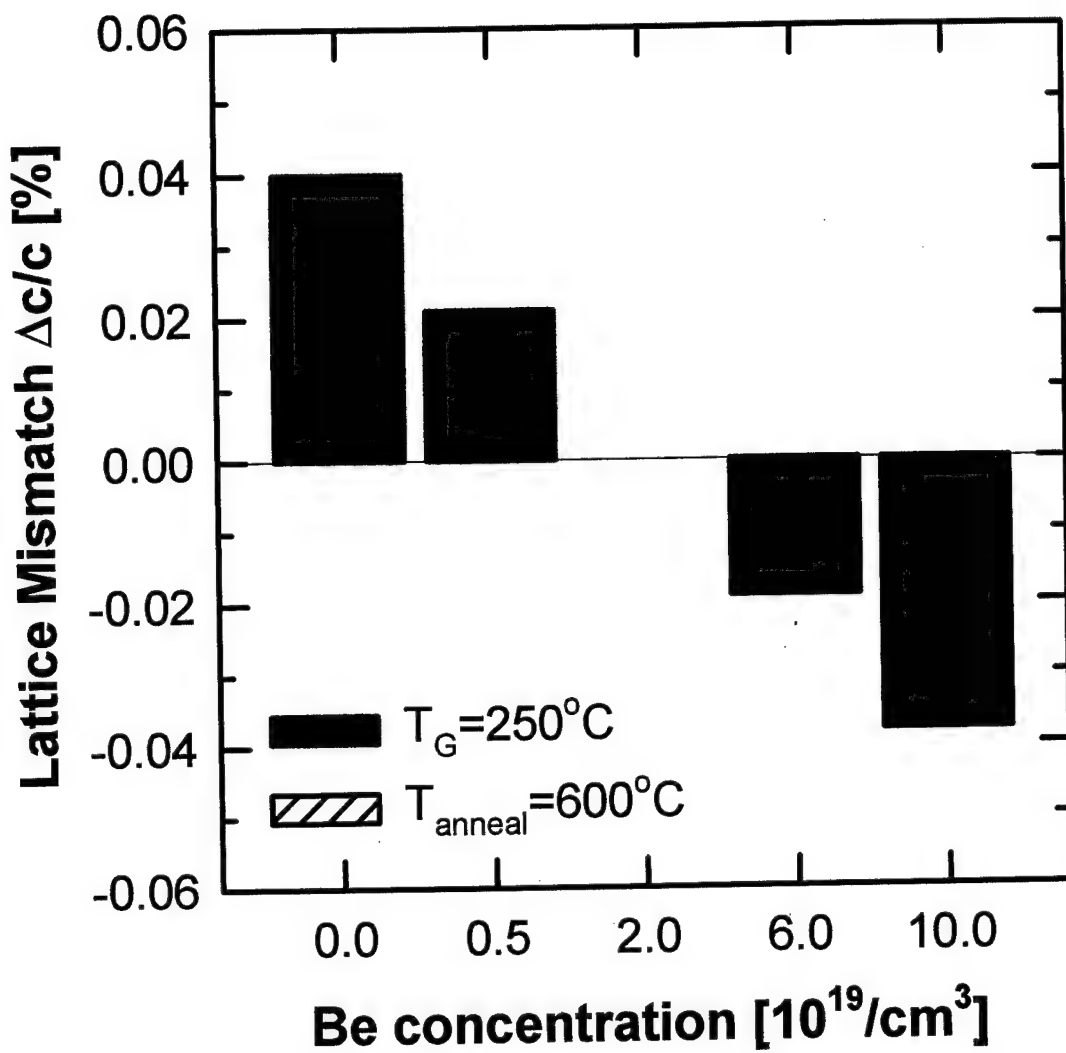


Figure 27

# Reduction in trapping time due to [Be]

(BEP=20, as-grown)

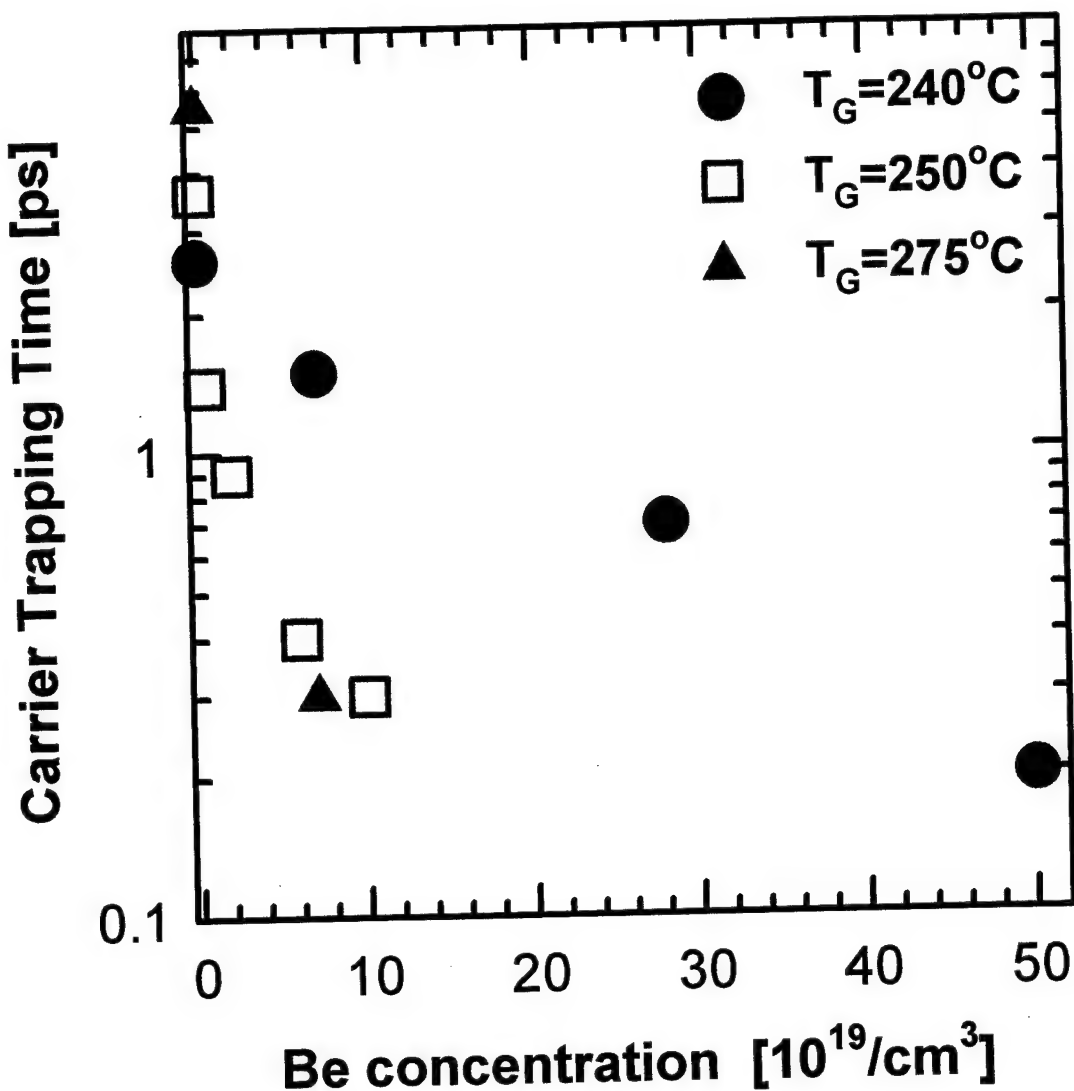


Figure 28

# T-dependence of the carrier trapping time

$[Be] = 5*10^{18}/\text{cm}^3$

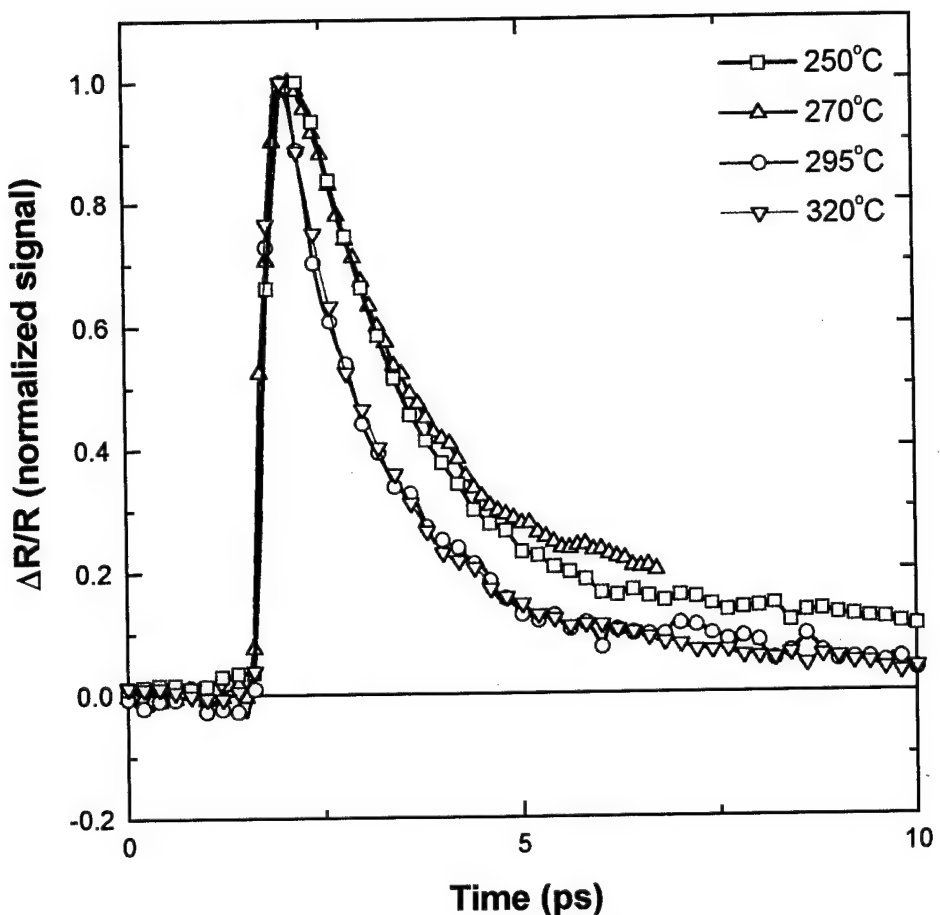


Figure 29

## Annealing behaviour of carrier trapping time

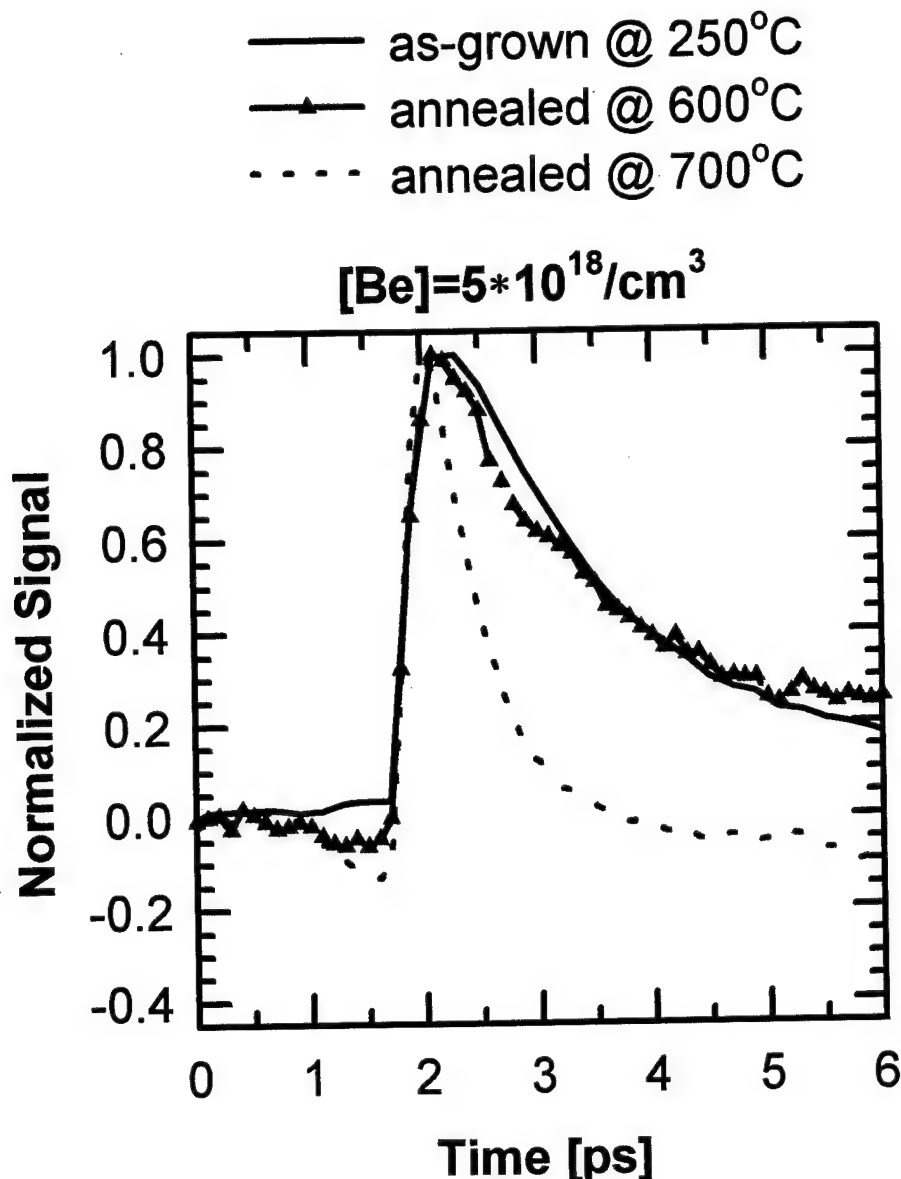


Figure 30.a

## Annealing behaviour of carrier trapping time

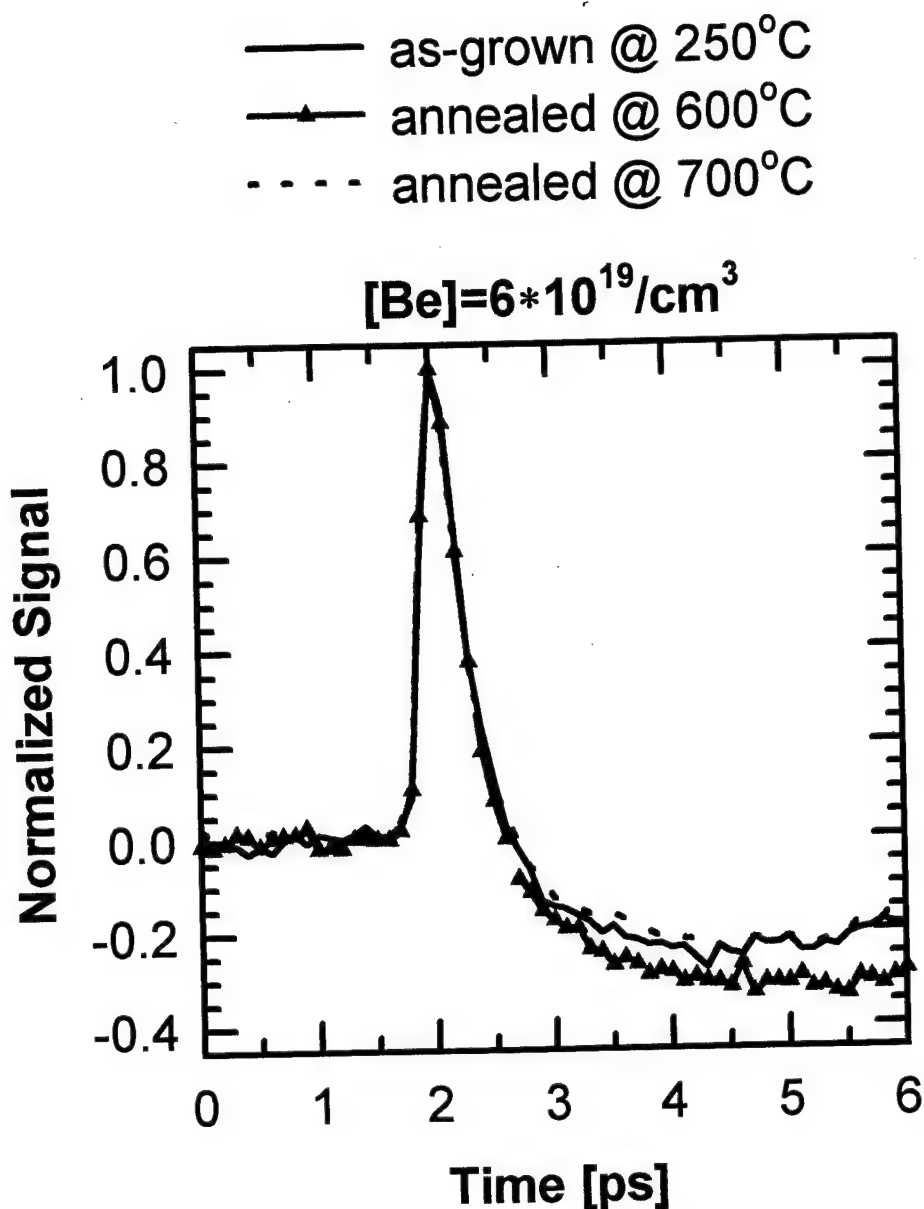


Figure 30.b

# Effective carrier capture cross section (LT-GaAs & neutron irrad. GaAs)

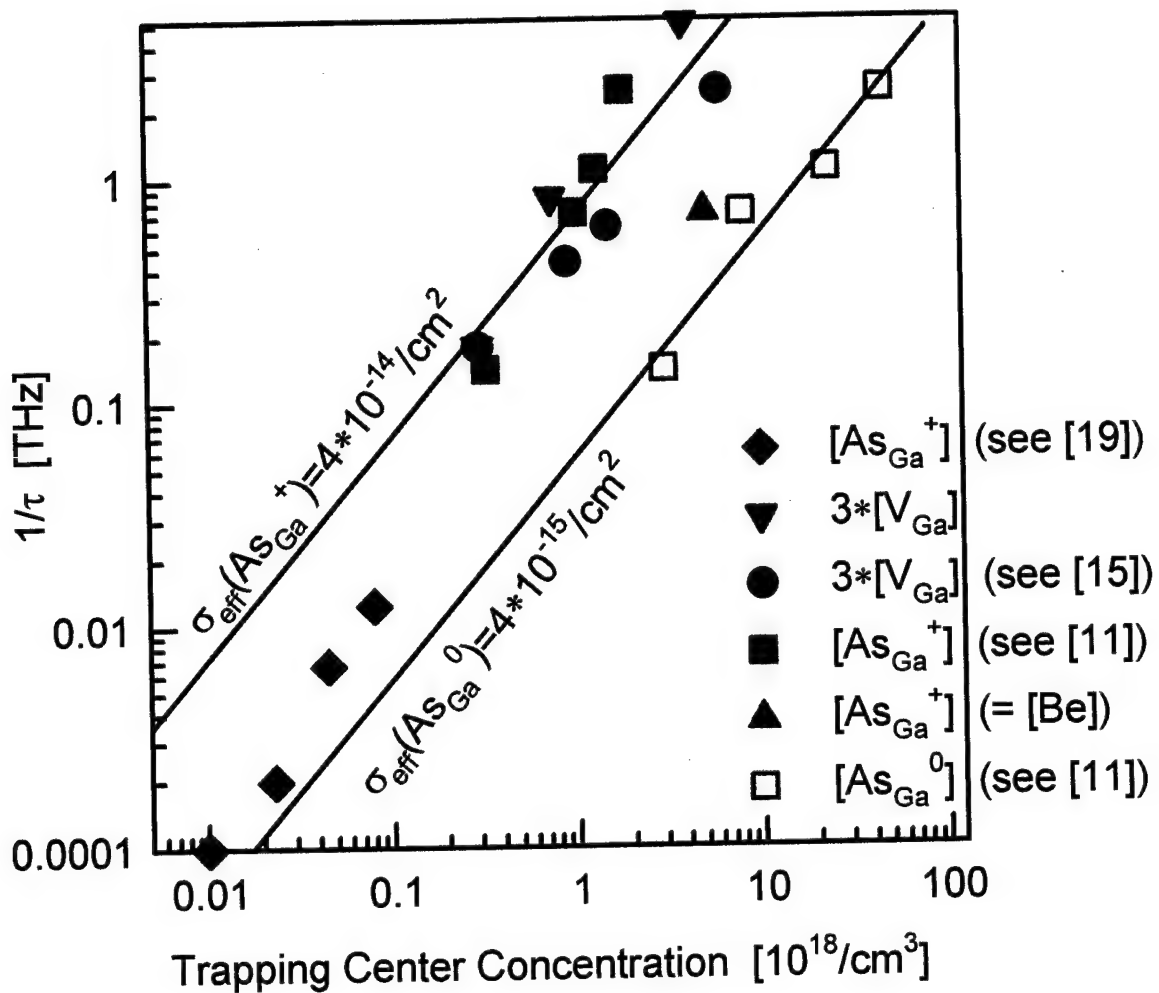


Figure 31

# Increased ionized & total $[\text{As}_{\text{Ga}}]$ due to Be-doping: $7 \times 10^{19} \text{ cm}^{-3}$

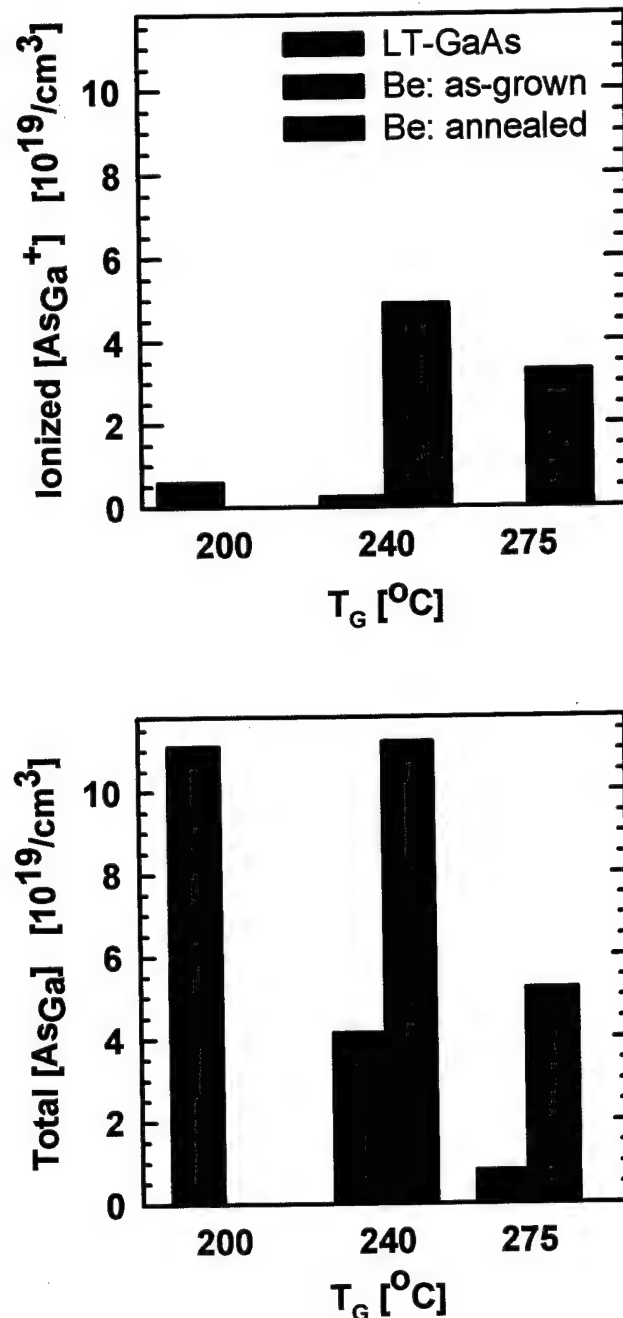


Figure 32

# SIMS profile of n-LT-GaAs:Be-n structure, as-grown

## PROCESSED DATA

15 Nov 97 Cs

Charles Evans & Associates

FILE: 70742w1a

Fig. 1a

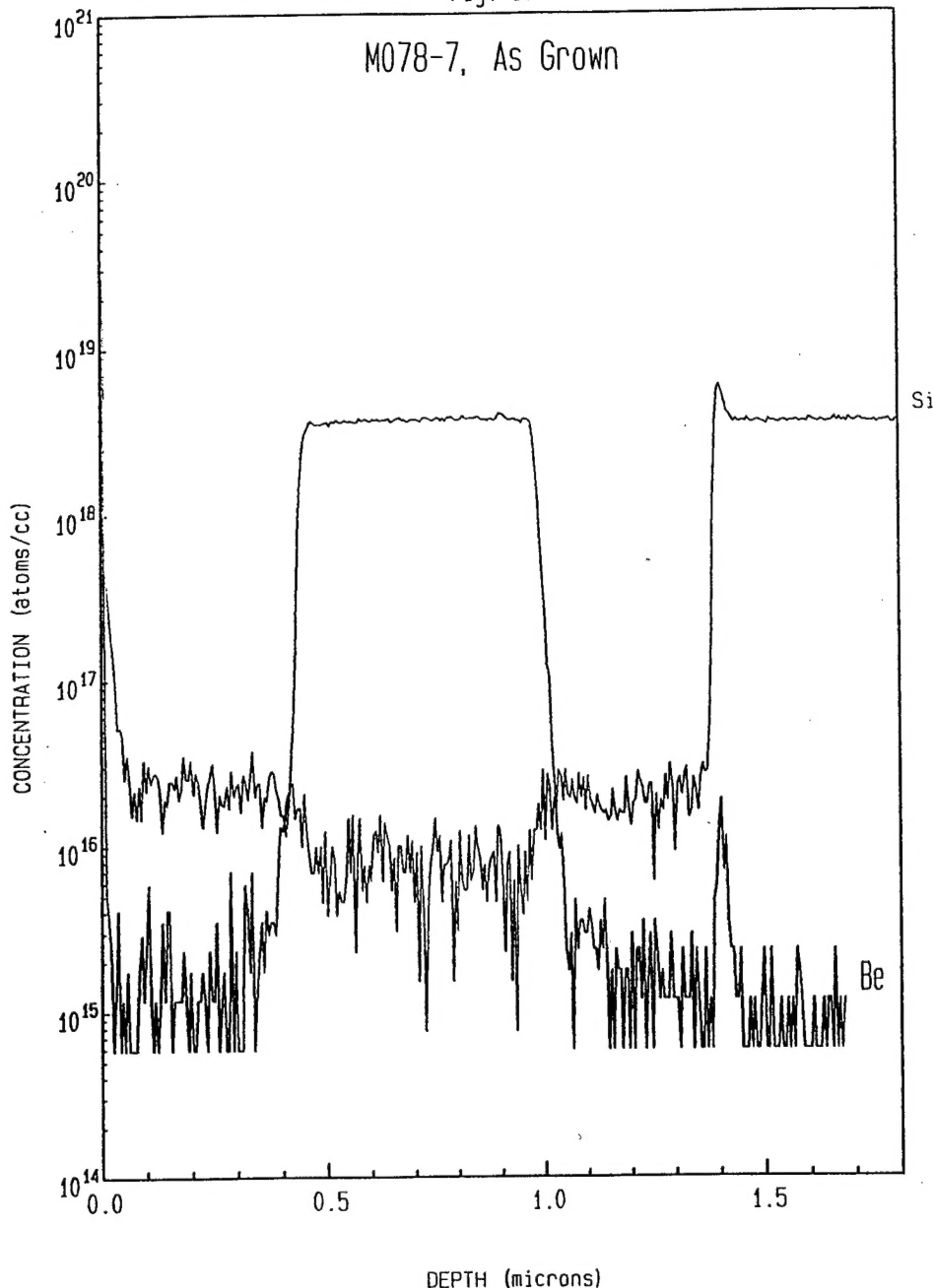


Figure 33.a

# SIMS profile of n-LT-GaAs:Be-n structure, 10 s at 850°C annealed

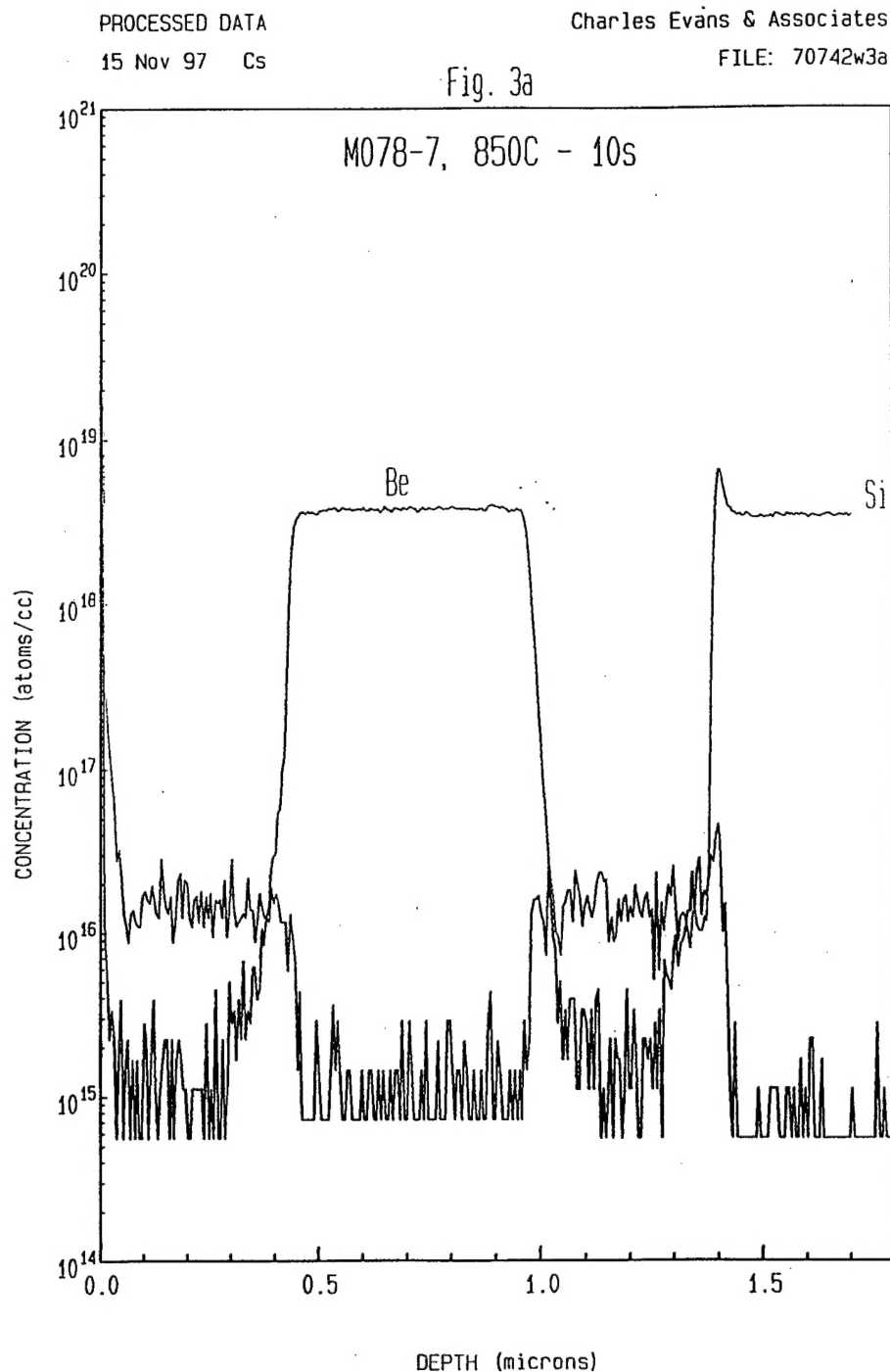


Figure 33.b

# SIMS profile of n-LT-GaAs:Be-n structure, 60 min. at 700°C annealed

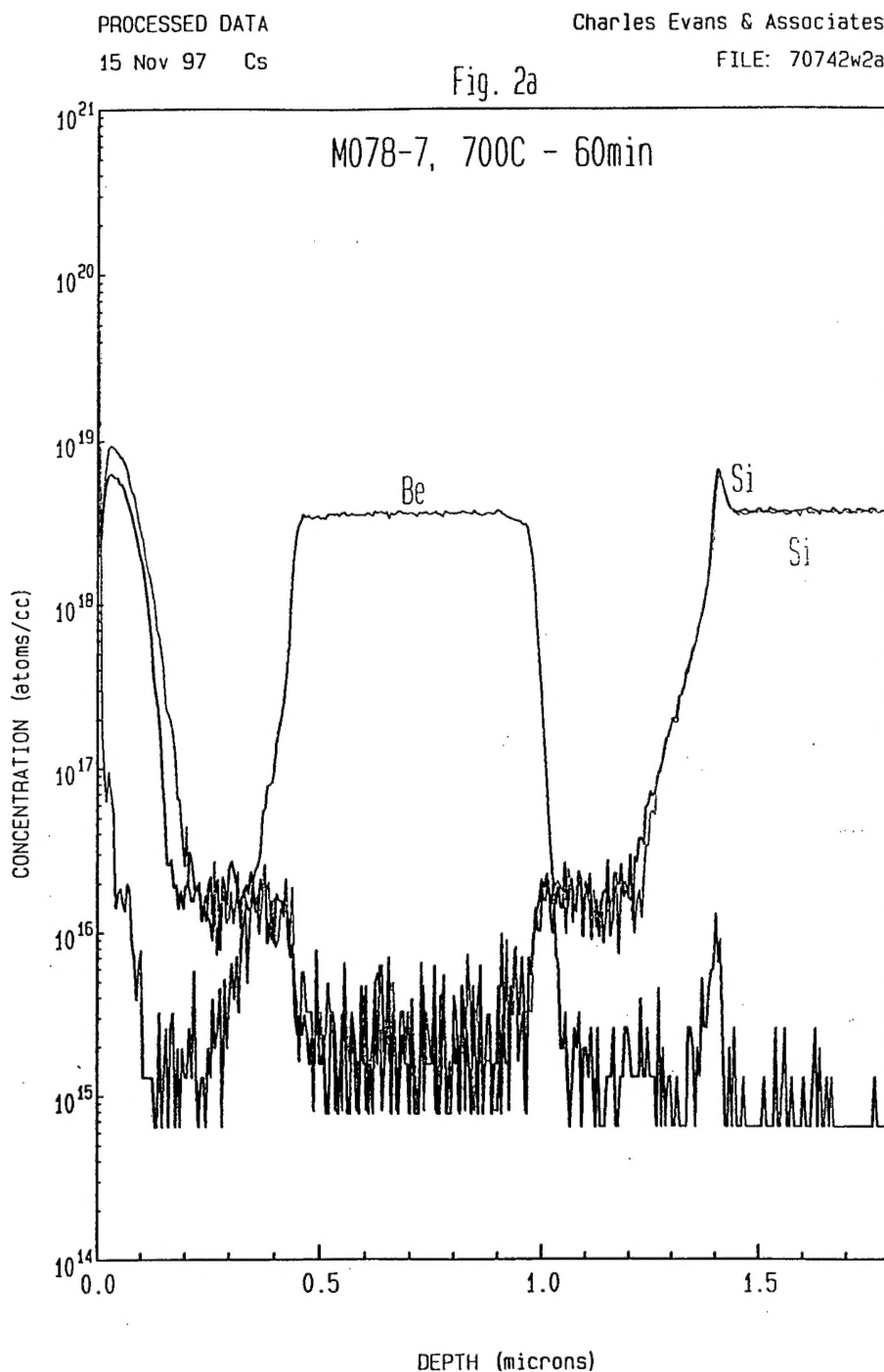


Figure 33.c

# Electrical resistivity of LT-GaAs:Be

$[Be]=10^{20}\text{cm}^{-3}$  : this study /  $[Be]=5*10^{19}\text{cm}^{-3}$  : [Ati.95]

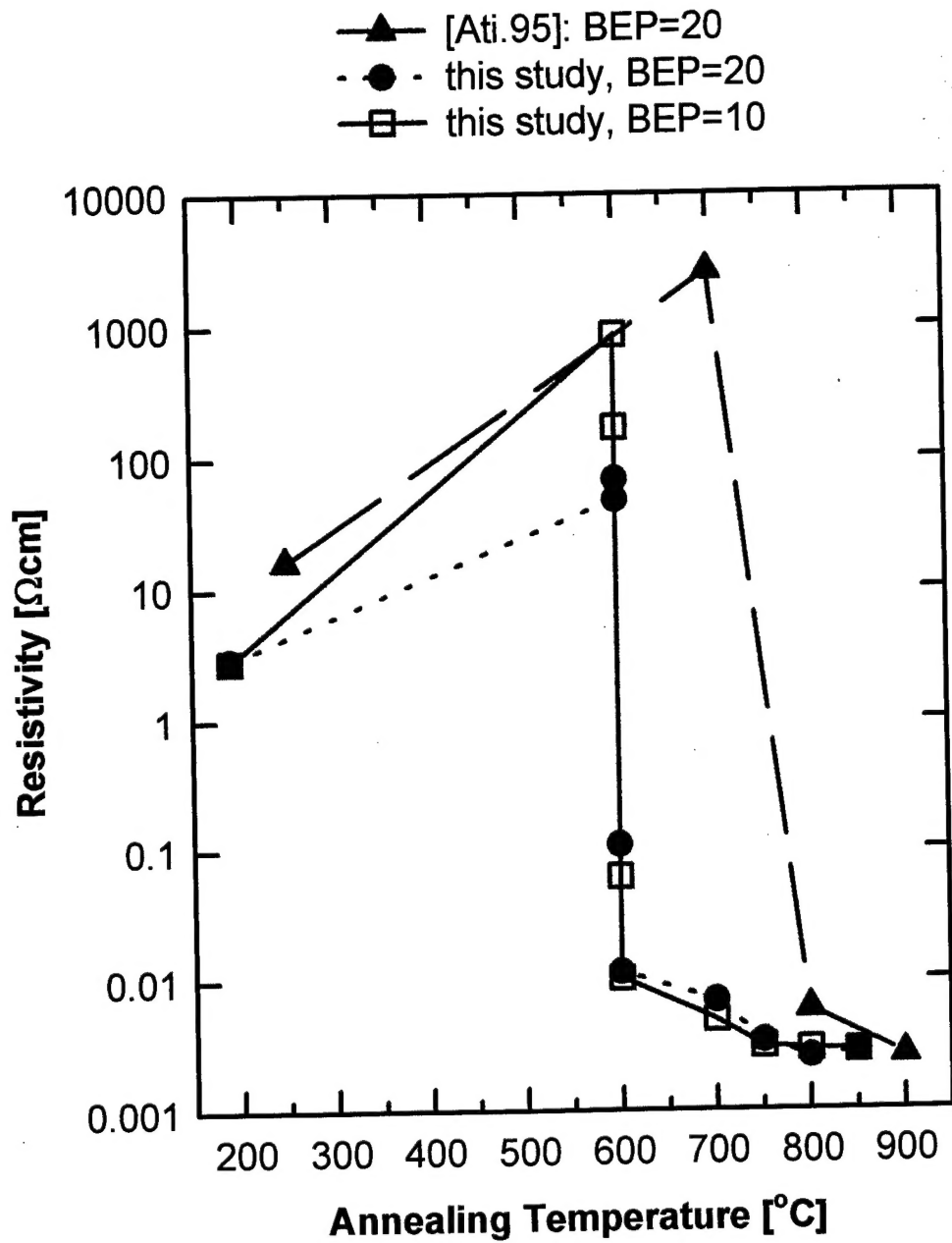


Figure 34